4-17-2013

Telemetry Controlled Brain Machine Interface To Train Cortical Circuits

Tina Marie DeCosta-Fortune

TELEMETRY CONTROLLED BRAIN MACHINE INTERFACE TO TRAIN CORTICAL CIRCUITS

by

Tina Marie DeCosta-Fortune

A Dissertation

Submitted in Partial Fulfillment of the

Requirements for the Degree of

Doctor of Philosophy

Major: Biomedical Engineering

The University of Memphis

May 2013

DEDICATION

for Robert

ACKNOWLEDGEMENTS

Without the guidance and persistent help from several people in and outside the University of Memphis and University of Tennessee Health Science Center joint biomedical engineering program, this dissertation would not have been possible. First, I would like to express my gratitude to Robert S. Waters, Ph.D. for allowing me the opportunity to become a member of his Anatomy and Neurobiology laboratory team, for sharing his passion for neuroscience, challenging me to reach new levels, and most of all for the time and energy he has invested in me. His patience and guidance are greatly appreciated.

Amy de Jongh Curry, Ph.D., thank you for introducing me to bioelectricity and allowing me to become a member of your electrophysiology laboratory team. The good advice, support, and guidance you have shared with me throughout this journey have been invaluable and for which I am grateful. I would also like to acknowledge the funding resources you made available for me to conduct my Ph.D. work.

I would also like to give special thanks to Dr. Bashir Morshed for his kindness, generosity of time, and availability at all hours to answer that 'quick question'. I am extremely appreciative for the opportunity to work with your team in the ESARP laboratory; it has proven instrumental. I am particularly grateful for your team's openness to teach, willingness to share knowledge, and offer ideas.

To Dr. Chen X. Li, I would like to thank you for taking the time to teach me my way around the laboratory, coaching me on the neurosurgery, histology, and pathway reconstruction procedures performed in these studies, and especially for the countless hours you selflessly spent in experimental studies; you are truly a master of your craft.

Dr. Jack W. Buchanan, thank you for your suggestions, comments, and overall advice you have given me.

To all my committee members, thank you for your continued support and participation.

Finally, to my wonderful, wonderful husband Robert to whom I am indebted for his devotion, patience, laughter, and most of all for reminding me of the important things in life.

ABSTRACT

DeCosta-Fortune, Tina Marie. Ph.D. The University of Memphis. May 2013. Telemetry Controlled Brain Machine Interface To Train Cortical Circuits. Major Professors: Amy L. de Jongh Curry, Ph.D. and Robert S. Waters, Ph.D.

The goal of this dissertation is to document functional reorganization in rat primary somatosensory (SI) cortex. This work proposes to strengthen the interhemispheric connection between homotopic sites in forelimb barrel cortex (FBC) through intracortical microstimulation (ICMS) and induce functional reorganization whereby neurons in FBC respond to new input from the ipsilateral forelimb. Furthermore, a wireless microstimulation and recording device was developed for producing enhancement and functional reorganization of cortical circuits in FBC.

The goal of Experiment One was to test the hypothesis that layer V neurons projected to homotopic sites in contralateral layer V FBC. Retrograde or anterograde neuronal tracer injections were made to characterize the distribution of callosal projecting neurons in contralateral SI that terminate in layer V FBC and where layer V callosal projecting neurons terminate in contralateral SI. The results showed a differential pattern of interhemispheric connectivity between homotopic forelimb representations in layer V FBC.

The goal of Experiment Two was to test the hypothesis that ICMS enhances the interhemispheric pathway and leads to functional reorganization. ICMS was delivered *in vivo* to the interhemispheric pathway between homotopic layer V barrel cortices and multiunit recordings were made to assess changes in firing rate. The results showed ICMS strengthens interhemispheric connectivity and leads to functional reorganization in rat FBC.

The goal of Experiment Three was to develop an interactive telemetry-based neural interface device for the controlled delivery of ICMS and recording response activity in rodent. The device successfully delivered microstimulation to a single electrode in SI and recorded evoked responses from a separate electrode in contralateral SI. Its performance was shown to be comparable to commercial stimulating and recording systems. This system serves as a prototype towards the implementation of a wearable compact device.

The data suggest that neurons in rat FBC can be induced to respond to new input from the ipsilateral forelimb by enhancing the interhemispheric pathway with ICMS. An interactive system for the controlled delivery of telemetry-based microstimulation and real-time recordings has been demonstrated *in vivo*. These studies provide the framework for subsequent studies of interhemispheric pathway enhancement and functional reorganization in freely moving rats.

PREFACE

The data collected during this research project has been organized to include two journal articles. Chapter II: Anatomical Tract Tracing Study will be submitted to *Experimental Brain Research* as an article entitled "Differential Pattern of Interhemispheric Connections between Homotopic Layer V Forelimb Representations in Rat Barrel Field Cortex." Chapter III: Chronic Microstimulation Study will also be submitted to *Experimental Brain Research*; it will be an article entitled "Intracortical Microstimulation Strengthens Interhemispheric Connections and Leads to Functional Reorganization."

TABLE OF CONTENTS

LIST OF TABLES

LIST OF FIGURES

CHAPTER I

INTRODUCTION

I. Goals and Objectives of Dissertation Research

The goals of this research project involve furthering our understanding of functional reorganization in rat primary somatosensory (SI) cortex. Despite the existence of callosal connectivity between SI cortices, neurons in forelimb SI respond only to input originating from the contralateral forelimb and not to input from the ipsilateral forelimb. The specific experimental questions addressed in this dissertation are focused on assessing the ability to strengthen the interhemispheric pathway between homotopic layer V forelimb representations and bring about functional reorganization in Sprague-Dawley rats by inducing SI forelimb neurons to respond to new input from the ipsilateral forelimb. Rat SI cortex provides a model system for these studies where layers IV and V are of particular interest. In rodents, cortical layer IV is characterized by regions of well-defined cell aggregates, termed barrels, which serve as morphological markers associated with the representation of punctate regions of the periphery. Additionally, layer IV granular cells receive direct somatic input from the thalamus (Jensen and Killackey, 1987a; Land et al., 1995). The pyramidal neurons in layer V provide a major output from the cortex, sending projections to neighboring cortical regions, contralateral cortex, and subcortical regions (White, 1989; Bernardo et al., 1990; Hattox and Nelson, 2007).

Rodent barrel cortex was chosen as the model system for this research because of the strong correlation between the morphology (structure) of the layer IV barrel subfields and their physiological representation (function) of peripheral regions including the vibrissa, forelimb, hindlimb, and axial body (Woolsey and Van Der Loos, 1970; Van Der

Loos and Woolsey, 1973; Welker, 1976; Chapin and Lin, 1984; Waters et al., 1995a; Pearson et al., 1996). Furthermore, the barrel cortex is organized into functional columns that run through all cortical lamina (Mountcastle, 1957; Woolsey and Van Der Loos, 1970; Favorov and Whitsel, 1988) and while barrels are confined to layer IV, cortical columns are in register with the well-defined clusters of cells located in layer IV (Lübke et al., 2000; Feldmeyer, 2012). Thus, the layer IV barrels provide an indication as where these cortical columns exist. The columnar organization of the barrel cortex allows for same body surface representation to be identified in those cortical layers that are devoid of morphological markers, such as layer V (infragranular layer). The focus of this dissertation is interhemispheric pathway enhancement and functional reorganization of layer V forelimb representation whereby a functional connection is established between ipsilateral forelimb barrel cortex and the ipsilateral forelimb. The forelimb representation is hereafter considered to include the forepaw, wrist, and forearm representations (Waters et al., 1995b).

The goals of **Experiment One** were to examine the details of layer V forelimb barrel cortex (FBC) interhemispheric connections and to test the hypothesis that layer V neurons in barrel cortex projected to homotopic sites in the contralateral layer V (FBC). Anatomical track tracing techniques were employed to examine the projection of layer V neurons to the contralateral cortex and determine an optimal interhemispheric circuit in which to study enhancement and functional reorganization. The retrograde tracer, cholera toxin-B subunit (CT-B), was used to identify the location of neurons in contralateral SI that terminate in layer V while the anterograde tracer, biotinylated

dextran amine (BDA), was used to determine where layer V callosal projecting neurons terminate in the opposite barrel cortex. The following questions were posed in Experiment One:

1. Do homotopic sites in SI forelimb representations receive reciprocal callosal projections?
2. What are the lamina that receive callosal projections from layer V SI cortex?
3. What are the lamina in contralateral SI that send callosal projections to layer V barrel cortex?

The goals of **Experiment Two** were to determine if transcallosal connectivity between homotopic layer V representations in FBC is enhanced through chronic microstimulation and whether this 'newly' strengthened pathway results in functional reorganization whereby input from the ipsilateral forelimb becomes expressed. Using chronic intracortical microstimulation (ICMS) and extracellular recording methods we were able to evaluate interhemispheric pathway enhancement through spike activity changes in response to cortical microstimulation. We were also able to determine occurrence of functional reorganization using the same extracellular recording method in conjunction with peripheral stimulation of the ipsilateral forelimb. The following questions were posed in Experiment Two:

1. Does chronic microstimulation enhance transcallosal connectivity between homotopic sites in layer V SI forelimb cortex?
2. What is the time course for enhancement?

3. Does an enhanced interhemispheric pathway result in functional reorganization whereby neurons in the forelimb barrel cortex respond to new input from the ipsilateral forelimb?

The goal of **Experiment Three** was to develop and test an interactive telemetry-based chronic microstimulation and recording device that can be used for producing enhancement and functional reorganization in rat FBC. The neural device addressed the following system requirements:

1. Generate monophasic, biphasic, and pseudomonophasic stimulation pulses of either positive or negative polarity.
2. Deliver a maximum biphasic stimulus intensity of 100 μA to a maximum load of 100 kΩ.
3. Allow real-time user control of stimulation amplitude, duration, frequency, and delay.
4. Operate in either a calibration (set # of pulses) or chronic (set time period) mode.
5. Record response activity following a specific number of consecutive stimulations at set intervals of time.
6. Wirelessly transmit stimulation parameters and recorded response data to and from the remote device, respectively.

Data gathered from these three experiments will provide valuable anatomical, physiological, and neural interfacing information that gives a unique insight into assessing our ability to train cortical circuits, which may play a role in our ability to modulate cortical reorganization.

II. Background and Significance

Injury- and treatment-induced cortical reorganization resulting from limb amputation and stroke recovery efforts, respectively, are widely recognized phenomenons. Approximately 1.7 million amputees and more than 7.0 million stroke survivors live in the United States and each year an estimated 185,000 Americans suffer the loss of a limb while nearly 795,000 suffer a stroke. One consequence of limb amputation and that takes place during post-stroke recovery is the reorganization (plasticity) of SI cortex. SI functional plasticity resulting from amputation has been associated with the phantom pain experienced by 50-85% of amputees (Knecht et al., 1995; Flor et al., 1998; MacIver et al., 2008) and the level of post-stroke motor recovery (Schaechter et al., 2006; Liepert et al., 2009; Murphy and Corbett, 2009; Roiha et al., 2011). Understanding this central neurological consequence is crucial for developing alternative compensation strategies and rehabilitation therapies.

A. Overview of the Somatic Sensory System

The somatic sensory system is arguably the most diverse of the sensory systems as it mediates a range of sensations that relate to touch (crude and discriminative), temperature, pain, and proprioception. In addition to responding to many different stimuli, the somatic sensory system differs from the other sensory systems [visual (seeing), auditory (hearing), gustatory (tasting), and olfactory (smelling)] in that its receptors are distributed throughout the body rather than being localized in a small, specialized area [eye (visual), ear (auditory), tongue (gustatory), nose (olfactory)]. Since somatic sensation deals with processing information related to four distinct sensations, various types of receptors are required to transduce the many types of stimuli. As such, a

specialized class of peripheral receptors exists for each modality; they include mechanoreceptors, thermoreceptors, nociceptors, and proprioceptors which are sensitive to touch, temperature, pain, and body position, respectively (Martin, 1989; Nolte, 2009). While each sensation is mediated by a different class of receptors, all somatosensory information from the body (trunk and limbs) is conveyed to SI by one of two ascending pathways: the dorsal column-medial lemniscal pathway and the spinothalamic (anterior and lateral) pathway. The former is the central pathway that carries information regarding tactile sensation (e.g. discriminative touch) and the latter is the primary pathway carrying information pertaining to temperature, pain, and crude touch (Martin, 1989; Tortora and Anagnostakos, 1990; Nolte, 2009). These tracts ascend ipsilaterally from the periphery and at a specific point along the pathway decussate (cross the midline) to the contralateral side before reaching SI; the dorsal column-medial lemniscal system decussates in the medulla whereas the spinothalamic system decussates in the spinal cord. After crossing the midline, both pathways project through the thalamus where the somatosensory thalamic nuclei send afferent projections to SI where they terminate; these thalamocortical neuronal terminations serve as the main source of somatosensory information input. The work conducted in this dissertation focuses on the somatic input of discriminative touch which is processed along the dorsal column-medial lemniscal pathway.

B. Anatomy and Physiology of the Dorsal Column-Medial Lemniscal System

The dorsal column-medial lemniscal pathway is the major route by which tactile information ascends to SI. It is comprised of three orders (primary, secondary, and tertiary) of sensory neurons that relay input from cutaneous mechanosensory receptors

distributed on the skin surface (Squire et al., 2008). The primary (1st order) sensory neuron is the dorsal root ganglion (DRG) neuron and when its terminals (mechanosensory receptors) are presented with the appropriate stimulus, somatic sensory signals (action potentials) are generated in response. The action potentials propagate from the terminal receptors along DRG afferents (distal and proximal processes) and enter the spinal cord through the dorsal root.

Upon entering the spinal cord, DRG neurons project ipsilaterally through the dorsal column to the lower medulla where they synapse onto secondary (2nd order) neurons located in the dorsal column nuclei (DCN). Projections from the secondary sensory neurons decussate in the medulla and ascend contralaterally in the medial lemniscus, which is a white matter tract that courses through the medulla, pons, and midbrain. Axons from the medial lemniscus project to the diencephalon region of the brain where they synapse onto tertiary (3rd order) neurons located in the ventroposterolateral (VPL) nucleus of the thalamus. Finally, afferent projections from thalamocortical neurons terminate, in large part, in SI (Jones, 1985; Jensen and Killackey, 1987a, 1987b; Arnold et al., 2001).

C. Anatomy and Physiology of the Somatosensory Cortex

Somatosensory cortical neurons are cytoarchitecturally arranged in a series of six horizontal layers, labeled I – VI from the outside (pial surface) in (white matter) (Brodmann, 1909). Somatic input from the periphery is transmitted through a series of afferent projecting neurons and relayed to the thalamus where thalamocortical neurons in the VPL send their axons to SI cortex, terminating primarily in layer IV (Jones, 1985; Jensen and Killackey, 1987a; Chmielowska et al., 1989; Land et al., 1995). As a result of

receiving direct input from the thalamus, layer IV cells exhibit shorter latency responses to somatic stimulation (Armstrong-James et al., 1992; Welker et al., 1993). Layer IV is densely populated with small granular cells that resemble grains of sand and is referred to as the granular layer; adjacent layers located immediately above (layer II/III) and below (layer V) contain pyramidal cells and these layers are referred to as the supra- and infragranular layers, respectively. Collectively, layers I – VI provide a horizontal lamina structure for SI.

In addition to their horizontal lamina organization, SI neurons are arranged in small vertical groupings that extend through all cortical layers forming a 'cortical column'; these groupings of neurons belong to a common modality and have a common peripheral receptive field location on the skin surface (Mountcastle, 1957). In 1978, Mountcastle hypothesized that cortical columns were comprised of several radial cell cords termed 'mini-columns' and that these mini-columns were the fundamental processing unit of the cerebral cortex (Mountcastle, 1978). Experimental evidence supporting a sub-columnar structure was provided from receptive field mapping studies carried out in SI of cat (Favorov et al., 1987; Favorov and Diamond, 1990) and monkey (Favorov and Whitsel, 1988). In rodent SI, cortical columns are easily identifiable as they are in register with the well-defined clusters of cells located in layer IV (Feldmeyer, 2012). Of the 19,000 neurons with a barrel related column, approximately 88% are excitatory and are distributed throughout the cortical lamina as follows: 5,000 (layer II/III), 4,000 (layer IV), 3,300 (layer V), and 4,500 (layer VI); the other 12% are non-excitatory interneurons (Meyer et al., 2010, 2011). Somatic input enters layer IV and through a series of interconnecting microcircuits, all neurons within a cortical column respond preferentially

to the same sensory stimulus (Mountcastle et al., 1955; Powell and Mountcastle, 1959; Mountcastle, 1978, 1997). The functional columnar arrangement of SI allows for precise receptive field mapping in cortical lamina devoid of morphological markers such as the infra- and supragranular layers.

D. Anatomy and Physiology of Rodent Barrel Field Cortex

The presence of cell aggregates in layer IV of rodent SI cortex was first identified by I. DeVries (DeVries, 1911) when he noted the formation of "small islands" from layer IV neurons. These small groupings of cells were later called 'glomeruli' after their unique bulb-like structure was observed in coronally sectioned rodent SI cortices (Lorente De No, 1922). However, it wasn't until the late 1960's that a physiological organization to these unique anatomical structures was suggested; through his work in SI of mouse, Woolsey (Woolsey, 1967) determined that movement (stimulation) of a single mystical vibrissa on the bilateral face evoked responses from neurons within an individual glomeruli. A later study conducted by Woolsey and Van der Loose characterized the morphological and physiological attributes of mouse vibrissa glomeruli using Nissl stained tangentially sectioned cortices and described the cell clusters as well-defined oval shaped structures composed of a dense granular wall surrounding a cell poor hollow center (Woolsey and Van Der Loos, 1970); because their shape resembled whisky barrels, the term "barrel" was coined to refer to a single cell cluster. In addition, cortical regions called "septa" were described as agranular zones surrounding and separating individual barrels from one another (Woolsey and Van Der Loos, 1970).

Individual barrels are segregated into barrel subfields, the first of which was associated with the representation of the mystacial vibrissa and sinus hairs on the snout of

the face and because of their location in SI, they were given the names of posteromedial barrel subfield (PMBSF) and the anterolateral barrel subfield (ALBSF), respectively (Woolsey and Van Der Loos, 1970; Van Der Loos and Woolsey, 1973; Welker and Woolsey, 1974). The PMBSF is described as a highly organized series of 5 anteroposterior running rows of barrels labeled A through E and each row contains 8 individual barrel units (Woolsey and Van Der Loos, 1970); a single barrel structure may contain several thousand cells and each of these cells has been physiologically associated with a single large mystical vibrissa on the bilateral face of the mouse (Woolsey, 1967; Woolsey and Van Der Loos, 1970; Welker, 1971). The ALBSF is a population of smaller barrels located anterior to the PMBSF consisting of approximately 100 barrel structures that are similar in shape to the PMBSF barrels but much smaller in size; these barrels respond preferentially to the somatic stimulation of the sinus hairs on the snout and lower lip on the bilateral face (Welker, 1971; Welker and Woolsey, 1974). The PMBSF and ALBSF are the two largest subfields, measuring 300 μm × 160 μm and 110 μm × 110 μm, respectively; together they occupy approximately 67% of the barrel field cortex (Dawson and Killackey, 1987).

Two additional barrel subfield, the forepaw and hindpaw barrel subfield (FBS and HBS, respectively), located medial to the PMBSF and ALBSF were recognized by Welker (Welker, 1971) while generating a physiological map of the entire body surface in layer IV of rat SI; they are physiologically associated with the contralateral forelimb and hindlimb (Welker, 1976; Dawson and Killackey, 1987; Waters et al., 1995a; Pearson et al., 1996). The FBS consists of a highly organized arrangement of approximately 25 barrels (Woolsey and Van Der Loos, 1970; Welker, 1976), measures 170 μm × 120 μm,

and occupies approximately 15% of the barrel field (Welker, 1976; Dawson and Killackey, 1987). The HBS, the smallest of all barrel subfields, consists of approximately 13 barrels and occupies 4% of the barrel cortex (Welker, 1976; Dawson and Killackey, 1987; Pearson et al., 1996).

In addition to the well-defined granular zones of the barrel subfield, the barrel cortex contains nebulous regions devoid of barrel like structures. The receptive fields within these cortical regions lack well demarcated boundaries; instead the boundaries are broad and more complex (Chapin et al., 1987). These layer IV cortical agranular regions receive sparse projections from the thalamus in comparison to the well-defined barrels. The most notable of these cortical regions is located immediately posterior to the discrete barrels of the FBS and responds to the stimulation of punctate regions on the wrist, arm, shoulder and the axial body (Welker, 1976; Dawson and Killackey, 1987; Waters et al., 1995a; Pearson et al., 1996).

An important aspect to modern day research is a technique to visualize the barrel subfield and the agranular regions, which lie adjacent to and in between the barrel fields, within a few sections of tissue. The technique was first introduced in 1976 by C. Welker and includes perfusing the brain with fixative, carefully separating the cortices from the white matter, flattening the cortices between two glass slides overnight, and sectioning the tissue in the tangential plane (Welker, 1976). Tangential sectioning of the cortex allows for the layer IV barrel field to be fully visualized within a few sections of tissue and thus providing a morphological map of the entire body surface, which is referred to

as the “rattunculus” (Welker, 1976). This method of tissue sectioning is commonly used to examine sites of electrolytic lesions and/or tracer labeling in relationship to the body surface map.

E. Anatomy and Physiology of the Forepaw Barrel Subfield

The forepaw barrel subfield (FBS) is located anteromedial to the PMBSF and can be found approximately 3.5 mm lateral to the midline Bregma. It is comprised of a highly organized array of barrels that are associated with the representation of the dorsal (hairy) and ventral (smooth) skin surfaces of the forelimb. Discrete regions have been associated with the dorsal and ventral digits and the digit pads while the wrist is represented by less defined regions of the FBS (Welker, 1976; Dawson and Killackey, 1987; Waters et al., 1995a). Some of the nearly 25 barrels are not the stereotypical whisky barrel shape; instead they are rectangular and ellipsoidal, giving the FBS an ovoid configuration. Bordering the FBS laterally, anteriorly, and medially are agrangular cortical areas that are non-responsive to somatic stimulation of the contralateral forelimb. Posterior to the FBS is a nebulous region devoid of barrel like structures that is responsive to the somatic stimulation of the wrist, forearm, upper arm, shoulder and trunk (Pearson et al., 1996).

Using extracellular recording and physiological mapping techniques, Waters et al. (1995a) generated a detailed map of the FBS digit, digit pads, and palmar pads. They reported within the forepaw representation, the digits are somatotopically organized along an anteroposterior axis. Digit one (D1) representation is associated with two large barrels located in the most anterolateral position of the FBS. Digits two through five (D2-D5) follow sequentially with D5 located in the most posteromedial position. D2-D5

is represented by the most apparent aspect of the FBS, 4 centrally located bands of well-defined barrels running along a mediolateral axis. Each barrel band is associated with the representation of a single glabrous digit. Within each band are 3-4 individual barrels representing the distal and proximal regions of D2-D5; the distal region is associated with the two most lateral barrels and the proximal region is associated with the two most medial barrels. Representation of the five digit pads lies medial to the glabrous digit representations and runs along an anteroposterior axis. The thenar pad (TH) is the most anterior pad located within the FBS. It is followed posteriorly by the three palmar pads (P1, P2, and P3) and finally, the hypothenar pad (HT) is the most posterior pad.

F. Transcallosal Connectivity between Somatosensory Cortices

The rodent barrel cortex has provided a discernible, well organized environment from which interhemispheric connectivity has been examined. Using axonal degeneration and anatomical tracing techniques, Wise and Jones (Wise and Jones, 1976) reported a differential pattern of connectivity between SI cortices. Callosal connectivity between ipsilateral and contralateral SI originates and terminates in all cortical lamina, predominately in the supra- and infragranular layers (layers II-III and V, respectively) with minimal connections located in the granular layer, layer IV (Wise and Jones, 1976; Akers and Killackey, 1978; Ivy and Killackey, 1981); the sparse labeling found in layer IV was confined to the agranular regions that lie alongside and in between the barrel fields (Wise and Jones, 1976; Akers and Killackey, 1978; Záborszky and Wolff, 1982). A subsequent study reported callosal connectivity within the barrel field generated a honeycomb-like pattern as track tracing techniques revealed labeling was localized within the agranular septa regions that surround and separate the individual barrels; the barrels

themselves were found to be relatively free of callosal connectivity (Olavarria et al., 1984). Furthermore, upon entering the contralateral SI cortex from the white matter, callosal fibers transcend, in bundles, normal to the cortical surface IV (Wise and Jones, 1976; Akers and Killackey, 1978; Ivy and Killackey, 1981). In relation to the body surface, callosal connections have been consistently described as being dense in cortical areas representing the midline or axial body whereas cortical areas associated with distal portions of the body, such as the forelimb, were reported relatively free of callosal connections and considered to be acallosal (Yorke and Caviness, 1975; Wise and Jones, 1976).

G. Bilateral and Ipsilateral Receptive Field Influences

In contrast to several studies that have reported neurons with bilateral receptive fields that receive input from both sides of the body to be exclusively associated with the midline structure of the body, such as the head and trunk (Dreyer et al., 1975; Manzoni et al., 1980, 1989; Ogawa et al., 1989), neurons with bilateral receptive fields associated with the forelimb have been identified in cat (Manzoni et al., 1980; Iwamura, 2000) and monkey (Iwamura et al., 1994, 2002; Taoka et al., 1998). However, in rodent neurons in FBC remain nonresponsive to bilateral input. In both cat (Favorov et al., 2006) and monkey (Lipton et al., 2006; Tommerdahl et al., 2006), ipsilateral forelimb stimulation has also been reported to influence evoked responses to stimulation of the homologous site on the contralateral forelimb.

Recording from neurons with bilateral peripheral receptive fields in cat SI, Innocenti and colleagues suggested that ipsilateral forelimb projections are modulated by callosal transfer from homotopic contralateral cortical regions (Innocenti et al., 1973). In

their study they examined responses to ipsilateral skin shocks and after blocking callosal input they reported responses to ipsilateral stimulation was reduced and therefore modulated by the callosal output of contralateral SI cortical region. Ipsilateral vibrissa input was also suggested to be mediated through the corpus callosum as ipsilateral responses were completely abolished following ablation of homotopic contralateral SI cortical regions (Pidoux and Verley, 1979). In rat SI, ipsilateral hindlimb inputs were also suppressed by inhibition from contralateral SI (Pluto et al., 2005).

H. Reorganization of Somatosensory Cortex

It was once a fundamentally accepted principle that cortical maps, after reaching a certain stage in development, were fixed entities and invariant to change. However, in the late 1970s, researchers began to reexamine this predominate viewpoint after reorganization was first illustrated in monkey visual cortex (VI) (Hubel and Wiesel, 1977; Hubel et al., 1977) and cat SI (Kalaska and Pomeranz, 1979). Subsequent studies have demonstrated cortical reorganization in SI of monkey (Merzenich et al., 1983; Florence and Kaas, 1995; Florence et al., 1996), flying fox (Calford and Tweedale, 1988), and rat (Waters et al., 1995b; Li and Waters, 1996; McCandlish et al., 1996; Pearson et al., 1999). Today it is universally recognized that adult cortical maps are not fixed but indeed dynamic in nature and are continuously reorganizing based on life experiences. The ability of neocortex to reorganize is a critical mechanism necessary for adapting to environmental changes and, more importantly, compensating for injury. This phenomenon has been well documented in humans following an amputation (Knecht et al., 1995, 1996; Flor et al., 1997, 1998; Borsook et al., 1998; Weiss et al., 2000), experiencing chronic back pain (Knecht et al., 1995; Flor et al., 1997), suffering from a

nervous system injury (Elbert et al., 1994), and recovering from a stroke (Schaechter et al., 2006; Roiha et al., 2011). While a considerable amount of research has been conducted over the past four decades on examining and characterizing cortical plasticity, it remains an area of great interest as the underlying mechanisms of this phenomenon are not well understood. The work in this dissertation proposes to extend our understanding of cortical reorganization by demonstrating that the interhemispheric pathway can be strengthened by chronic microstimulation and the enhancement leads to functional reorganization.

I. Mechanisms Underlying Cortical Plasticity

Extracellular physiological recording and mapping techniques have been employed to demonstrate the forepaw is somatotopically represented by the barrels within the layer IV FBS and that each individual barrel is associated with the representation of a punctate region of the forepaw skin surface (Welker, 1976; Angel and Banks, 1983; Dawson and Killackey, 1987; Waters et al., 1995b). While this methodology is commonly used to provide a general understanding of cortical organization, it is limited in that it only reveals information relating to somatic suprathreshold input. Intracellular recording methods provide a more complete understanding by revealing information relating to both supra- and subthreshold somatic input to a single cortical neuron. Using intracellular recordings, our lab, has previously shown that neurons within the individual barrels of the FBS receive both short latency suprathreshold input from a principle location on the forepaw as well as long latency subthreshold input from adjacent forepaw skin surfaces (Li & Waters 1996). Similarly, other investigators have reported neurons

within the individual barrels of the PMBSF respond to the displacement of a primary vibrissa (suprathreshold input) as well as adjacent vibrissae (subthreshold input) (Carvell and Simons 1988; Moore and Nelson 1998).

Cortical plasticity in the form of an expanded receptive field is thought to be the result of preexisting subthreshold input from adjacent regions being raised to suprathreshold firing levels and becoming the newly expressed receptive field (Li et al., 1996). Expanded receptive fields have been induced through peripheral deafferentation (Smits et al., 1991; Li and Waters, 1996; Moore et al., 1998), blocking callosal inputs from opposite cortical region in contralateral SI (Clarey et al., 1996), suppressing GABAergic inhibition (Smits et al., 1991; Li and Waters, 1996; Li et al., 2002), and short-term electrical stimulation (1.5× threshold) of the periphery (Li et al., 1996). Furthermore, these expanded receptive fields are expressed in homotopic regions in contralateral SI through callosal fiber pathways; although the cortical region remains nonresponsive to input from the ipsilateral periphery (Calford and Tweedale, 1990).

J. Chronic Stimulation

The body of work represented in this dissertation concentrates on cortical reorganization brought about by an increase in sensory input through chronic microstimulation of the interhemispheric pathway between homotopic layer V forelimb representations. The concept that chronic stimulation induces reorganization by strengthening callosal connectivity is based on Hebb's cell assembly theory wherein the connection between two cells is strengthened when one cell repeatedly or persistently participates in the excitation and firing of a second cell (Hebb, 1949). High frequency cortical stimulation has been reported to induce long-term potentiation (LTP) lasting

several hours (Lee and Ebner, 1992; Aroniadou-Anderjaska and Keller, 1995; Glazewski et al., 1998), associated with increases in neuronal firing rates (Lee and Ebner, 1992), and enhanced the interhemispheric pathway by increasing the number of transcallosal connections as well as their efficiency (Bogdanova and Sil'kis, 2002).

K. Brain Machine Interfaces

Electrical stimulation (Ranck, 1975; Tehovnik, 1996) and recording of neural activity (Salinas and Sejnowski, 2001) are fundamental techniques used in neurophysiologal research and clinical studies for investigating brain function such as the cortical remodeling that occurs following amputation (Kelahan et al., 1981; Florence and Kaas, 1995; Borsook et al., 1998) and during post stroke recovery (Liepert et al., 2009; Murphy and Corbett, 2009; Kerr et al., 2011; Roiha et al., 2011). Conventional methods employing these techniques use large racked-mount commercial equipment that typically requires some degree of restraint or sedation of the subject. However, advancements in neuroscience and neuroengineering have enabled these fundamental tools to be developed into smaller more portable electronic devices, commonly referred to as Brain Machine Interfaces (BMIs), in an effort to minimize and, in some cases, remove the restrictions imposed by conventional methods.

Many of the existing BMIs used in research have been employed to function as either a neural stimulator (Xu et al., 2004; Thurgood et al., 2008, 2009; Arfin et al., 2009) or a neural data acquisition system (Obeid et al., 2004; Farshchi et al., 2006; Harrison et al., 2007, 2008; Fan et al., 2011); only two systems incorporating both capabilities were found reported (Jackson et al., 2006a, 2007; Fernando et al., 2007). Jackson et al. (2006a, 2007) developed a neural device consisting of two separate circuits, one for

stimulation and the other for neural signal data acquisition, that could be connected together and operate as one unit. Their device was used to create an artificial connection between two sites in the primary motor cortex (MI) of monkey by using the firing activity recorded at one site to trigger pre-defined stimulation to the second site. Their results showed that activity from the recording site resembled the activity at the stimulating site after only a few days of continuous operation. Fernando et al. (2007) developed a neural stimulator (mA range) and integrated its capabilities into an existing miniaturized wireless neural data acquisition system fabricated by Farshci (2006). Their stimulator system was focused on developing both a constant current and voltage controlled source. Their system provides milliamp level stimulation and its features were demonstrated *in vitro*. Unfortunately, these investigators did not present simultaneous stimulation and recording *in vivo*.

III. Relevance To Dissertation Research

A specific literature review has been conducted for each experiment and presented in their respective chapters to provide the necessary background information to understand the research presented in this dissertation.

The goal of Experiment One is to elucidate the projection patterns of callosal projecting neurons in layer V SI forepaw, wrist, forearm, and shoulder representations to determine if layer V neurons project to homotopic sites in layer V of contralateral barrel cortex. Using focal injections of CT-B, this work intends to identify the location of callosal neurons in contralateral barrel cortex that terminate in layer V; focal injections of BDA will be used to identify where layer V callosal projecting neurons terminate in the opposite barrel cortex. Regional distribution of the projection patterns will be used to

determine if the projections are homotopic. Chapter II will provide data that support homotopic projections between specific forelimb cortical regions and their respective site in contralateral cortex. The data will also show that layer V barrel cortex receive callosal inputs primarily from layer V and layer III of contralateral barrel cortex.

Experiment Two will test whether transcallosal connections are strengthened by chronic microstimulation and if the newly enhanced interhemispheric pathway leads to functional reorganization. Based on the anatomical track tracing study results of dense patches of reciprocal transcallosal connectivity between specific homotopic layer V forelimb representations in SI of rodent, a rigorous evaluation of functional reorganization in the wrist representation was performed in by strengthening its transcallosal connections. Chapter III will provide data that support chronic microstimulation induces enhancement of the interhemispheric pathway between homotopic layer V forelimb representations in rat SI; the data will also demonstrate that neurons in the forelimb cortex can become responsive to new input from the ipsilateral forelimb following enhancement of the transcallosal connectivity between ipsilateral and contralateral forelimb cortices.

The results of Experiment Two provided proof of principle that an interhemispheric pathway between SI cortices can be enhanced and the enhancement leads to functional reorganization. Experiment Three contributes the development of an interactive telemetry-based embedded system for the controlled delivery of chronic microstimulation and real time monitoring of response activity. Functional performance and Bluetooth communication capabilities of this device will be demonstrated on a bench-top, in a saline-based solution, and *in vivo* with Sprague-Dawley rats. Design of this device will

serve as a prototype for use with anesthetized rats to evaluate functional requirements prior to studying interhemispheric pathway enhancement and functional reorganization in freely moving rats. Chapter IV will provide data demonstrating the capacity of this device to deliver microstimulation of varying waveform, intensity, duration, delay, and frequency. Data will also be presented showing recording of evoked response activity and the ability to modify experimental controls real-time.

CHAPTER II

ANATOMICAL TRACT TRACING STUDY

I. Specific Literature Review

The primary somatosensory (SI) cortex is somatotopically organized, arranged into cortical columns, receives input, in large part, from the opposite side of the body surface, and sends projections to both ipsilateral and contralateral SI as well as to subcortical sites. In rodents, cortical layer IV is characterized by regions of well-defined cell aggregates, termed barrels, which are segregated into subfields associated with the representation of the mystacial vibrissae (Woolsey and Van Der Loos, 1970; Van Der Loos and Woolsey, 1973; Welker, 1976), forepaw (Welker, 1976; Chapin and Lin, 1984; Waters et al., 1995a), and hindpaw (Pearson et al., 1996). In addition, layer IV contains a nebulous region devoid of barrel like structures located immediately posterior to the forepaw barrel subfield (FBS) that is associated with the representation of the wrist, forearm, trunk, and shoulder (Pearson et al., 1996). The distinctive relationship between barrel field structure and function makes the barrel cortex an attractive model system for examining connectivity between ipsilateral and contralateral SI cortices.

Interhemispheric connectivity between SI cortices has been studied in a variety of species that include non-human primate (Weller et al., 1987; Manzoni, 1997; Iwamura et al., 2001), cat (Manzoni et al., 1980; Barbaresi et al., 1987), rabbit (Ledoux et al., 1987), raccoon (Ebner and Myers, 1965; Herron and Johnson, 1987), and rodent (Wise and Jones, 1976; Olavarria et al., 1984; Hayama and Ogawa, 1997; Henry and Catania, 2006). Wise and Jones (1976) transected the corpus callosum, hemisected the neocortex, or injected retrograde and anterograde tracers throughout SI and reported a differential

pattern of connectivity in contralateral SI which was subsequently corroborated by several investigators (Akers and Killackey, 1978; Ivy and Killackey, 1981). Upon leaving the white matter and entering the contralateral SI, commissural fibers transverse orthogonally through layer VI towards the pial surface to make dense connections in layers III and V (Wise and Jones, 1976; Akers and Killackey, 1978; Ivy and Killackey, 1981). In contrast, sparse labeling was noted in layer IV (Wise and Jones, 1976; Akers and Killackey, 1978; Ivy and Killackey, 1981) and the label observed was localized to agranular regions that lie outside and between the granularly organized barrel subfields (Wise and Jones, 1976; Akers and Killackey, 1978; Záborszky and Wolff, 1982). When tracers were injected into layer IV of the vibrissa representation (Olavarria et al., 1984) or layers III and IV of the jaw representation (Hayama and Ogawa, 1997), the resulting labeling was restricted to agranular septal regions that lie between individual barrels in the contralateral SI barrel field cortex. Similarly, injections that were localized to layers III and IV in the forelimb representation resulted in dense labeling in contralateral agranular regions bordering the forelimb site (Henry and Catania, 2006), and sparse labeling within the forelimb barrel cortex (FBC) (Hayama and Ogawa, 1997; Henry and Catania, 2006).

Callosal projections in rodent SI originate, in large part, from pyramidal neurons in layers III and V (Yorke and Caviness, 1975; Wise and Jones, 1976; White and DeAmicis, 1977). It was subsequently reported that layer V callosal projections were localized to pyramidal neurons in layer Va (Ivy and Killackey, 1981; Koralek et al., 1990; Hattox and Nelson, 2007) although layer Va cells also project to neighboring motor cortex and subcortical regions that include the striatum (Wise and Jones, 1977a; White, 1989;

Bernardo et al., 1990; Hoeflinger et al., 1995). Layer Va neurons have small somas and thin non-bifurcating apical dendrites that terminate in layer I, in contrast to layer Vb projecting neurons that have large somas and thick bifurcating apical dendrites that also terminate in layer I (Hattox and Nelson, 2007; Feldmeyer, 2012).

Clear evidence for connectivity between ipsilateral and contralateral SI in rodents has been demonstrated by injecting large amounts of tracer into SI, or examining degenerating axons following inactivation of large SI cortical regions (Yorke and Caviness, 1975; Wise and Jones, 1976; Akers and Killackey, 1978; Ivy and Killackey, 1981; Weller et al., 1987; Koralek and Killackey, 1990). When connectivity was studied by making more restricted injections into layers III or IV of the forelimb representation labeling was sparse or absent within the contralateral homotopic forepaw representation (Hayama and Ogawa, 1997; Henry and Catania, 2006) although, dense patches of labeling were found in regions bordering the forelimb representation (Henry and Catania, 2006). Unfortunately, these investigators did not specify the laminar distribution of labeling (Hayama and Ogawa, 1997; Henry and Catania, 2006).

To the best of our knowledge, no rodent studies have examined interhemispheric callosal connections between homotopic sites from injections targeted to layer V forelimb or shoulder cortex. In the present study we made anterograde or retrograde injections in layer V within the forepaw, wrist, forearm, and shoulder representations in rat to test the hypothesis that layer V neurons projected to homotopic regions in layer V. Our results suggest that wrist, forearm, and shoulder SI cortices project to homotopic regions of contralateral SI. In contrast, little evidence was found to support a homotopic relationship between forepaw cortices. The observations obtained from the current study

provided a framework for the subsequent study of interhemispheric pathway enhancement and functional reorganization in rat SI which has been presented in abstract form (DeCosta-Fortune et al., 2009).

II. Materials and Methods

A. Animals

A total of 17 Sprague-Dawley rats of either sex with an average age of 11.6 wks (± 3.67 wks) and average weight of 285.1 g (± 62.28 g) were used to examine interhemispheric connectivity between SI cortices. Of this number, 6 rats were studied using a retrograde tracer and 11 rats were studied using anterograde tracer. The experiments conformed to *the Principles of Laboratory Animal Care* (NIH publication No. 86-23, revised 1985) and were approved by the University of Tennessee Health Science Center (UTHSC) Institutional Animal Care and Use Committee (IACUC).

B. Animal Preparation

Rats were anesthetized with Ketamine/Xylazine (100 mg/kg, i.m.) and supplemented regularly (10% of initial dose) in order to maintain areflexia. The hair on top of the head and forelimb was shaved. The animal was placed on a water-circulating heating pad to maintain body temperature between 36.5º C and 38.0º C and the head was secured in a stereotaxic frame. A local anesthetic (Carbocaine) was injected into the scalp and a midsagittal incision was made in the skin to expose the underlying bone. Anterior-posterior and medial-lateral measurements were taken in reference to Bregma and one or two small holes (1 mm diameter) were drilled in the skull over presumptive regions of SI representing the forepaw, wrist, forearm, or shoulder. The dura was then removed and the brain surface was infused with warm saline (0.9%) to prevent drying. A

digital image of the SI cortical surface was taken and enhanced using PhotoShop CS4 (Adobe); the image was then used to mark the surface location(s) of electrode penetrations into the brain.

C. Receptive Field Identification

A carbon fiber electrode (Armstrong-James and Millar, 1979), attached to a Canberra-type Narishige microdrive, was inserted into SI to physiologically identify sites in the forelimb or shoulder representation. Receptive field(s) of SI neurons were measured using hand-held probes that consisted of a blunt-tipped medal rod (00 gauge) attached to the end of a wooded dowel. Extracellular responses were amplified using a custom built amplifier (1500×), fed into an audio monitor, and viewed on an analog oscilloscope. Receptive fields were defined by using minimal somatic stimulation that evoked a maximal cortical response.

Receptive field identification was initiated by inserting the recording electrode to a depth of 700 μm which had previously been reported to lie within the layer IV barrel field and to yield the strongest response to minimal peripheral stimulation (Waters et al., 1995b). If a receptive field of interest was identified, the electrode was then systematically advanced in 100 μm increments to layer V (approximate depths of 900–1,400 μm) and the receptive field was re-measured at each increment. Whenever a match between layer IV and V receptive fields was found, the site in layer V was chosen for injection of tracer. All receptive fields were plotted on a standardized body map of the shoulder, forelimb, and forepaw regions as shown collectively in Fig. 1.

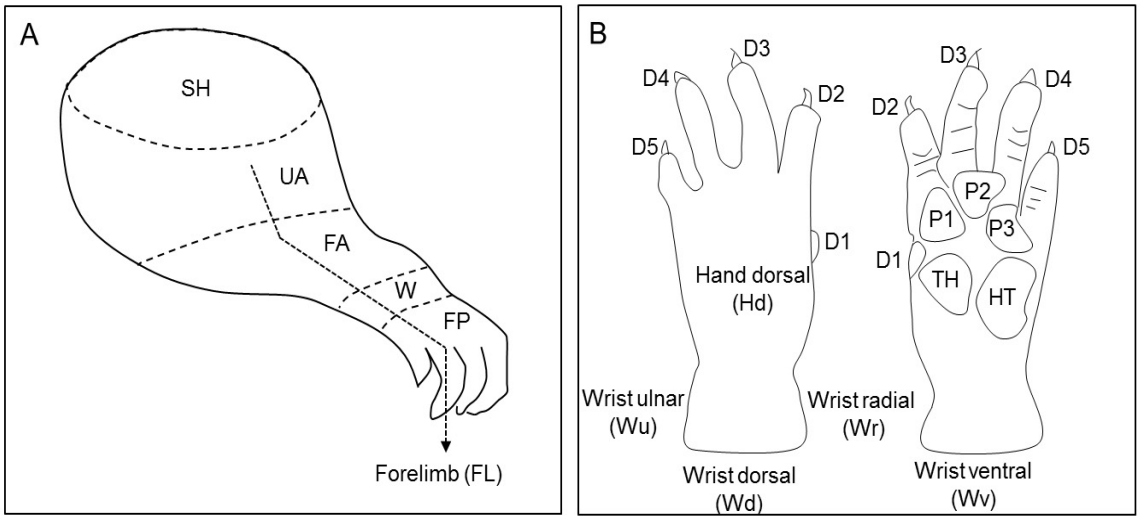

Figure 1 – Line drawings of shoulder, forelimb, and forepaw maps with nomenclature used for plotting receptive fields. **A:** Shoulder and forelimb map nomenclature: FA = forearm; FL = forelimb; FP = forepaw; SH = shoulder; UA =upper arm; W = wrist. **B:** Forepaw map nomenclature: D = digit; H = hand; P = pad; TH = thenar pad; HT = hypothenar pad. Sub-nomenclature: d = dorsal; r = radial; u = ulnar; v = ventral.

D. Tract Tracing

Following physiological identification of a receptive field in the presumptive layer V forelimb or shoulder representation, the carbon fiber electrode was replaced with a glass micropipette containing a 2% solution of either the retrograde tracer, cholera toxin-B subunit (CT-B), or the anterograde tracer, biotinylated dextran amine (BDA), in 1M K-Acetate. The pipette was then lowered into the presumptive layer V where the tracer was iontophoresed into the brain tissue using a digital precision current source (Midgard, Stoelting Co.). CT-B (*n* = 6 rats) was iontophoresed for 10 min using a 10-40 µm tip diameter, +5 or +7 µA of current, and a 7 sec duty cycle; BDA (*n* = 11 rats) was iontophoresed for 7 min using a 7-10 µm tip diameter, +1 µA of current, and a 7 sec duty cycle. The pipette then remained in the tissue for 2 min before withdrawal. Following the injection(s), the opening(s) in the skull was closed with dental cement and the

overlying skin was sutured. The animal received post-operative care that included administering an antibiotic (Penicillin G Potassium; 0.5 mL, i.m.) and a sedative (Buprenorphine Hydrochloride; 0.03 mg/kg, i.m.).

E. Tissue Processing

After a 5-7 day survival, animals were administered a lethal dose of Nembutal (100 mg/kg, i.m.) and transcardially perfused with 0.9% saline followed by chilled 4% paraformaldehyde in 0.3 M sodium phosphate-buffered saline (NaPBS, pH 7.4, 21˚ C). The brain was removed; cortices were blocked, and prepared for sectioning in the coronal plane. In some cases, hemispheres were flattened between two Plexiglas plates in preparation for sectioning in a plane tangential to the pial surface (Welker and Woolsey, 1974). Tissue was fixed in 4% paraformaldehyde at 4˚ C and refrigerated overnight. The following day, tissue was sectioned in the coronal or tangential plane at 100 µm thickness using a Vibratome.

1. CT-B Processing

Sections were rinsed (3 × 10 min) with 0.01 M potassium phosphate-buffered saline (KPBS, pH 7.4, 21˚ C) and incubated overnight in 1˚ antibody (goat anti-choleragenoid, List Biological Laboratories) at 4˚ C. The next day, tissue was reacted with 2˚ antibody (biotinylated donkey anti-goat, List Biological Laboratories) for 1 hr. and placed in Avidin-Biotin Complex Elite (ABC, Vector Laboratories) solution (1:200 in 0.01 M KPBS) for 1 hr.; sections were washed (3 × 10 min) in 0.01 M KPBS (pH 7.4, 21˚ C) before and after each reaction step. Sections were reacted with 0.05% 3, 3’ diamino benzidine (DAB) KPBS (intensified with 30% hydrogen peroxide + 1% nickel ammonium sulfate) until the desired level of staining was achieved to visualize CT-B

labeled neurons and neuronal processes, and then rinsed (2 × 5 min) in buffer. Sections were incubated in CO contained within a DAB-sucrose-PBS mixture and placed in a warm water (38˚ C) bath until barrels were visible (Wong-Riley and Welt, 1980). Sections were then rinsed (2 × 5 min) in buffer, mounted in distilled water on gelatin-coated glass slides, air dried overnight, and coverslipped.

2. BDA Processing

Sections were incubated in ABC Elite (1:200 in 0.01 M KPBS) for 4 hrs. and rinsed (3 × 10 min) in 0.01 M KPBS (pH 7.4, 21˚ C). Tissue was reacted with a 0.05% 3, 3' DAB-KPBS intensified with a nickel ammonium sulfate (1%) and hydrogen peroxide (30%) solution to achieve desired level of staining to visualize BDA impregnated neurons and neuronal processes. Sections were rinsed (2 × 5 min) in 0.01 M KPBS, counterstained with CO until barrels were visible, rinsed (2 × 5 min) in buffer, mounted, air dried overnight, and coverslipped.

F. Pathway Reconstruction

All tissue sections were scanned into a whole slide digital imaging scanning system (Aperio ScanScope XT) and examined using ImageScope (Aperio). Sections of interest containing injection, target, or corticocortical axonal labeling were imported into PhotoShop CS4 (Adobe).

In coronally sectioned tissue, an anatomical map of the interhemispheric pathway was built by reconstructing the injection and target sites in relation to the cortical layers which were made visible by CO staining; orthogonal measurements were made from the

pial surface to each visible lamina. The site where the interhemispheric pathway crossed the midline was determined by reconstructing labeled axons visible in the corpus callosum.

In tangentially sectioned tissue, the projection pathway was reconstructed in relation to the layer IV barrel subfields that were identified from CO stained sections, typically visible across 3 sections. The section with the most complete FBS was designated as the center (~700 μm) of the FBS. Layers II and III, which make up the supragranular zone, were formed from the tissue sections preceding the visible barrel fields and the succeeding sections constituted the infragranular zone of layers V and VI. An outline of the FBS was superimposed onto each reconstructed cortical layer using blood vessels as fiducials.

G. Data Analysis

Injection sites consisted of an inner dense core (IDC) and a surrounding outer core (SOC). In coronal sectioned tissue, IDCs were studied in relation to the cortical layer as measured from the pial surface and the cortical column as measured from the midline, whereas in flattened sections, IDCs were studied in relationship to the layer IV barrel field. The location of the IDC was determined by measuring the area using PhotoShop CS4 (Adobe) density threshold settings (CT-B: 20%; BDA: 40%); these threshold settings were established from the smallest injections made and allowed for a well-defined spherical shaped IDC to be visualized. Target sites were defined by the most prominent labeling (CT-B: cell bodies; BDA: terminal branches and fields) observed per cortical layer. In flattened sections, target site locations were also examined in relationship to the body part representation in the barrel field. In cases where multiple

injections were made that included an injection into the forepaw representation, an area equivalent to the FBS was centered on the cortical region contralateral to the injection site and used to assess the amount of labeling generated from each independent tracer injection. The location at which the interhemispheric pathway crossed the midline was examined in coronally sectioned tissue; the transverse point was defined as the location where the maximal amount of labeled corpus callosum fiber segments was observed in a region perpendicular to pial surface and within a 1 mm radius of the midline. Areal and linear distance measurements were made using PhotoShop CS4 (Adobe). Single-factor Analysis of Variance (ANOVA) and Student Newman-Keuls (SNK) post-comparison tests were used to assess statistical significance ($p < 0.05$) of target labeling distribution between cortical layers.

III. Results

From a total of 17 rats, 29 injections of retrograde ($n = 10$) or anterograde ($n = 19$) tracer were iontophoresed into a physiologically identified site(s) in the forepaw ($n = 14$), wrist ($n = 10$), forearm ($n = 2$), shoulder ($n = 2$), or jaw ($n = 1$) representations. Injections were made at depths ranging from 875 μm to 1,350 μm corresponding to layer V. In 5 rats, single injections were made into physiologically identified sites in SI; in 12 rats, single injections were made into two separate physiologically identified sites in the same animal. Injections were spherical in shape, consisted of an IDC and a SOC; IDCs were targeted to layer V of the desired representation. Projection labeling in the contralateral SI was distributed across all cortical laminar with the greatest density found in layer V. Injection and target site parameters are summarized in Table 1.

Table 1 – Summary of anatomical retrograde and anterograde tracer data. Injection sites localized in SI layer V at an average depth of 1,162.1 ± 214.13 μm project predominately to contralateral SI layer V at an average depth of 1,242.8 ± 249.65 μm. Projections from wrist, forearm, and shoulder representations terminate primarily to their respective homotopic contralateral cortex fields whereas forepaw projections terminate in a neighboring cortical area outside the barrel field in contralateral SI. Dash (-) indicates not applicable.

Experiment No.	Cutting Plane	Receptive Field Location	Injection Site Depth (μm)	Cortical Layer	Electrode Tip Diameter (μm)	Current (μA)	Duration (min)	Duty Cycle (sec)	IDC Area (mm^2)	Cutting Plane	Relationship to Layer IV Barrel Field	Target Site Depth (μm) and layer
CTB-1	Tangential	Shoulder Forepaw	1,100 1,100	V V	20 20	5 5	10 10	7 7	0.77 0.76	Tangential	Shoulder Outside FBS	980 (V) 980 (V)
CTB-2	Coronal	Shoulder Forepaw	1,063 1,330	V V	15-20 40	5 5	10 10	7 7	0.18 0.39	Tangential	Shoulder Outside FBS	560 (II/III) 1,400 (V)
CTB-3	Coronal	Forearm Forepaw	1,310 1,049	V V	20 20	5 5	10 10	7 7	0.37 0.45	Tangential	Forearm Outside FBS	980 (V) 1,120 (V)
CTB-4	Coronal	Forearm Forepaw	1,127 1,220	V V	20 20	5 5	10 10	7 7	0.45 0.39	Tangential	Forearm Outside FBS	1,260 (V) 1,260 (V)
CTB-5	Coronal	Wrist	1,100	V	10	7	10	7	0.26	Coronal	-	1,640 (V)
CTB-6	Coronal	Wrist	1,227	V	10	7	10	7	0.65	Coronal	-	1,120 (V)
BDA-1	Tangential	Hypothenar Pad Forepaw	1,283 1,283	V V	7 7	1 1	7 7.5	7 7	0.18 0.24	Coronal	-	1,260 (V) 1,334 (V)
BDA-2	Tangential	Wrist Forepaw (edge)	875 875	V V	10 10	1 1	7 7	7 7	0.15 0.15	Tangential	Wrist Outside FBS	1,400 (V) 1,400 (V)
BDA-3	Tangential	Wrist Forepaw	1,400 1,120	V V	10 10	1 1	7 7	7 7	0.16 0.11	Tangential	Wrist Outside FBS	1,750 (V) 1,050 (V)
BDA-4	Coronal	Wrist Forepaw	1,220 990	V V	10 10	1 1	7 7	7 7	0.14 0.17	Coronal	-	1,344 (V) 1,290 (V)
BDA-5	Tangential	Wrist Forepaw (edge)	1,300 1,100	V V	10 10	1 1	7 7	7 7	0.07 0.10	Tangential	Wrist FBS (edge)	1,600 (V) 1,600 (V)
BDA-6	Coronal	Wrist Forepaw	1,000 1,347	V V	10 10	1 1	7 7	7 7	0.07 0.21	Coronal	-	1,160 (V) 1,220 (V)
BDA-7	Coronal	Wrist Forepaw	1,042 1,307	V V	10 10	1 1	7 7	7 7	0.18 0.16	Coronal	-	1,064 (V) 1,095 (V)
BDA-8	Tangential	Wrist	1,983	V	10	1	7	7	0.19	Tangential	Wrist	1,400 (V)
BDA-9	Coronal	Wrist Forepaw	1,103 1,001	V V	10 10	1 1	7 7	7 7	0.39 0.32	Coronal	-	1,358 (V) 1,406 (V)
BDA-10	Tangential	Forepaw	963	V	10	1	7	7	0.11	Tangential	Outside FBS	1,000 (V)
BDA-11	Tangential	Jaw	1,000	V	10	1	7	7	0.06	Tangential	Jaw	1,011 (V)

A. Retrograde Projections – Distribution of Callosal Projecting Neurons

To examine the distribution of interhemispheric layer V projection neurons, we injected 6 rats with the retrograde tracer CT-B. In these rats, 10 injections were made into physiologically identified sites in layer V within the forepaw, wrist, forearm, or shoulder representation. Target labeling in the contralateral SI was distributed across all cortical lamina, although the densest labeling was located in layer V. Following an injection into the wrist, forearm, or shoulder representation, retrogradely labeled cells in contralateral SI were found concentrated in homotopic fields whereas an injection into the forepaw representation resulted in target labeling primarily outside the FBS.

An example of a CT-B injection into the shoulder and forepaw representations in the same rat and resulting labeling in contralateral SI is shown in Fig. 2. Both injection and target cortices were flattened and tangentially sectioned to reveal the barrel field map. Injections sites (Fig. 2A) in layer V are shown in relationship to the projected layer IV body map (dotted line) that was superimposed onto the layer V injection sites. Injection IDCs were localized to the shoulder and glabrous forepaw representation regions at a depth of approximately 1,100 μm; however, the SOCs spilled over to the neighboring agranular sites. Shoulder and forepaw IDCs (solid white outline) are shown in Fig. 2B and Fig. 2C, respectively. A composite of labeled callosal neurons (black dots) from contralateral SI is superimposed onto the layer IV barrel field and is illustrated in Fig. 2D. Note that target labeling is largely confined to the shoulder representation while the densest forepaw labeling (93%) lies in the agranular region outside the FBS. Examples of 100 μm thick-sections through layer V (depth = 1,260 μm) where the

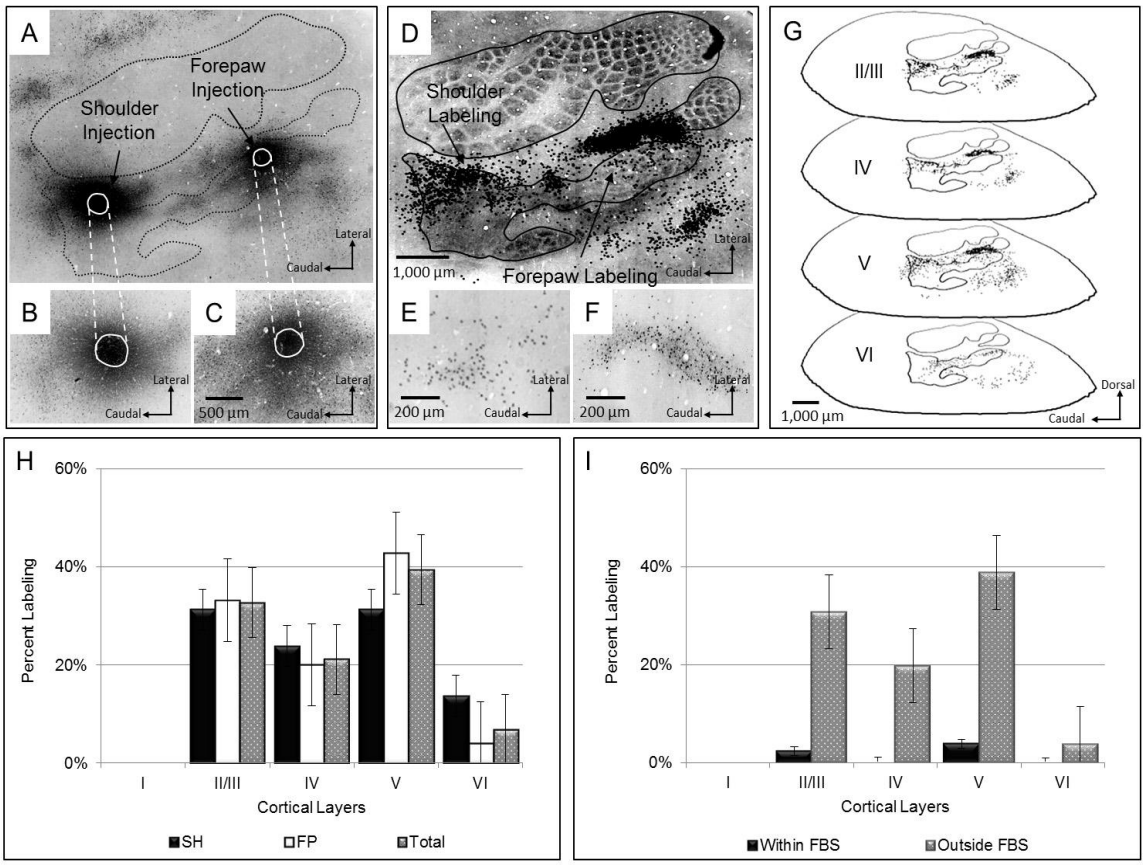

Figure 2 – Transcallosal projection pattern following independent CT-B injections into physiologically identified layer V shoulder and forepaw representations. **A-C:** Injection Site - Photomicrograph of layer V (A) showing locations (arrows) of injections into the shoulder and forepaw representations. An outline of the layer IV barrel field (dotted line) has been superimposed onto injections sites. Photomicrographs showing IDC (solid white outline) labeled regions of the respective injection sites, shoulder representation (B) and forepaw representation (C) at 5× magnification. **D-G:** Target Site – Photomicrograph of layer IV (D) showing location (arrows) of CT-B impregnated labeled cells (black dots) in relation to the barrel subfield in contralateral cortex; reconstruction of target labeling throughout all cortical lamina has been superimposed onto layer IV. Example of heaviest layer V target labeling at 1,260 µm in the shoulder (E) and forepaw (F) representations at 5 × magnification. Morphological reconstruction (G) of labeled neurons across distributed across cortical layers and shown in relation to the layer IV barrel field; the FBS outline obtained from 700 µm has been superimposed on each reconstructed layer. **H-I:** Projection Distribution – Laminar distribution of cell counts presented as percent labeling in shoulder, forepaw, and combined total; densest labeling found in layer V (43%) followed by layers II/III (33%). Forepaw labeling was further subdivided into cortical regions within the FBS and outside the FBS.

densest labeling was found are shown in Fig. 2E (shoulder representation) and Fig. 2F (forepaw representation). The distribution of labeled cells observed within presumed cortical lamina is illustrated in Fig. 2G; note for perspective, a line drawing of the barrel field in layer IV was superposed onto each reconstructed layer. Percent label in shoulder and forepaw representations as well as the total percent labeling for each lamina is presented in Fig. 2H; the greatest percent labeling is found in layer V (shoulder: 31%, forepaw: 42.7%, total: 39%). Presumptive labeling from the forepaw injection was further divided into labeled cells within and outside the FBS and this is shown Fig. 2I. While the forepaw and shoulder injection IDCs were similar in size (area ≈ 0.77 mm^2), there was a greater amount of target labeling following an injection into the forepaw representation then following an injection into the shoulder representation within layer V (forepaw: 42.7%, shoulder: 31%) and the combined total labeling (forepaw: 70.8%, shoulder: 29.2%). For purposes of this analysis, labeling in the presumptive motor cortex (MI) medial to the FBS was not described as the projection from each representation could not be readily discerned.

A second example of CT-B injections into layer V shoulder (depth = 1,063 μm) and forepaw (depth = 1,330 μm) representations and resulting labeling in contralateral SI is shown in Fig. 3. In this example, the injection cortex was coronally sectioned while the target cortex was flattened and sectioned in the tangential plane. Injection site locations (arrows) in layer V of the shoulder and glabrous forepaw representations are shown in the photomicrographs in Fig. 3A and Fig. 3B, respectively; insets depict the injection sites with respect to the distance from the midline (shoulder: 2.50 mm, forepaw: 2.23 mm).

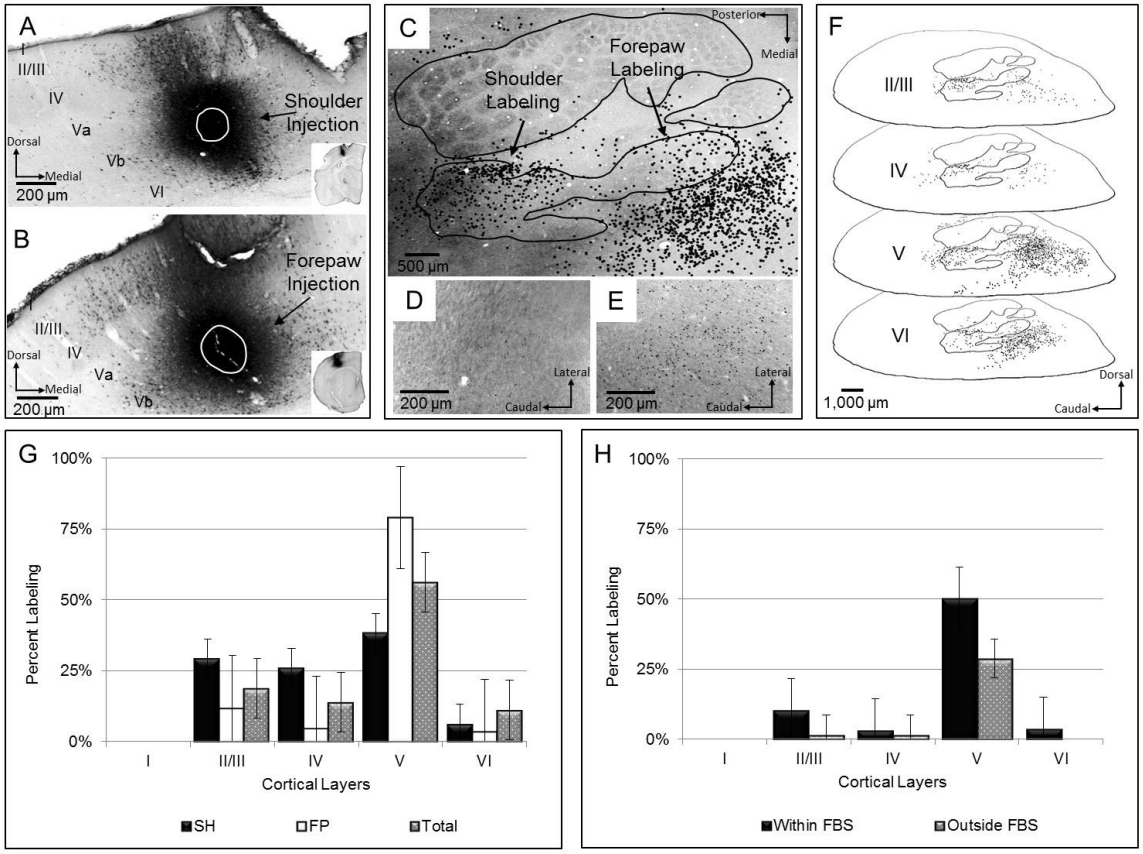

Figure 3 – Terminal field labeling following injection of CT-B into the physiologically identified layer V shoulder and forepaw representations. **A-B:** Injection Site – Photomicrographs showing location (arrows) of CT-B injection in shoulder (A) and forepaw representation (B); white outlines denote IDC (solid line) labeled regions and insets show location of injection sites with respect to midline. **C-E:** Target Site – Photomicrograph showing location (arrows) of CT-B labeled neurons in contralateral cortex. Reconstruction of target labeling (black dots) from layers I - VI µm has been superimposed onto layer IV barrel fields. Example of maximum labeling found in shoulder (D) and forepaw (E) representations within a single tissue section (100 µm thickness). **F:** Composite – Morphological analysis and reconstruction of target site labeled cell bodies as seen over the cortical layers; barrel field obtained from 700 µm has been superimposed on each reconstructed cortical layer. **G-H:** Projection Distribution – Cell counts of laminar distribution (G) depict that the most prominent target labeling was observed in layer V (79%). Further subdivision of presumptive forepaw representation labeling (H) also shows layer V contains the densest labeling.

Both IDCs, denoted by solid white lines, are centered in layer Vb. The composite labeled cell bodies (black dots) from the contralateral SI target cortex were superimposed onto the layer IV barrel field (Fig. 3C). Once again, the shoulder projection targets the homotopic shoulder cortex in contralateral SI while the forepaw representation injection predominately targets the cortical regions adjacent to the presumed FBS. Examples of the heaviest layer V target labeling from a single tissue section are shown in Fig. 3D (shoulder representation) and Fig. 3E (forepaw representation). A reconstruction of the labeled neurons throughout the presumptive cortical lamina is illustrated in Fig. 3F; the layer IV barrel field has been superimposed onto each cortical layer. The percent labeling, within each cortical lamina, for both shoulder and forepaw injections is presented in Fig. 3G. Following an injection into the shoulder representation, 38% of the labeled cell bodies were found in layer V and 29% in layer II/III. The densest labeling within the presumed FBS was also located in layer V (79%). Collectively, the densest labeling observed in contralateral SI was observed in layer V (56%) followed by layer II/III (19%). Presumptive labeling from the forepaw injection was further divided into labeled cells within and outside the FBS and this is shown Fig. 3H. In this example a greater amount of labeling occurs within the contralateral FBS because labeling in the presumptive MI was not described.

In 2 rats, injections were made into adjacent sites in the forearm and forepaw representations and an example for 1 rat is shown in Fig. 4. In this case, the injection site was sectioned in the coronal plane while the target site was flattened and tangentially sectioned, both at a 100 μm thickness. The injection sites in layer Vb (depth = 1,310 μm) in the forearm and layer Va (depth = 1,049 μm) in the forepaw representations are shown

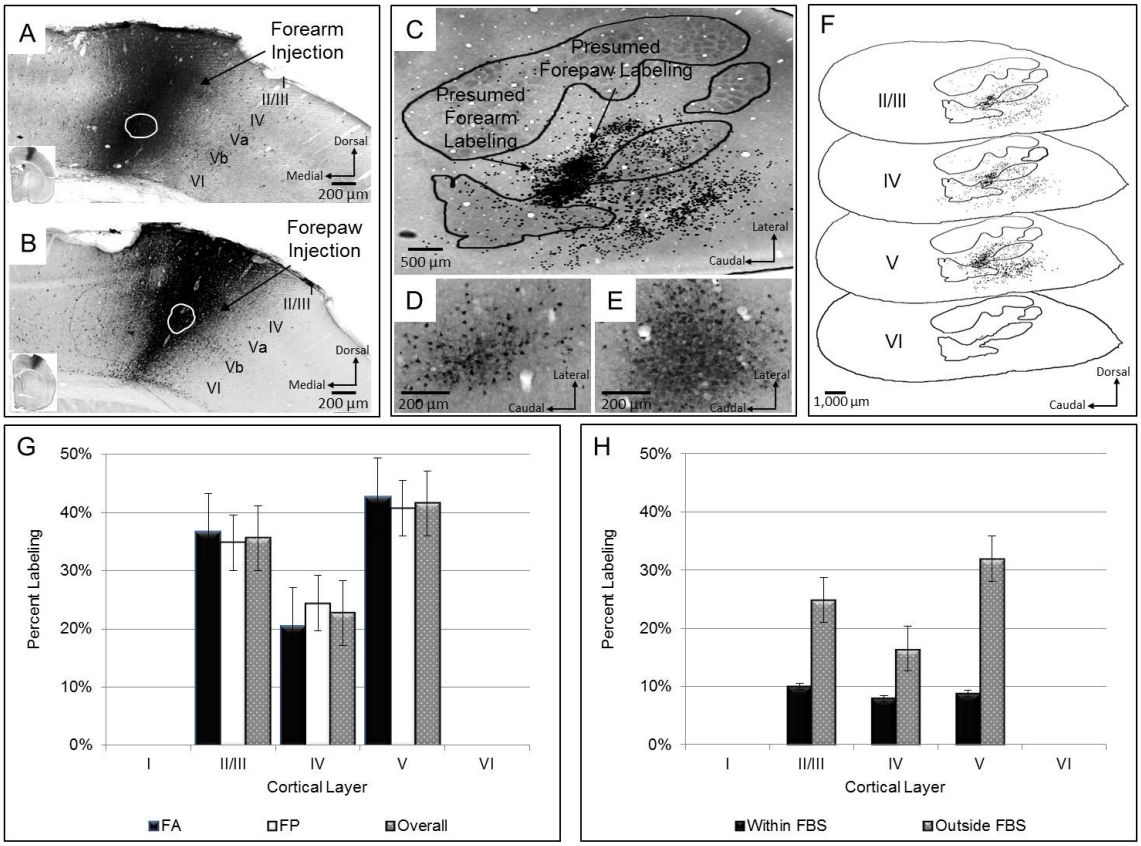

Figure 4 – Projection pattern following an injection of the retrograde tracer CT-B into the physiologically identified layer V forearm and forepaw representations. **A-B:** Injection Site – Photomicrographs showing location (arrows) of CT-B injection into layer V forearm (A) and forepaw (B) representations; white outlines denote IDC (solid line) labeled regions; insets show location of injection sites with respect to midline. **C-E:** Target Site - Photomicrograph showing location (arrows) of CT-B labeled neurons in contralateral cortex. Reconstruction of target labeling (black dots) from layers I – VI has been superimposed onto layer IV barrel fields. Example of maximum labeling found within a single 100 µm thick tissue section in shoulder (D) and forepaw (E) representations at depths of approximately 980 µm and 1,120 µm, respectively. **F:** Composite – Reconstruction of target labeling distributed across the cortical layers and in relation to the layer IV barrel field (superimposed onto each reconstructed cortical layer). **G-H:** Projection Distribution – CT-B labeled cell bodies were distributed across the cortical lamina (G); the most prominent target labeling was observed in layers II/III (36%) and V (42%). Labeling outside the FBS (H) was most prominent in layer V.

in Fig. 4A and Fig. 4B, respectively. The composite labeling (black dots) in contralateral SI is superimposed onto the layer IV barrel field illustrating presumptive forearm and forepaw labeling in relation to the body map and this is shown in Fig. 4C. Note that the labeling within the presumptive forearm barrel cortex is concentrated in the homotopic forearm representation compared to the presumptive labeling from the forepaw injection which is concentrated outside the projected FBS territory. Examples of labeling in layer V are shown in Figs. 4D and 4E for the forearm and forepaw representations, respectively. The differential distribution of laminar labeling is illustrated in Fig. 4F, an outline drawing of the layer IV barrel field has been superimposed onto each reconstructed layer. Cell counts for the laminar distribution of labeling are presented in Fig. 4G. The greatest percentage of labeling was found in layer V (forearm: 43%, forepaw: 41%, total: 42%) followed closely by layer II/III (forearm: 37%, forepaw: 35%, total: 36%). The majority of target labeling following the forepaw injection was localized outside the FBS and this is shown in Fig. 4H. Note that within layer V, 32% of the labeling was found bordering the projected FBS territory while 9% was located within the projected FBS territory.

The previous examples have shown the areal distribution of callosal projecting neurons with respect to the body part representation. Because the target cortices were flattened and sectioned tangentially, cortical layer demarcations were approximations. To precisely examine laminar labeling, both injection and target sites were cut along a coronal plane (Fig. 5). An example of an injection made into layer Vb wrist representation at a depth of 1,230 μm is shown in Fig. 5A along with its IDC (white outline); the inset depicts the location of the injection site 2.60 mm lateral to the midline.

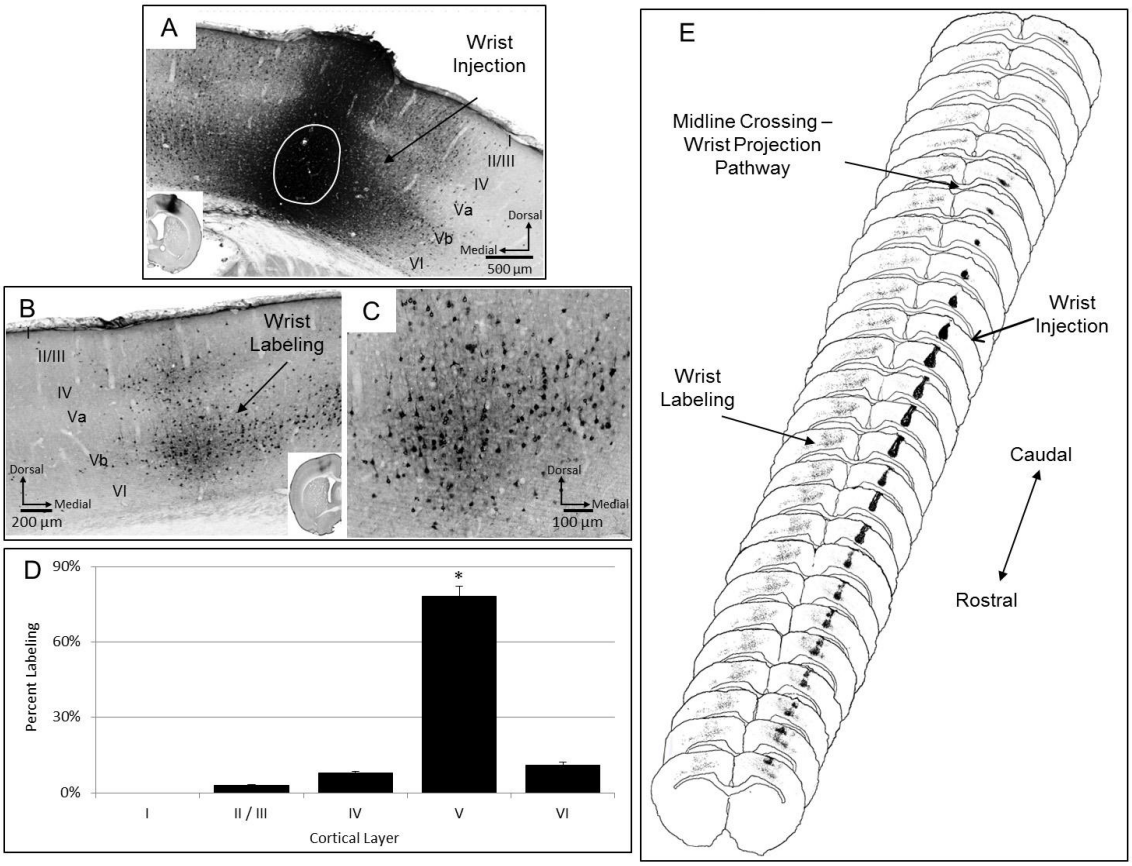

Figure 5 – A representative example of a coronally sectioned transcallosal projection pattern following injection of CT-B into the physiologically identified layer V wrist representation. **A:** Injection Site – Photomicrograph showing location (arrows) of CT-B injection in wrist representation at cortical layer Vb at a depth of approximately 1,120 µm; solid white lined circle identifies the position of the IDC. The inset shows location of injection site with respect to midline. **B-C:** Laminar Target Labeling – Photomicrograph of single 100 µm thick-section showing CT-B labeled cell bodies in contralateral cortex. Layer V target labeling at 5× (B) and 20× (C) magnification. **D:** Projection Distribution – Greatest number of labeled cells was observed in layer V (78%); asterisk (*) denotes statistical significance at $\alpha = 0.05$ level. **F:** Composite – Morphological reconstruction at selected cortical sections (100 µm thick) of wrist injection site (left hemisphere) and target labeling (right hemisphere). Densest target labeling in layer V was 400 µm anterior to the injection site. The interhemispheric pathway crossed the midline 500 µm posterior to the wrist injection site.

The resulting labeled cells in contralateral SI are distributed across layers II – VI as shown in Fig. 5B. In this rat, the densest labeling occurred in layer Vb; the location of the target site with respect to the midline is shown in the inset. An example of the densest layer V labeling is shown in Fig. 5C for a single 100 µm thick-section. The percent labeling throughout the lamina is presented in Fig. 5D. Since a clear separation between layers II and III could not be made, these layers are collapsed. In this rat, a significant percentage of the labeled cells (78%) was located in layer V as determined using a paired t-test. Reconstruction of injection and target cortices is illustrated in Fig. 5E; that the callosal midline crossing is most dense approximately 500 µm caudal to the injection site while the heaviest labeling in contralateral SI – target site – is approximately 300 µm anterior to the injection site.

B. Anterograde Projections – Distribution of Callosal Axons and Terminals

To examine the distribution of callosal axons and terminals originating from layer V callosal projecting neurons in contralateral SI, 11 rats were injected with the anterograde tracer BDA. In these rats, a total of 19 injections was made into physiologically identified sites in forepaw, wrist, and forearm representations. Layer V callosal projecting neurons send axons to contralateral SI that have terminal connections distributed across all cortical lamina with the densest labeling occurring in layer V. Injections made into the wrist and forearm representations terminated in homotopic fields in contralateral SI while injections made into the forepaw representation terminate primarily outside the FBS.

An example of a BDA injection in the wrist and forepaw representations and resulting labeling in contralateral SI is shown in Fig. 6. In this rat, both injection and

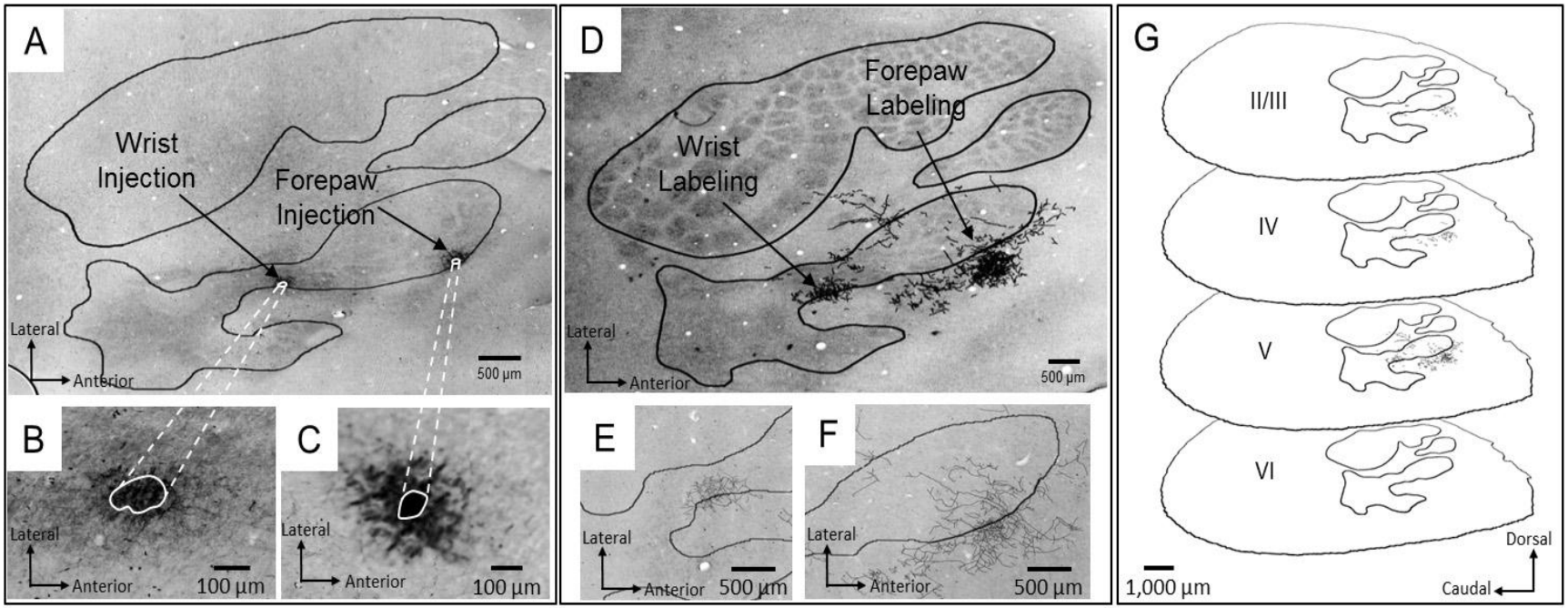

Figure 6 – Transcallosal projection pattern of labeled fibers following BDA injection into the physiologically identified wrist and forepaw representations in layer V. **A-C:** Injection Site – Photomicrograph showing locations (arrows) of BDA injections in layer V wrist and forepaw representations, an outline of visible barrel fields (black dotted lines) from layer IV has been superimposed onto injections sites in layer V; sites of IDC (solid while line) labeled regions of the wrist (B) and forepaw (C) representations. **D-F:** Target Site – Photomicrograph showing location (arrows) of BDA labeled axons and terminal branches in contralateral cortex; reconstruction from layers I – VI has been superimposed on the layer IV barrel fields. Examples of layer V labeled terminal branching (black lines) found in a single 100 µm thick-section in wrist (E) and forepaw (F). **G:** Composite – Morphological analysis and reconstruction of target labeled axons and terminal branches as seen across the cortical layers; barrel field obtained from 700 µm has been superimposed on each reconstructed cortical layer.

target site cortices were flattened and sectioned in the tangential plane to examine homotopic connectivity. Each injection (Fig. 6A) was made in SI at a depth of approximately 1,000 µm; one was targeted to the dorsal wrist representation and the second was targeted to a region of the forepaw cortex responsive to input from digit three (D3) and digit four (D4). An outline of the layer IV barrel field (black line) has been superimposed onto the injection sites; both injections were localized to their respective receptive fields and the IDCs (dotted white outline) are shown in Fig. 6B (wrist representation) and Fig. 6C (forepaw representation). The photomicrograph in Fig. 6D shows a composite (black lines) of target labeling (labeled axons and terminal branches) from all cortical lamina superimposed on to the layer IV barrel field. Following a BDA injection into the wrist representation, labeled axons were localized in contralateral SI wrist representation. However, following an injection into the forepaw representation, labeled axons were found in contralateral SI that were aligned to the projected region outside the FBS. An example of labeling from a single 100 µm thick-section in layer V is shown in Fig. 6E (wrist representation) and Fig. 6F (forepaw representation). A reconstruction of the callosal projection pattern as seen over the cortical layers is illustrated in Fig. 6G. A line drawing of the barrel fields has been superimposed onto each reconstructed layer. Note that terminal labeling was observed in layers II – V, with the greatest amount occurring in layer V.

An example of a BDA injection in the forepaw representation in layer V and resulting labeling is illustrated in Fig. 7. In this rat, a single injection was made in SI, and both injection and target sites were flattened. BDA was injected at a depth of 1,000 µm in a site where the neurons responded to input from digit two (D2). This injection was

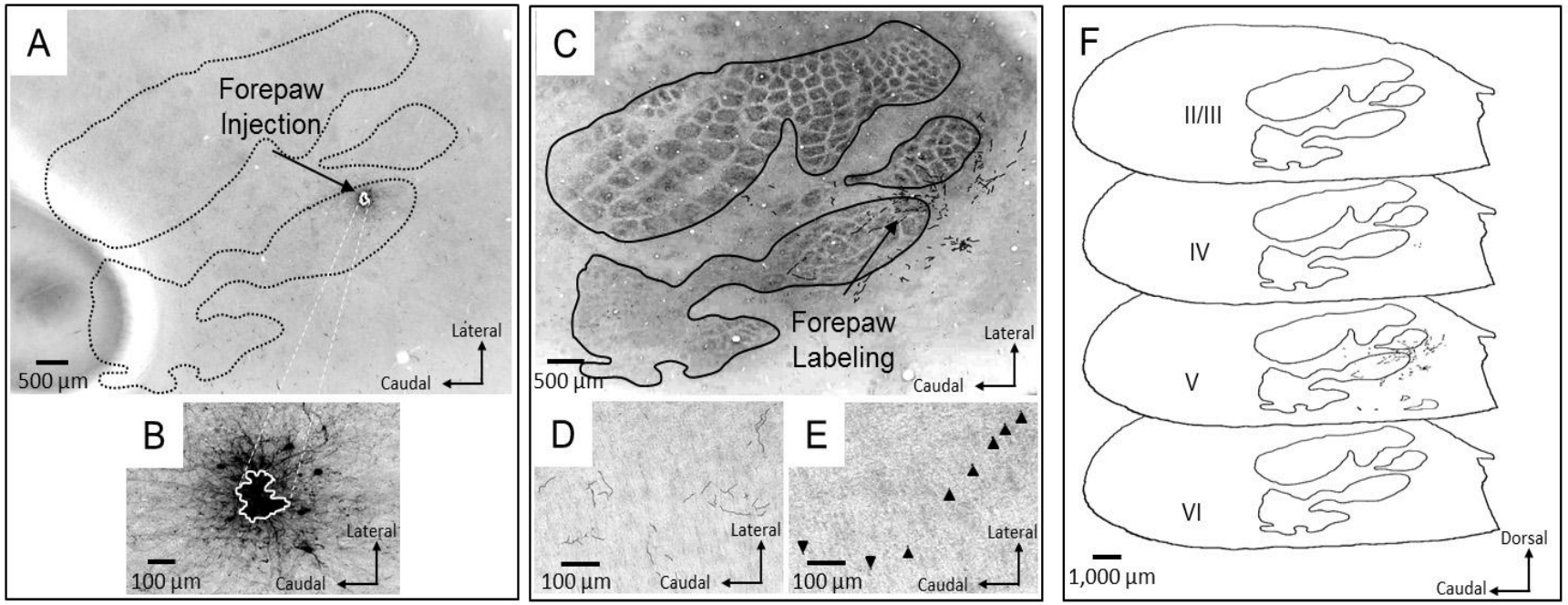

Figure 7 – Projection pattern example of labeled fibers following BDA injection into the physiologically identified forepaw representation in layer V. **A-B:** Injection site – Photomicrograph showing location (arrow) of BDA injection in FP representation at a depth of 1,200 µm. Outline of layer IV barrel fields superimposed onto injection site. IDC labeling (white outline) of injection site (B). **C-E:** Target site – Photomicrograph showing location (arrow) of BDA labeled axons in contralateral SI. Reconstruction of composite target labeling (for depths ranging from approximately 156 µm to 1,556 µm) superimposed on layer IV barrel cortex (C). Forepaw representation target projection in contralateral SI at 1,000 µm of fiber labeling (D) and axonal varicosities (arrows) (E). **F:** Composite - Morphological analysis and reconstruction of target labeling. The barrel field obtained from 700 µm is superimposed on each reconstructed cortical layer.

small and confined within the FBS (Fig. 7A); the white outline in Fig. 7B denotes the IDC. The photomicrograph in Fig. 7C shows a composite of laminar labeling projected to layer IV; the fibers are seen to course through the FBS but the majority of labeling was localized in the agranular regions adjacent to the FBS. Examples of labeled fibers and axonal varicosities in layer V (depth = 1,000 μm) are shown in Figs. 7D and 7E, respectively. A laminar reconstruction of labeled axons is illustrated in Fig. 7F along with a superimposed line drawing of the barrel field. The heaviest labeling was found in layer V.

To examine the lamina distribution of callosal projection axons, BDA was injected into the wrist and glabrous forepaw digit representations and the tissue was sectioned in a coronal plane (Fig. 8). The injection sites for the wrist and forepaw representations, are shown in the photomicrographs in Fig. 8A and Fig. 8B, respectively; the insets show injection site locations in relation to the midline measuring 3.23 mm (wrist representation) and 3.49 mm (forepaw representation). Both injection sites were centered in layer Vb and are spherical in shape. Photomicrographs in Fig. 8C and Fig. 8D show labeled axons in contralateral wrist and forepaw regions, respectively; axonal varicosities (black dots) are shown in Fig. 8E and Fig. 8F. While the IDCs were approximately the same size (average of 0.35 mm^2), target labeling in the contralateral homotopic sites was greater in the presumed wrist representation compared to the forepaw representation. In both target sites, labeled axons were found throughout cortical layers II-VI and labeled terminal branching and varicosities were observed in layers II-VI. A reconstruction of the projection pathway between the injection and target sites is illustrated in Fig. 8G. The section(s) containing the heaviest labeling at the midline was defined as the primary

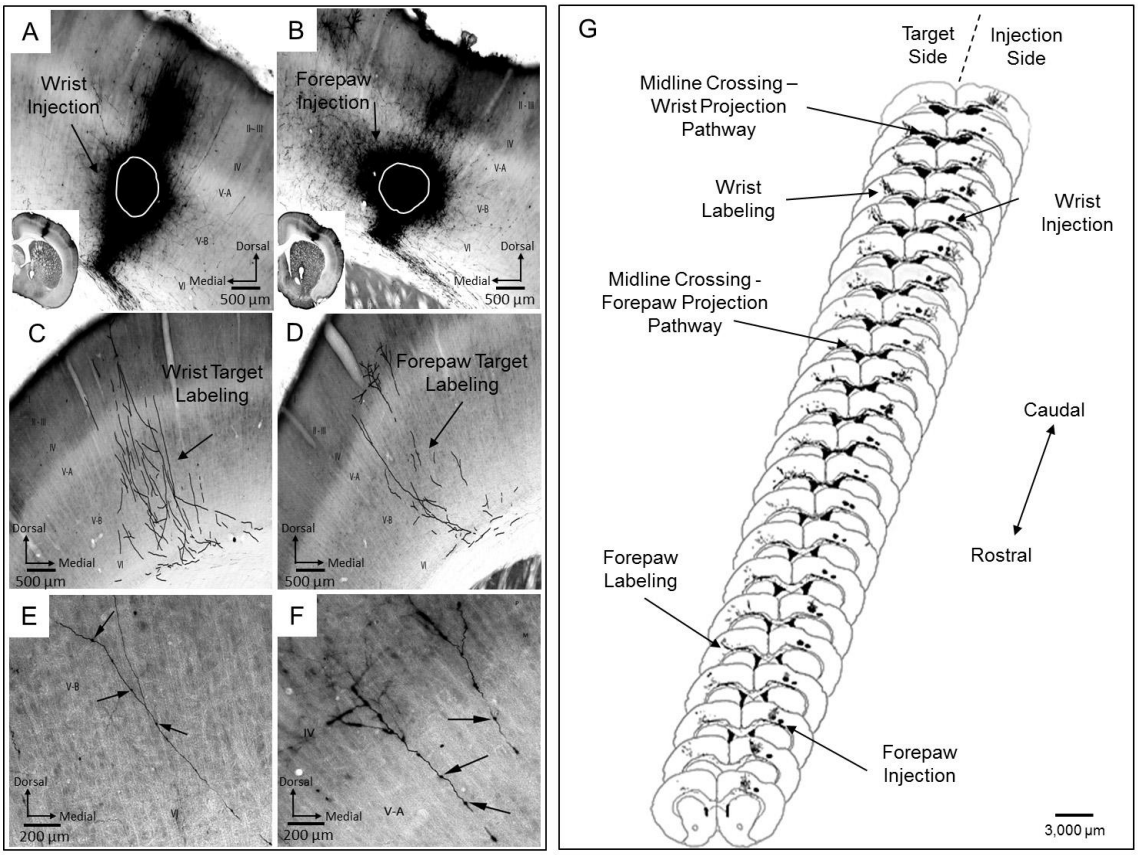

Figure 8 – Coronally sectioned transcallosal projection pattern of labeled fibers following BDA injection into the physiologically identified wrist and forepaw representations in layer V. **A-C:** Injection Site – Photomicrograph showing locations (arrows) of BDA injections in layer V wrist and forepaw representations, an outline of visible barrel fields (black dotted lines) from layer IV has been superimposed onto injections sites in layer V; sites of IDC (solid while line) labeled regions of the wrist (B) and forepaw (C) representations. **D-F:** Target Site – Photomicrograph showing location (arrows) of BDA labeled axons and terminal branches in contralateral cortex; reconstruction from layers I – VI has been superimposed on the layer IV barrel fields. Examples of layer V labeled terminal branching (black lines) found in a single 100 µm thick-section in wrist (E) and forepaw (F). **G:** Composite – Morphological analysis and reconstruction of target labeled axons and terminal branches as seen across the cortical layers; barrel field obtained from 700 µm has been superimposed on each reconstructed cortical layer.

cross-over site. Commissural fibers labeled from the forepaw injection traveled nearly 1,100 μm before crossing over to the contralateral SI as compared to the commissural fibers labeled from the wrist representation which traveled only 300 μm before traversing the midline.

C. Regional Distribution of Interhemispheric Projections

Injection of tracers into layer V in physiological identified sites in the forepaw, wrist, arm, or shoulder resulted in a differential pattern of labeling in the contralateral SI. An interpreted summary fitted to layer IV barrel field is illustrated in Fig. 9. This summary was generated from 5 sets (injection and target sites) of tangentially sectioned and flattened tissue processed for CT-B or BDA. Injection sites and their respective densest target sites were transposed from each individual set to representative locations; collectively this data is representative of the areal distribution patterns observed. Injections made into shoulder, wrist, and forearm regions project to their respective homotopic sites in contralateral SI; interestingly, these regions are devoid of barrel-like structures. In contrast, the highly organized FBS projected primarily to neighboring cortical regions outside the presumed contralateral FBS.

D. Laminar Distribution of Interhemispheric Projections

Following an injection of CT-B into layer V of SI cortex, labeled cell bodies were observed in layer II-VI in the contralateral SI. The percentage of cells labeled in each experiment with respect to laminar locations is presented in Fig. 10. In some cases it was difficult to distinguish the layer II/III boundary so these layers were combined. The percentage of labeling throughout the different laminar obtained from 10 injections (forepaw: 4, forearm: 2, wrist: 2, and shoulder: 2) is shown in Fig. 10A. Cells of origin

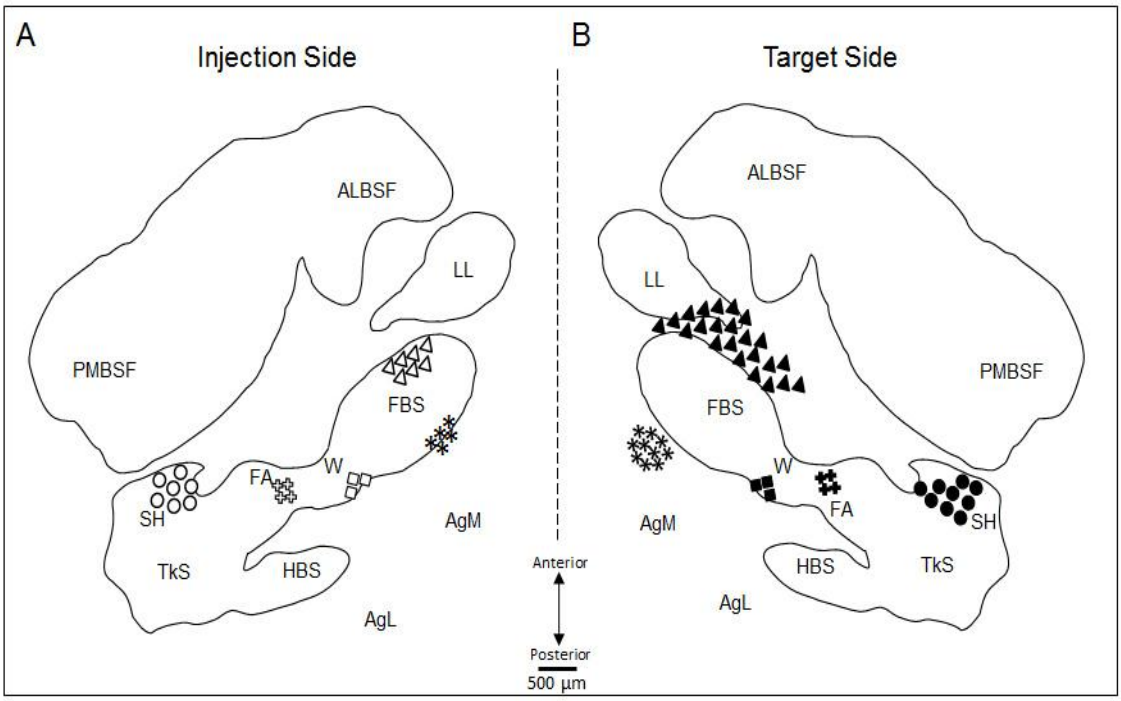

Figure 9 – Caricature presenting our visual interpretation of the interhemispheric regional distribution projection patterns from layer V forelimb and shoulder representations. A line drawing of the barrel field cortex at 700 µm was used to identify location of the shoulder (SH), forearm (FA), wrist (W), forepaw barrel subfield (FBS), hindpaw barrel subfield (HBS), posteromedial barrel subfield (PMBSF), and anterolateral barrel subfield (ALBSF), and the motor cortex medial agranular field (AgM) and lateral agranular field (AgL). **A:** Injection Side – A representative sample (n = 5) of independent injection sites of CT-B and BDA into the forepaw (n = 2), wrist (n = 1), forearm (n = 1), and shoulder (n = 1) representations in layer V is shown in relation to the body map of layer IV. Injection locations are denoted by black outlined triangles, crosses, diamonds, stars, and circles, respectively. **B:** Target Side – Composite projection pattern of callosal terminal labeling consisting of CTB-B impregnated cell bodies and BDA labeled fibers whose origins are the respective sites in (A). The cortical regions with the densest target labeling are represented. Target sites are denoted by filled triangles, crosses, diamonds, stars, and circles, respectively. Note that the area and location of injection and target site labeling are representative illustrations based on visual inspection of 5 injections and their respective target labeling.

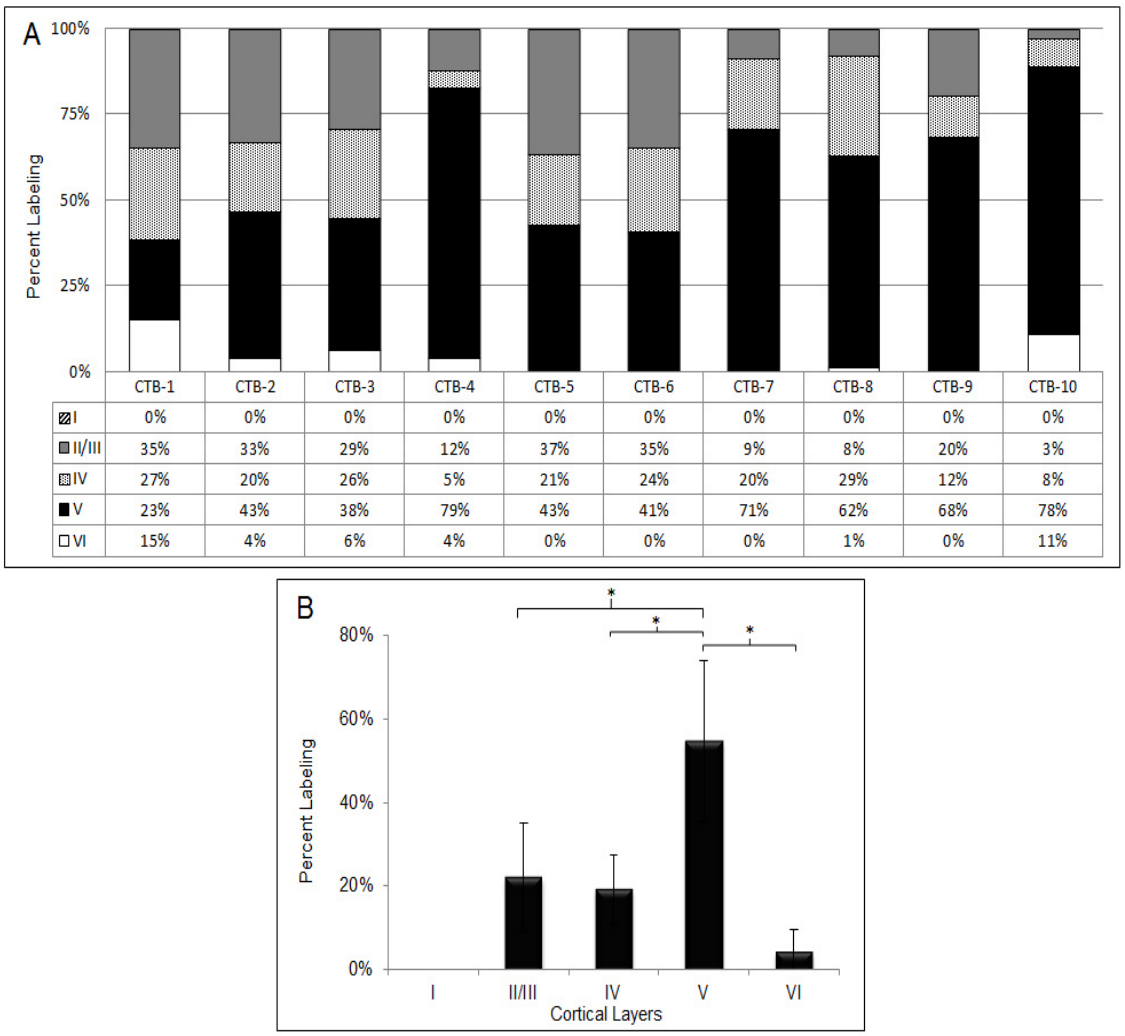

	CTB-1	CTB-2	CTB-3	CTB-4	CTB-5	CTB-6	CTB-7	CTB-8	CTB-9	CTB-10
I	0%	0%	0%	0%	0%	0%	0%	0%	0%	0%
II/III	35%	33%	29%	12%	37%	35%	9%	8%	20%	3%
IV	27%	20%	26%	5%	21%	24%	20%	29%	12%	8%
V	23%	43%	38%	79%	43%	41%	71%	62%	68%	78%
VI	15%	4%	6%	4%	0%	0%	0%	1%	0%	11%

Figure 10 – Distribution summary of projection labeling across cortical lamina following injection of CT-B into contralateral forelimb and shoulder representations. **A:** Composite – Percent of counted labeled cell bodies as seen distributed across the cortical layers following 10 CTB injections (4 forepaw, 2 forearm, 2 wrist, and 2 shoulder in layer V of the contralateral cortex. Target labeling was observed in cortical layers II/III – VI. **B:** Projection Distribution – Distribution of labeled CT-B cells. Average labeling observed (II/III: 22.0 ± 13.2%, IV: 19.2 ± 8.3%, V: 54.6 ± 19.3%, VI: 4.2 ± 5.3%). Most prominent target labeling occurred in layer V followed by layer II/II. The difference between layer V and layers II/III, IV, and VI was shown to be statistically significant ($p < 0.001$) using paired t-Tests for two sample means.

were found in layers II – VI. The average labeling distribution across lamina (I: 0.0%, I/III: 22.7 ± 12.2%, IV: 16.4 ± 6.7%, V: 58.2 ± 12.8%, VI: 2.6 ± 3.8%) is shown in Fig. 10B. The largest percent of labeled cells were found in layer V. Analysis of Variance (ANOVA) revealed this distribution difference to be statistically significant ($F_{crit} = 2.759$; $p < 0.005$). A Student-Newman-Keuls (SNK) post-hoc test showed a statistically significant *($p < 0.01$)* difference between layer V and layers II/III ($q_{test} = 9.21$), IV ($q_{test} = 10.85$), and VI ($q_{test} = 14.42$). The difference between layer II/III and VI ($q_{test} = 5.21$) as well as layer IV and VI ($q_{test} = 3.56$) was also found to be statistically significant ($p < 0.05$). Note that CTB-1 had a greater percent labeling in layer IV than in layer V; this may be due, in large part, to the target cortex having been flattened and cut tangentially, thus the lamina demarcations were approximates.

IV. Discussion

In the present study, anterograde or retrograde tracers were injected into physiologically identified sites in layer V of the forelimb-shoulder barrel cortex to test the hypothesis that layer V neurons in the forepaw, wrist, forearm, and shoulder representations project to homotopic sites in the contralateral SI cortex. Our results support previous findings of a transcallosal connection between SI cortices and provide evidence for differential homotopic connectivity between forelimb and shoulderrepresentations. The major findings are: (a) tracers injected into the wrist, forearm, and shoulder representations in layer V of SI, densely labeled their respective homotopic sites in contralateral SI cortex, (b) tracers injected into the forepaw representation in layer V sparsely labeled their contralateral homotopic site, but instead labeled regions adjacent to the forepaw representation, (c) retrograde tracers injected into

layer V predominately labeled cell bodies in lamina III and V in contralateral SI, although sparse labeling was also found in the other lamina; similarly, anterograde tracers injected into layer V showed a similar distribution of axon labeling in contralateral SI, (d) layer IV barrels and barrel-like regions received sparse projections from contralateral layer V, although the labeling that was observed following injections into the wrist, forearm, and shoulder representations was localized to the respective homotopic site, while the labeling found in layer IV following an injection into the forepaw representation was predominately localized non-barrel regions adjacent to the FBS, and (e) labeled interhemispheric projections from all representations examined in this study transversed the midline posteriorly and terminated predominately anteriorly to their respective injection sites, albeit the forepaw projection crossed the midline at a greater distance from the injection site in comparison to the wrist, forearm, and shoulder projection pathways. These results lay the groundwork for a subsequent study on interhemispheric enhancement and functional reorganization.

A. Technical Considerations

1. Homotopy

The notion of homotopic connectivity within ipsilateral cortex implies that two cortical regions receive input from similar parts of the body surface. Conversely, homotopic connectivity between sites in ipsilateral and contralateral cortices implies that the separate cortical regions receive input from similar parts of the body surface but on opposite sides of the body. In the present study, injections were made at a physiological identified site in one hemisphere and homotopic connectivity was defined by how closely the labeling in the contralateral hemisphere was matched to the body representation at the

injection site. To accomplish this, we relied on the presence of a forelimb body map in SI cortex in rodents, where the forelimb was represented by barrels and barrel-like structures in layer IV that were revealed in cortical tissue that had been flattened and cut on a tangential plane (Waters et al., 1995b; Pearson et al., 1999). The barrel field was then aligned with other cortical laminae/sections, using blood vessels as fiducials, to plot a projected body surface map that could be used to assess homotopic relationships between ipsilateral and contralateral SI cortices.

While the flattening procedure provided a methodology for assessing homotopy, it was a less precise method in determining cortical depth for sections outside the layer IV barrels. We have previously reported that the center of the forelimb barrel field lies approximately 700 μm below the cortical surface (Waters et al., 1995b). In the present study, all cortical/tangential sections were cut at a 100 μm thickness, and from a total of 19 hemispheres that were flattened and cut on a tangential plane, an average of 6 tissues sections (range 5–8) was required to reach the center of the FBS. Therefore, the two sections immediately superficial or deep to the center of the barrel field were judged sufficient to move into the adjacent cortical lamina. Of course, adjacent laminar determination was not an issue in sections that were cut on the coronal plane.

2. Tracer Injection Site Determination

All injections were guided by prior physiological identification of layer V forelimb and shoulder representations. First, sites of interest were initially identified by recording receptive fields in layer IV since the forelimb and shoulder representations were clearly demarcated at this layer. The electrode was then systematically advanced in 100 microns steps to a depth of 1,400 microns and the receptive field(s) of neurons reexamined at each

step. Injection depth was chosen as that location having a strong receptive field that matched the receptive field recorded in layer IV that lay between 900 and 1,400 microns. All injections were targeted to a specific forelimb or shoulder site in layer V and although the injection IDCs were localized to the respective representation and centered in layer V, the boundaries of the injection were not always confined to the specific site as observed in flattened or coronally cut sections. Larger injections provided maximal visualization of cortical connectivity in the opposite barrel cortex while smaller focal injections led to labeling of more localized sites in the contralateral SI.

3. Multiple Injections

In 12 rats, injections were made at two separate physiological identified sites one of which was in the forepaw representation. The resulting contralateral labeling could always be partitioned into separate locations, but often times, sparser labeling appeared between these zones that could not be associated with one injection site or the other. In these cases, the labeling was not counted. Furthermore, sparse labeling also was found in the presumptive MI that could not be associated with one injection site or the other and was therefore excluded from assessment; this exclusion had no effect on our analysis as our focus was on target labeling in cortical regions homotopic to the injection site.

B. SI Columnar Organization

SI neurons are arranged in small vertical groupings that extend through all cortical layers forming a ‘cortical column’; these groupings of neurons belong to a common modality and have a common peripheral receptive field location on the skin surface (Mountcastle, 1957). Mountcastle hypothesized that cortical columns were divided into radial cell cords termed ‘mini-columns’ and were the fundamental processing units of the

cerebral cortex (Mountcastle, 1978). Experimental evidence supporting a sub-columnar structure was provided from receptive field mapping studies carried out in SI of cat (Favorov et al., 1987; Favorov and Diamond, 1990) and monkey (Favorov and Whitsel, 1988). By recording unit responses in the forelimb region of area 1, Favorov and Whitsel (1988) found that the receptive fields recorded from neurons within a mini-column were very similar in size, configuration, and location on the skin surface. However, considerable variability in these same receptive field attributes was recorded from neurons located in adjacent mini-columns. While neurons within a cortical column, may exhibit variability in size and configuration of receptive fields, they all shared a small common receptive field center on the surface of the skin. The functional columnar arrangement of SI neurons allows for precise receptive field mapping as systematic shifts in receptive field position on the skin surface occurs between neighboring cortical columns and not within. In rodent SI, cortical columns are easily identifiable as they are associated with the well-defined barrels of layer IV (Feldmeyer, 2012). Of the 19,000 neurons within a barrel related column, approximately 88% are excitatory which are distributed throughout the cortical lamina as follows: 5,000 (layer II/III), 4,000 (layer IV), 3,300 (layer V), and 4,500 (layer VI); the other 12% are non-excitatory interneurons (Meyer et al., 2010, 2011).

C. Layer V Injection Sites

Prior to making a tracer injection into layer V, the receptive field was first mapped in layer IV. When a desired receptive field in the forelimb or shoulder representation was identified in the barrel field, the recording electrode was systematically advanced into layer V. Injections were then made into a location in layer V where tactile stimulation

evoked the strong response between 900-1,400 microns. Recording similar receptive fields in layers IV and V ensured the injection position was within a cortical column as described by Favorov and Whitsel (1988).

D. Regional Distribution of Layer V Forelimb and Shoulder Interhemispheric Projections

Our findings both support and contrast previous reports of interhemispheric connections between SI forelimb cortices. The presence of sparse interhemispheric projections to homotopic forelimb sites is consistent with earlier findings that cortical regions associated with appendicular (lateralized) representations such as the forepaw and wrist project to non-homotopic sites, while projections from more axial sites terminate homotopically (Yorke and Caviness, 1975; Wise and Jones, 1976); this is commonly referred to as the midline rule (Innocenti, 1986). Given that the shoulder is technically located at an interface between axial and lateralized body locations, and plays a role in skeletal movement, our results from injections in shoulder, arm, or wrist representations do not support a midline rule. However, homotopic connections do not appear to exist between forepaw representations. These discrepancies may be due, in part, to differences in neuronal tracing methods, injection sizes or sites of injections. More recently, focal injections were made in layers III and IV in sites responsive to input from both wrist and proximal forepaw, and in these cases, sparse labeling was reported within homotopic regions in contralateral SI, although dense patches of labeling were found bordering the homotopic region (Hayama and Ogawa, 1997; Henry and Catania, 2006). Although our injections were targeted to layer V, our findings are consistent with their forepaw results but differ in that we observed homotopic labeling following injections into the wrist

representation. To the best of our knowledge, focal injections have not been made in the shoulder representation to study interhemispheric connectivity in rat barrel cortex.

E. Lamina Distribution of Layer V Interhemispheric Projections

Our results are consistent with previous descriptions of callosal afferents arising from and terminating in all cortical layers, primarily in layers III and V with minimal connectivity in layer IV (Yorke and Caviness, 1975; Wise and Jones, 1976; Ivy and Killackey, 1981). The scarcity of callosal connectivity within layer IV was initially described as being restricted to the agranular region and absent in the granular regions of the barrel subfields (Yorke and Caviness, 1975; Wise and Jones, 1976; Ivy and Killackey, 1981). It was subsequently reported that layer IV labeling has a honeycomb-like distribution pattern generated by the label being located in the septa regions surrounding and separating the individual barrels, while the barrels themselves remained relatively free of label (Olavarria et al., 1984; Hayama and Ogawa, 1997). In the present study we observed label cell bodies scattered in the nebulous non-barrel like structure representing the shoulder and in the well-defined barrel structure of the FBS in layer IV; in addition, labeled axon segments and terminals were also found running along the anteroposterior axis of the FBS. Although the wrist, arm, shoulder, and trunk representation do not have precise barrel-like structures, they are still described as being part of granular cortex; granular cortex is defined from Nissl staining of small granular type neurons, this distinction, however, cannot be made with CO staining. While there are no barrels in the wrist, arm, shoulder, and truck representations, the outline of these can still be seen in CO stained sections that correspond to granular cortex.

Previous interhemispheric connectivity studies in rodent SI either made a single large injection or multiple injections that led to the labeling of a large number of callosal projections (Yorke and Caviness, 1975; Wise and Jones, 1976; Ivy and Killackey, 1981; Koralek et al., 1990). The cells of origin and points of termination in the opposite SI were described to provide a 'macroscopic' organization of the SI callosal system. Unfortunately, these investigators did not specifically describe the depths at which the injections were made (Yorke and Caviness, 1975; Wise and Jones, 1976; Ivy and Killackey, 1981; Koralek et al., 1990). In one study carried out in the SI of tree shrews investigators made multiple injections of HRP in the forelimb representation at depths that included layer V and reported variability in label density that supported the midline rule for callosal projections(Weller et al., 1987). When more localized injections were made into the forelimb representation in SI of rodent, injections were made into layers III and IV (Hayama and Ogawa, 1997; Henry and Catania, 2006). To the best of our knowledge, focal injections have not been made in rodent SI layer V to study interhemispheric connectivity between barrel cortices.

F. Comparison of Present Study with Previous Interhemispheric Connectivity Studies in Rodent

Over the past four decades anatomical track tracing (Yorke and Caviness, 1975; Wise and Jones, 1976; Ivy and Killackey, 1981; Olavarria et al., 1984; Koralek et al., 1990; Hayama and Ogawa, 1997; Henry and Catania, 2006) and/or axonal degeneration (Wise and Jones, 1976; Akers and Killackey, 1978) techniques have been employed to characterize the interhemispheric connectivity between SI cortices in rodent. Wise and Jones (1976) conducted an exhaustive study in which they injected large amounts of

tracer in SI and examined axonal degeneration following a commisurotomy or hemidecortication to reveal the total pattern of callosal connectivity between the ipsilateral and contralateral SI. Their findings describe callosal projections originating from cells distributed throughout all cortical laminae but predominately in layers III and V, callosal axons transversing all cortical layers of contralateral SI in a series of vertical bands with terminals densely located in layer III and V, and callosal connectivity originating and terminating primarily in cortical areas that lie alongside and in between the layer IV barrel subfields. Likewise, a majority of the previous studies conducted in rodent either made large tracer injections into SI (Yorke and Caviness, 1975; Ivy and Killackey, 1981; Olavarria et al., 1984; Koralek et al., 1990) or inactivated large regions of SI (Akers and Killackey, 1978) and reported a similar differential lamina and areal distribution pattern of interhemispheric connectivity. A few neuronal tracer studies were conducted whereby focal injections were made into layers III and IV of the forelimb representation (Hayama and Ogawa, 1997; Henry and Catania, 2006). Following an injection of wheat germ agglutinin-conjugated horseradish peroxidase (WGA-HRP) at a depth of approximately 500-700 μm (layers III and IV) callosal connections were found to be sparse or completely lacking in the site homotopic to the injection site (Hayama and Ogawa, 1997). Labeling instead was confined to the cortical regions bordering the homotopic forelimb representation (Henry and Catania, 2006). However, the authors (Henry and Catania, 2006) did not specifically describe the lamina distribution of the callosally derived labeling.

Our interhemispheric connectivity distribution pattern share many similarities to those previously described and where differences were observed, we had the advantage

of examining labeled projections after making focal injections. The present study supports the description of callosal projections arising and terminating in all cortical layers, predominately in layers III and V. Previous studies have consistently reported projection label in the forelimb representation being located in the cortical regions adjacent to the forelimb representation while minimal label occurs with the homotopic site. However, a majority of these studies do not characterize the specific forelimb representation sub-regions examined such as the forepaw, wrist, and forearm. Our findings revealed a similar pattern of distribution in the forepaw representation; projection label in the wrist and forearm are in contrast as we found dense labeling within the respective homotopic sites. We also present new data showing layer V shoulder representation projects to homotopic shoulder in contralateral barrel cortex.

Modulation of cortical circuitry requires a thorough grounding of the underlying anatomical connectivity. The regional and laminar distribution patterns characterized in our study supplied the data necessary to determine an optimal interhemispheric circuit in which to study enhancement and functional reorganization. Based on the consistency of dense localized populations of transcallosal connections, the interhemispheric pathway connecting homotopic layer V wrist representations in SI cortex was selected as the primary site for enhancement in Experiment Two. Provided that little evidence was found to support a homotopic relationship between forepaw cortices, the forepaw representation was selected as a comparison.

CHAPTER III

CHRONIC MICROSTIMULATION STUDY

I. Specific Literature Review

Neurons in cat primary somatosensory (SI) cortex were first described as receiving somatosensory input exclusively from the contralateral body surface (Mountcastle, 1957; Mountcastle et al., 1957). This description was altered by reports that SI cortical neurons also received bilateral input in monkey (Manzoni et al., 1989; Ogawa et al., 1989; Iwamura et al., 1996; Taoka et al., 1999; Lipton et al., 2006; Tommerdahl et al., 2006), cat (Innocenti et al., 1973; Mann, 1979; Manzoni et al., 1980), and rodent (Angel and Lemon, 1975; Pidoux and Verley, 1979; Chapin and Lin, 1984; Armstrong-James and George, 1988; Shuler et al., 2001; Pluto et al., 2005). It was suggested these neurons were restricted to receiving bilateral input from the midline body structures that included the head (Dreyer et al., 1975), face (Schwarz and Fredrickson, 1971), and axial trunk in large part because dense populations of bilateral receptive field neurons were reported in SI cortical regions dense with callosal connections (Manzoni et al., 1980; Innocenti, 1986; Conti et al., 1986); callosal connections were primarily associated with the midline representation of the trunk, face, or head and were considered devoid in cortical regions associated with the lateralized functions of the limbs (Yorke and Caviness, 1975; Wise and Jones, 1977b; Manzoni et al., 1980).

More recently investigators have reported that SI neurons also receive bilateral input that is not associated with the representation of the midline body structures. For example, SI cortical neurons in cat (Brooks et al., 1961a, 1961b; Manzoni et al., 1980; Tommerdahl et al., 2006), monkey (Iwamura et al., 1994, 2002; Toda et al., 1996; Taoka

et al., 1998) and flying fox (Calford and Tweedale, 1988) receive bilateral forelimb input although no evidence exists that any receive exclusive input from the ipsilateral forelimb alone. Neurons with bilateral receptive fields that are not associated with the midline body structures were also found in cortical regions coexisting with patches of callosal connections (Toda et al., 1996). In rat SI, data has been presented describing bilateral input from the hindlimbs (Angel and Lemon, 1975; Chapin and Lin, 1984; Armstrong-James and George, 1988; Pluto et al., 2005) and vibrissa (Pidoux and Verley, 1979; Shuler et al., 2001); however, no evidence exists of neurons receiving bilateral input in rodent SI forelimb cortex (Shin et al., 1997) despite callosal connections between homotopic forelimb representations in SI cortex (Welker, 1971; DeCosta-Fortune et al., 2010).

Neurons responsive to bilateral input have receptive field centers located on homologous contra- and ipsilateral skin surfaces (Pidoux and Verley, 1979; Calford and Tweedale, 1988; Armstrong-James and George, 1988) and changes in receptive fields resulting from activity-dependent plasticity are immediately reflected in the contralateral site (Calford and Tweedale, 1990). In flying fox and monkey, following a local lidocaine injection into the center of a forelimb receptive field, the receptive field region on both the locally anesthetized forelimb and the homologous skin surface of the contralateral forelimb expanded; after the anesthesia effects had diminished, both newly expanded receptive field regions gradually reduced to their prior size (Calford and Tweedale, 1990). Expansion of receptive field size has also been induced through blocking callosal

inputs from opposite cortical region in contralateral SI (Clarey et al., 1996) and chronic stimulation of the periphery (Recanzone et al., 1992a; Diamond et al., 1993; Wang et al., 1995; Li et al., 1996; Rema et al., 2006; Quairiaux et al., 2007).

Ipsilateral projections can modify the response to a stimulus in contralateral cortex in monkey (Calford and Tweedale, 1990; Korvenoja et al., 1995; Clarey et al., 1996; Lipton et al., 2006; Tommerdahl et al., 2006), cat (Favorov et al., 2006), and rat (Shin et al., 1997; Shuler et al., 2001); heightening or diminishing of ipsilateral input has been reported to have a suppressing effect on the responsiveness to homologous contralateral stimuli (Tommerdahl et al., 2006) ; reduction in responsiveness ranges from 20% (Shin et al., 1997) to 47% (Rema and Ebner, 2003). Simultaneous delivery of contralateral and ipsilateral vibrotactile hand stimulation, in monkey, resulted in an average response reduction of approximately 35% when compared to contralateral-only stimulation; in the absence of contralateral stimulation, ipsilateral-only stimulation evoked a very weak nonspecific response in SI (Tommerdahl et al., 2006). Conversely, in rat SI, suppressed responsiveness to contralateral input has been accompanied by deafferentation of ipsilateral peripheral sensory input (Shin et al., 1997; Rema and Ebner, 2003) and deactivation of homotopic site in the ipsilateral SI (Li et al., 2005). Viewed collectively, these findings provide convincing experimental evidence that ipsilateral input has a modulatory effect on the responsiveness to contralateral input.

Response to ipsilateral stimuli is likely mediated through transcallosal connections between homotopic sites in SI cortices (Innocenti et al., 1973; Pidoux and Verley, 1979; Iwamura et al., 1994) where the corpus callosum serves as an anatomical substrate integrating both contralateral and ipsilateral input (White and DeAmicis, 1977; Olavarria

et al., 1984; Koralek et al., 1990; Shuler et al., 2001). Several studies have demonstrated that ipsilateral responsiveness is either abolished or significantly reduced following inactivation of callosal inputs from the homotopic site using polarizing currents (Innocenti et al., 1973) or inactivation of the SI contralateral homotopic site through ablation (Pidoux and Verley, 1979; Iwamura et al., 1994) or pharmacological application (Shuler et al., 2001). Evoked response latencies further suggest that the interhemispheric pathway mediates ipsilateral responses. For instance, response recordings in rat vibrissa SI cortex demonstrated average layer IV response latencies of 14.67 ± 0.02 ms, 15.07 ± 0.02 ms, and 23.78 ± 0.04 ms to the deflection of contra-, bi-, and ipsilateral principle whisker, respectively (Wiest et al., 2005) and average layer V response latencies of 11 ± 3.4 ms, and 23 ± 4.7 ms to contra- and ipsilateral whisker stimulation, respectively (Shuler et al., 2001). The additional latency time of approximately 10 ms is attributed to the amount of time it takes for the ipsilateral sensory input to be relayed from the contra- to ipsilateral cortex.

As a precursor to this study, we reported in abstract form that layer V neurons send strong interhemispheric projections to layer V of contralateral SI (DeCosta-Fortune et al., 2010). The aim of the present study was to test the hypothesis that transcallosal connections can be strengthened by chronic intracortical microstimulation (ICMS) leading to enhancement of the interhemispheric pathway and functional reorganization. Our work is based on Hebb's theory that the connection between two neurons is strengthened when the projecting neuron repeatedly contributes to the activation of the target neuron (Hebb, 1949; Morris, 1999). Repetitive stimulation applied *in vivo* to rat SI has been shown to induce representational plasticity (Recanzone et al., 1992b; Dinse et

al., 1993; Heusler et al., 2000; Kalarickal and Marshall, 2002); plasticity of callosal connections has been demonstrated *in vitro* rat slice preparations by data showing tetanic stimulation of the white matter enhances responsiveness (Lee, 1982; Bindman et al., 1988; Artola et al., 1990) and *in vivo* in rodent barrel cortex by data showing absence of interhemispheric activity down regulates responses in contralateral barrel cortex (Li et al., 2005). However, only one study was found where chronic stimulation induced long-term plasticity of transcallosal excitatory connections *in vivo* (Bogdanova and Sil'kis, 2002). In the present study, chronic microstimulation was used to enhance the interhemispheric pathway and peripheral stimulation of the ipsilateral forelimb was used to test for ipsilateral input to the enhanced SI cortex. Our results provide the first data demonstrating strengthening of transcallosal connections between homotopic SI layer V forelimb cortices in rat that leads to functional reorganization whereby ipsilateral responsiveness is obtained.

II. Materials and Methods

A. Animals

A total of 10 Sprague-Dawley rats of either sex with an average age of 11.22 wks (± 1.76 wks) and average weight of 324.59 g (± 30.51 g) were used to examine interhemispheric pathway enhancement and functional reorganization in SI forelimb representation. Enhancement of callosal connectivity between homotopic forepaw sites was studied in 1 rat, between homotopic wrist sites in 8 rats, and between homotopic forearm sites in 1 rat; following chronic stimulation of the interhemispheric pathway, functional reorganization within the respective site was tested. The experiments

conformed to *the Principles of Laboratory Animal Care* (NIH publication No. 86-23, revised 1985) and were approved by the University of Tennessee Health Science Center (UTHSC) Institutional Animal Care and Use Committee (IACUC).

B. Animal Preparation

Rats were anesthetized with Ketamine/Xylazine (100 mg/kg, i.m.) and supplemented regularly throughout the experiment (10% of initial dose) in order to maintain areflexia. The hair on top of the head and both forelimbs were shaved. The animal was placed on a water-circulating heating pad to maintain body temperature between 36.5º C and 38.0º C while the head was secured in a stereotaxic frame. A local anesthetic (Carbocaine) was injected into the scalp and a midsagittal incision was made in the skin to expose the underlying bone. Anterior-posterior (A-P) and medial-lateral (M-L) measurements were taken in reference to Bregma and a large bilateral opening approximately 4 mm (A-P) by 4 mm (M-L) was made overlying the frontal and parietal cortices exposing the forepaw, wrist, and forearm barrel subfields in SI of both hemispheres. The dura was incised and reflected outward and the brain surface was infused with warm saline (0.9%) to prevent drying. A recording chamber was constructed using dental cement and the exposed cortices were bathed in warm silicon fluid (10,000 cs). Digitally enhanced (PhotoShop CS4, Adobe) images of the SI cortical surface were used to mark the location of electrode penetrations into the brain.

C. Receptive Field Identification in Each Hemisphere

A carbon fiber electrode (Armstrong-James and Millar, 1979), attached to a Canberra-type Narishige microdrive, was inserted into SI to identify sites in the forelimb representation; for purposes of this study the forelimb representation is defined as

containing the forepaw, wrist, and forearm sites. Receptive field(s) of SI neurons were identified by responses elicited from mechanical stimulation of the skin surface using hand-held probes consisting of a blunt-tipped medal rod (00 gauge) attached to the end of a wooded dowel. Unit responses were amplified using a custom built amplifier, fed into an audio monitor, and viewed on an oscilloscope. Receptive fields were defined by using minimal somatic stimulation that evoked a maximal cortical response.

Receptive field identification began by inserting the recording electrode to a depth of 700 μm which had previously been reported to lie within the layer IV barrel field and to yield the strongest response to peripheral stimulation (Waters et al., 1995b). If a forepaw, wrist, or forearm receptive field was identified in layer IV, the electrode was then systematically advanced in 100 μm increments to layer V at a depth of approximately 1,400 μm; to ensure the electrode penetration remained with the cortical column, the receptive field was re-measured at each increment. When the receptive field measured in layer V was similar to that measured in layer IV the electrode was fixed at that location; it's A-P and M-L coordinates and cortical depth were documented. A second carbon-fiber electrode attached to an independent microdrive was inserted into the opposite barrel field cortex and the process was repeated to locate a similar site in layer V. All receptive fields were plotted on a standardized body map of the forearm and forepaw as shown in Fig. 9.

D. Microstimulation and Interhemispheric Pathway Enhancement

Once the receptive fields were matched in each hemisphere and the two recording electrodes were fixed in place, transcallosal connectivity between the homotopic representations was examined by delivering intracortical microstimulation (ICMS) to one

electrode (stimulating electrode) and recording evoked responses from the second electrode (recording electrode) in contralateral cortex. Slight adjustments were made to the depth of the recording electrode to achieve a maximal evoked response using a minimal amount of stimulus current. The carbon fiber stimulating electrode was replaced with a tungsten electrode (Frederick Haer Company) and the receptive field was reexamined. ICMS (cathodal pulse, 1.5 × threshold, 1.0 ms pulse duration, 1 Hz) was delivered in layer V for 1-5 hrs. Responses to 20-50 consecutive microstimulations were recorded and collected at the beginning of stimulation to establish a baseline level of response activity, during ICMS delivery at 30 min intervals to monitor changes in spike occurrence, and at the end of stimulation to determine level of enhancement.

E. Peripheral Stimulation and Functional Reorganization

After similar representations in each barrel cortex were identified and the interhemispheric connection between them was established, baseline peripheral responses were measured in contralateral and ipsilateral SI cortices. The mechanical stimulus used to stimulate the periphery during mapping was replaced with a bipolar stimulating electrode which was fashioned from a pair of twisted silver chloride wires and used to deliver current (1.5× threshold, 1.0 ms pulse duration , 1 Hz) onto the forelimb skin surface. Baseline responses to 20-50 consecutive electrical stimulations of the forelimb skin surface were collected before (T_{ICMS} = 0.0 hrs.) chronic microstimulation was delivered. To assess the occurrence of functional reorganization, responses to the same number consecutive stimulations were collected at 30 min intervals (T_{ICMS} = 0.5, 1.0, …, 2.5 hrs.) during ICMS and again afterwards ($T_{ICMS} \geq 3.0$ hrs.).

F. Tissue Processing

Following recording, electrolytic lesions (5 µA, 10 sec) were made at both the stimulating and recording sites. Animals were then administered a lethal dose of Nembutal (100 mg/kg, i.m.) and transcardially perfused with 0.9% saline followed by chilled 4% paraformaldehyde in 0.3 M sodium phosphate-buffered saline (NaPBS, pH 7.4, 21˚ C). The brain was removed; cortices were blocked, and prepared for sectioning in the coronal plane. Tissue was fixed in 4% paraformaldehyde at 4˚ C and refrigerated overnight. The following day, tissue was coronally sectioned at 100 µm thickness using a Vibratome. Sections were rinsed (3 × 10 min) with 0.01 M potassium phosphate-buffered saline (KPBS, pH 7.4, 21˚ C) and counterstained with cytochrome oxidase (CO). Tissue was then incubated in a DAB-sucrose-PBS mixture and placed in a warm water (38˚ C) bath until barrels were visible (Wong-Riley and Welt, 1980). Sections were then rinsed (3 × 10 min) in buffer, mounted in distilled water on gelatin-coated glass slides, air dried overnight, and coverslipped.

G. Data Analysis

Extracellular responses to cortical and peripheral stimulation were recorded and digitally sampled at 30k Hz using IGOR Pro 6.20 (Wavemetrics). With the stimulus set to occur at a 10 ms delay, the first 120 ms of response data was captured and exported for offline analysis using a custom spike detection algorithm developed in Matlab (Mathworks). Each trace was segmented into a pre-stimulus period (t_{pre} = 0-10 ms), a stimulus period with accompanying artifact (t_{art} = 10-14 ms), and a post-stimulus period (t_{post} = 14-120 ms) containing the stimulus response activity which was then further sub-divided into three response 'windows' (t_{resp1} = 14-40 ms, t_{resp2} = 40-80 ms, and t_{resp3} = 80-

120 ms). Enhancement of the interhemispheric pathway was characterized by an increase (1.5× baseline) in evoked response firing rate during the post-stimulus period. Functional reorganization was defined by the appearance of newly evoked responses in ipsilateral forelimb cortex following stimulation of the ipsilateral forelimb that was not present prior to enhancing the interhemispheric pathway between homotopic forelimb sites.

1. Spike Detection

Responses to 20-50 consecutive cortical stimulations were collected before (T_{ICMS} = 0.0 hrs.), during (T_{ICMS} = 0.5, 1.0, …, 2.5 hrs.) and after (T_{ICMS} = 3.0 hrs.) ICMS. Each recorded response trace was bandpass filtered with low and high cutoff frequencies set to 300 Hz and 1000 Hz, respectively (Quiroga et al., 2004; Rutishauser et al., 2006). Spike detection was performed by applying an amplitude threshold to each filtered response trace. For responses to cortical stimulation, the detection threshold, V_{thr}, was established from the baseline post-stimulus period (t_{post} = 14-120 ms); careful consideration was given to minimize Type I (false positives) and Type II (false negatives) errors. Type I errors occur when the threshold is set too low and noise crosses over thereby creating false positives while Type II errors occur when the threshold is set tool high and spikes are missed thereby creating false negatives. When testing for functional reorganization each recorded response trace was examined for evoked responses following ipsilateral forelimb stimulation. In cases where spontaneous or bursting neuronal activity was observed in the ipsilateral barrel cortex, emphasis was placed on response activity with a latency of 16-20 ms to set the detection threshold; this time frame was selected based on previous reports of ipsilateral response temporal attributes (Shuler et al., 2001; Wiest et al., 2005) and in a previous pilot study we determined that evoked responses to cortical

stimulation and contralateral forelimb stimulation had latency of 8-10 ms. We predicted responses to ipsilateral forelimb stimulation would be relayed from the contralateral to the ipsilateral cortex and therefore have a latency of 16-20 ms.

Each recorded data point *k* was assessed against 3 criteria [$k \geq V_{thr}$, $k \geq (k\text{-}1)$, and $k \geq (k\text{+}1)$] to determine spike occurrence. When all 3 criteria were met, the spike detection counter was incremented by 1 and both the amplitude and time of occurrence were logged. Spike activity histograms and raster plots were generated for t = 0-120 ms in 2 ms time bins. Evoked response onset, latency, and duration were calculated using the spike activity peri-stimulus time histograms. Onset of the evoked response was defined as having occurred when the number of post-stimulus spikes within a 2 ms time bin reached 1.5× the average number of pre-stimulus spikes. Latency was measured from the onset of the stimulus artifact (t = 10 ms) to the onset of the evoked response. Duration of the evoked response was measured from its onset to the time when pre-stimulus activity levels resumed.

2. Time Course for Enhancement

To examine the time course of interhemispheric pathway enhancement a repeated measures Analysis of Variance (ANOVA) and Student-Newman-Keuls (SNK) post-comparison test were used to assess statistical significance ($p < 0.05$) of the changes in the number spikes detected throughout the microstimulation period; changes in response duration and latency were also assessed.

III. Results

From a total of 10 rats, interhemispheric pathway enhancement and functional reorganization in layer V SI cortex was studied between homotopic forepaw (n = 1), wrist

(n = 8), and forearm (n = 1) representations. Similar layer V receptive fields were physiologically identified in the barrel cortex of each hemisphere; one receptive field served as the stimulating site while the other served as the recording site. A case example showing the locations of both the stimulating and recording sites, as marked my electrolytic lesions, is shown in the photomicrograph (Fig. 11) of a single 100 µm thick tissue section. ICMS was delivered to the stimulating site for a period of 1.0 hrs. to 5.0 hrs. at depths of 1,300 µm to 1,400 µm and extracellular responses to 20-50 consecutive stimulations were collected from the recording site at depths ranging from 1,100 µm to 1,500 µm; both stimulating and recording sites correspond to layer V. Chronic ICMS induced change in contralateral SI firing rate in all 10 rats and these changes led to functional reorganization in 7 rats. Experimental parameters for stimulation, recording, interhemispheric pathway changes, and ipsilateral responsiveness are summarized in Table 2.

A. Interhemispheric Pathway Enhancement

To examine changes in firing rate of transcallosal connections, we delivered chronic ICMS to the interhemispheric pathway between physiologically identified homotopic sites in layer V of 10 rats for 1.0 hrs. to 5.0 hrs. and recorded the response activity in 3 primary 'windows' (t_{resp1} = 14-40 ms, t_{resp2} = 40-80 ms, t_{resp3} = 80-120 ms). Of these, 9 rats, 9 (FA: n = 1, W: n = 7, FP: n = 1) displayed an increase in evoked response firing activity while 1 rat experienced a reduction in response firing activity. The criterion for enhancement (50% increase) was met or exceeded in 7 of the 9 rats experiencing an increased firing rate; in one rat, the percent increase could not be precisely measured although an increase in spike activity was clearly visible and in a second rat, the percent

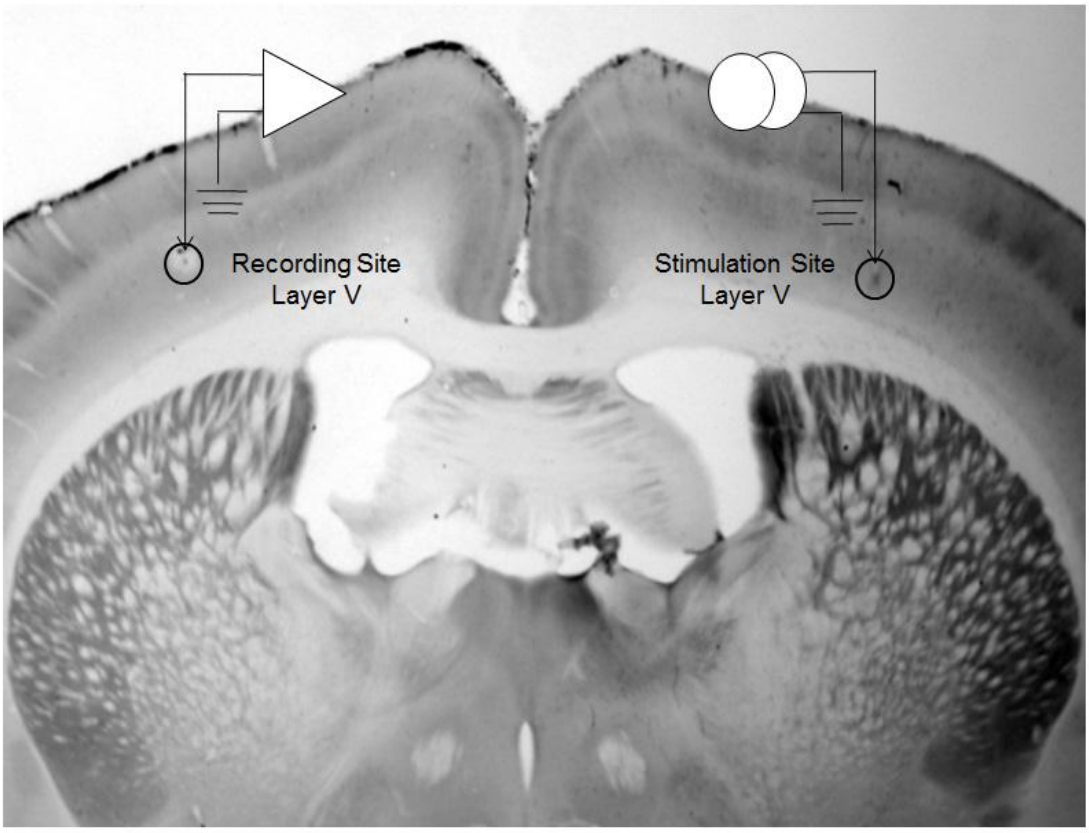

Figure 11 – Photomicrograph showing an example of the locations of the stimulation and recording sites in SI layer V forelimb cortex. Similar receptive fields on the wrist representation were physiologically identified in each SI. Chronic microstimulation was delivered for a period of 1.0 – 5.0 hrs. at a depth of 1,400 μm and multiunit responses to 20-50 consecutive stimulations were recorded in the contralateral barrel cortex at a depth of 1,100 μm.

Table 2 – Interhemispheric pathway enhancement and functional reorganization summary data. ICMS delivered in SI layer V (depth = 1,373 ± 46.71 μm) strengthened the interhemispheric pathway between homotopic layer V forelimb representations; an increase in firing rate was observed in 9 of the 10 rats, of which, 7 of which satisfied the criterion for enhancement (1.5× over baseline). However, in one case, responsiveness decreased (-37%). An average of 1.5 hrs. of ICMS delivery was required to obtain enhancement. Enhancement of transcallosal connections induced a functional connection between ipsilateral forelimb and ipsilateral barrel cortex in 7 rats. Note, the * indicates a case where an increase in firing rate was observed but could not be accurately measured.

Experiment No.	Stimulation Site (SI Cortex)							Recording Site (Contralateral SI Cortex)				Interhemispheric Pathway Enhancement		Functional Reorganization
	Receptive Field	Depth (μm)	Cortical Layer	Cathodic Current 1.5× threshold (μA)	Pulse Duration (ms)	Frequency (Hz)	ICMS Duration (hrs.)	Receptive Field	Depth (μm)	Cortical Layer	Consecutive Responses	Maximum % Change	Time of Max Change (hrs.)	Ipsilateral Response
CS-1	Forearm	1,400	V	60	1	0.5	1.5	Forearm	1,100	V	50	*	1.5	Y
CS-2	Wrist	1,400	V	50	1	0.5	3.0	Wrist	1,100	V	40	134%	3.0	Y
CS-3	Wrist	1,400	V	30	1	0.5	3.0	Wrist	1,100	V	50	82%	3.0	Y
CS-4	Wrist	1,400	V	70	1	0.5	3.0	Wrist	1,100	V	50	111%	2.5	Y
CS-5	Wrist	1,300	V	30	1	0.5	1.5	Wrist	1,500	V	50	59%	1.0	Y
CS-6	Wrist	1,300	V	30	1	0.5	3.0	Wrist	1,300	V	50	-37%	2.5	N
CS-7	Forepaw	1,400	V	30	1	0.5	3.0	Forepaw	1,100	V	20	76%	1.5	N
CS-8	Wrist	1,400	V	30	1	0.5	1.0	Wrist	1,100	V	50	23%	1.0	N
CS-9	Wrist	1,400	V	30	1	0.5	3.0	Wrist	1,100	V	50	91%	3.0	Y
CS-10	Wrist	1,400	V	50	1	0.5	5.0	Wrist	1,400	V	25	585%	5.0	Y
Mean		1,373		42.73	1	0.5	3.0		1,200		41	127%	2.4	
Std Dev		46.71		15.55	0	0	1.19		148.32		13.06	178%	1.2	

increase did not meet the criterion for enhancement. The average ICMS duration to reach enhancement was 1.5 hrs. Latency of evoked responses to chronic stimulation was consistently measured to range between 6 ms to 10 ms, averaging 7.43 ms (± 1.15 ms) and the response duration ranged from 8 ms to 24 ms, averaging 12.29 ms (± 2.92 ms); both of which were not significantly different ($p > 0.05$) following interhemispheric enhancement as determined using a repeated measures ANOVA.

An example of interhemispheric pathway enhancement between homotopic layer V wrist representations is depicted in Fig. 12. Intracortical microstimulation (-50 μA, 0.5 Hz, 1.0 ms pulse duration) was delivered for 3.0 hrs. in the physiologically identified wrist representation in SI cortex at a depth of 1,400 μm while extracellular responses were recorded in layer V at a depth of 1,100 μm from a homotopic site in contralateral barrel cortex. Response recordings to 40 consecutive stimulations were gathered at the beginning and at the end of 3.0 hrs. of ICMS, the first 25 of which are shown in Fig. 12A and Fig. 12B, respectively. These recordings illustrate the increase in activity responsiveness to the stimulus; a sample of 10 responses is shown in the respective insets. Following 3.0 hrs. of microstimulation a clustering of activity was observed primarily in the t_{resp1} = 14-40 ms response window as seen from the raster plots (Fig. 12C and Fig. 12D). This clustering of activity occurs with a latency of 8 ms. In addition, the raster plots show a reduction in spontaneous activity following the evoked response. The corresponding peri-stimulus time histograms are shown in Fig. 12E and Fig. 12F and depict the number of spikes (2 ms bins) detected which exceed the voltage amplitude threshold (V_{th} = 6 mV) increased from 119 (Fig. 12E) to 278 (Fig. 12F) in the response window t_{resp1} = 14-40 ms which is an increase of 2.34× over baseline. During the time

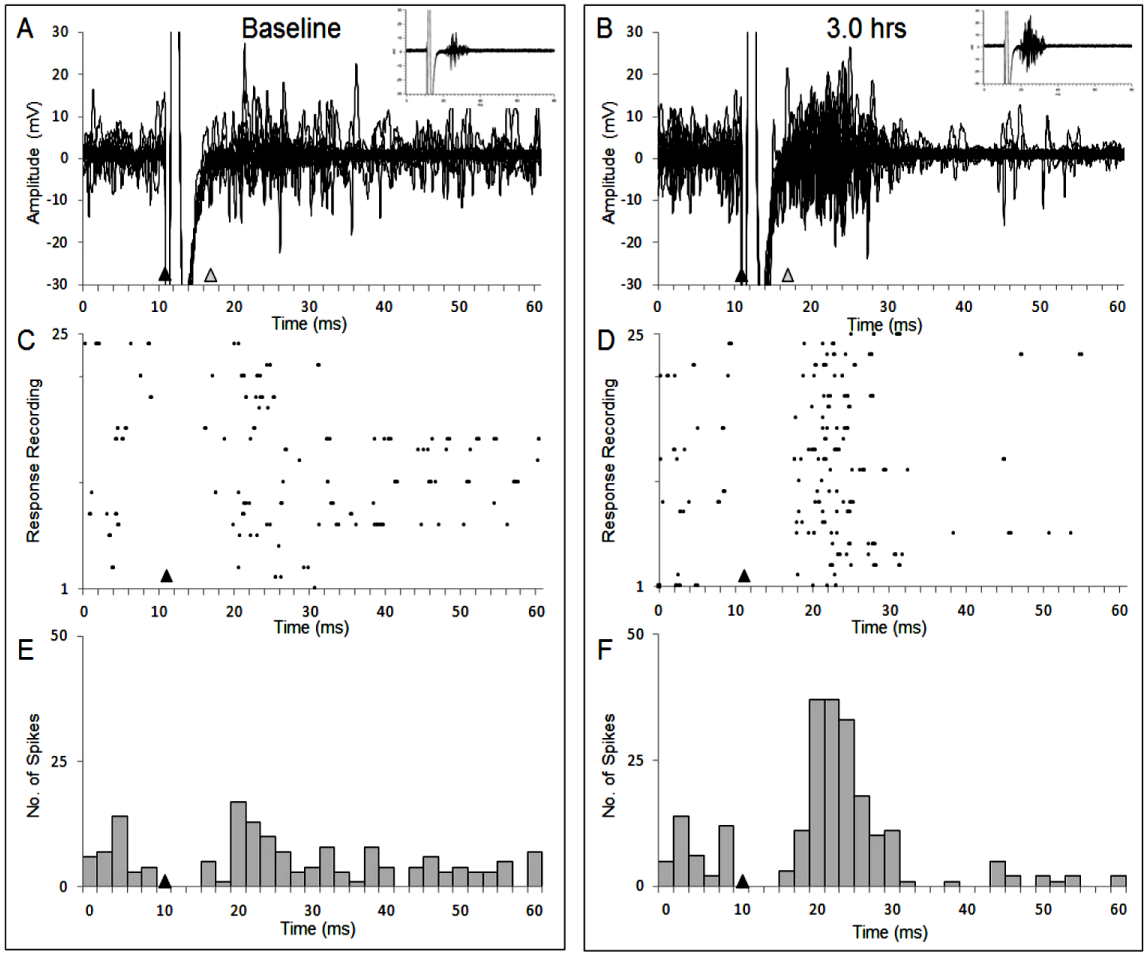

Figure 12 - Interhemispheric pathway enhancement between layer V wrist representations in ipsilateral and contralateral SI cortices following ICMS (-50 µA, 1.0 ms duration, 0.5 Hz, 3 hrs.). **A-B:** Composite of 25 response recordings at baseline (A) and after enhancement (B). **C-D:** Raster plots (C and D) for the corresponding response traces shown in A and B, respectively; after ICMS, response activity (t_{resp} = 16-30 ms) increased while spontaneous activity (t_{resp} > 30 ms) decreased. **E-F:** The peri-stimulus time histograms (2 ms bins) depict the number of spikes detected exceeding the voltage threshold (approximately 6 mV) before (E) and after (F) ICMS. The number of spikes during the response window t_{resp1} = 14-40 ms increased from 119 to 278, resulting in a 134% increase over baseline. Evoked response latency and duration ranged from 8-10 ms and 6-12 ms, respectively. Filled and hollow triangles denote onset of stimulus and evoked response, respectively.

period of interhemispheric pathway enhancement, the evoked response latency ranged from 8-10 ms averaging 9.714 ms (± 0.76 ms) and the duration averaged 8.57 ms (± 1.90 ms) ranging from 6-12 ms. The onset of the stimulus and the evoked response are indicated by the filled and hollow triangles, respectively.

Additional examples of interhemispheric enhancement between homotopic layer V wrist representations are presented in Fig. 13. In both examples (Fig. 13A and Fig. 13B), the wrist representation was physiologically identified in layer V of both SI cortices and chronic microstimulation was delivered for a minimum of 3.0 hours. Similar to the previous example, the increase in firing activity and spikes detected was concentrated in the t_{resp1} = 14-40 ms response window. Also, enhancement of the interhemispheric pathway did not affect the response onset which measured 7.71 ms (Fig. 13A) and 6.74 ms (Fig. 13B) nor did it affect the response duration measuring an average of 17.43 ms (Fig. 13A) and 14.00 ms (Fig. 13B). The filled triangles denote the stimulus onset while the hollow triangles denote the onset of the evoked response.

As a comparison to modulating transcallosal connections between forelimb sites with homotopic projections, we examined interhemispheric pathway enhancement between layer V forepaw representations, which do not have homotopic projections, in 1 rat and is shown in Fig. 14. The forepaw digit three (D3) representation was physiologically identified in layer V of the barrel cortex at a depth of approximately 1,400 μm and was chronically stimulated (-30 μA, 0.5 Hz, 1.0 ms pulse duration) for a period of 3.0 hrs. Extracellular responses were recorded from layer V (depth = 1,100 μm) of the homotopic site in the opposite barrel cortex. Figs. 14A and Fig. 14B show the composite responses to 20 consecutive stimulations collected at the beginning (T_{ICMS} =

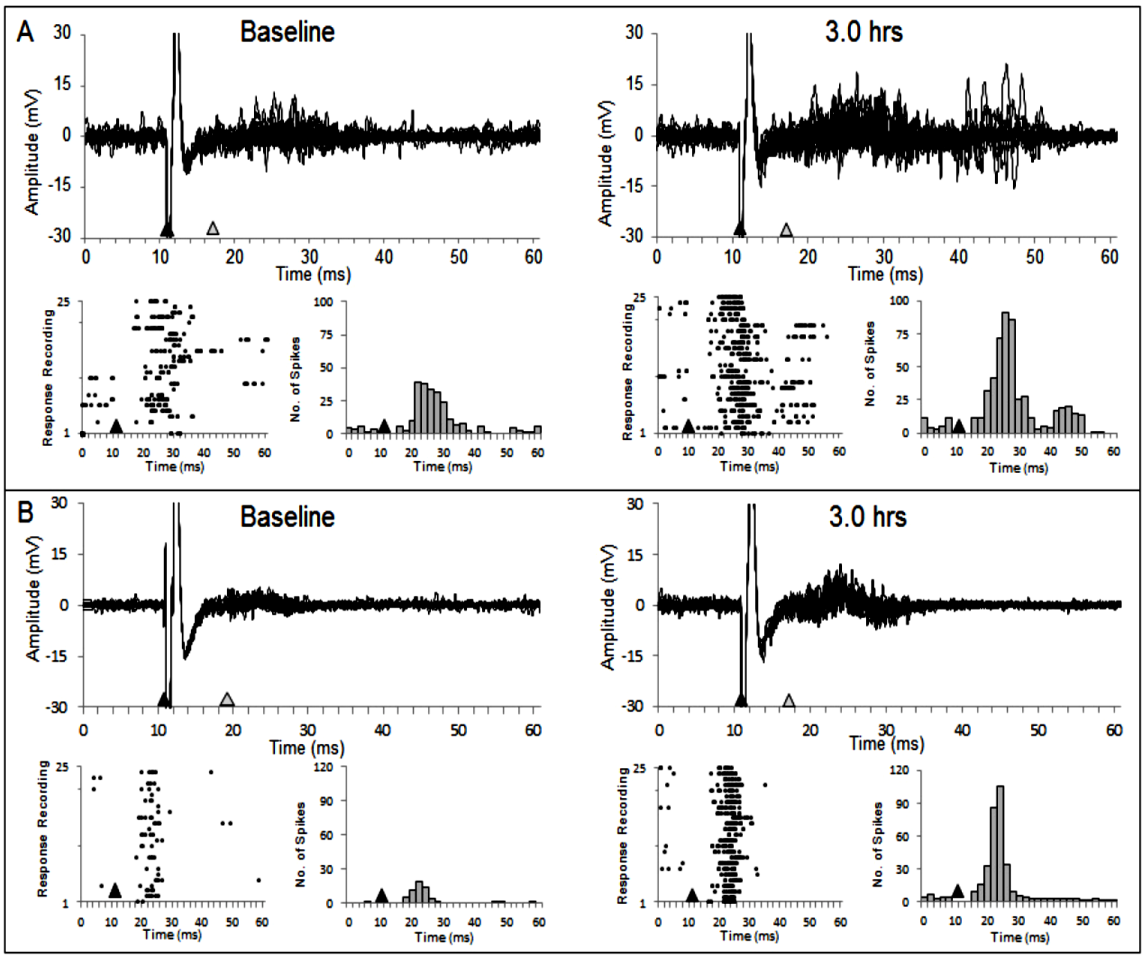

Figure 13 – Additional examples of increased response activity between homotopic layer V wrist representations in barrel cortex following ICMS. **A-B:** Composite of 25 response recordings taken before (baseline) and after (3.0 hrs.) chronic microstimulation. Both rats received a 1.0 ms pulse duration cathode (A: -30 µA, B: -50 µA) pulse delivered at 0.5 Hz for 3 hrs. (A) and 5 hrs. (B); data for B is shown at 3.0 hrs. as a comparison. Corresponding raster plots and peri-stimulus time histograms illustrate an increase in spikes detected in 2 ms bins. In both rats, enhancement in firing rate was concentrated between 14 ms and 40 ms; number of spike detected (V_{th} = 2 mV) increased 91% (A) and 111% (B). Evoked response latency averaged 7.71 ± 1.38 ms (A) and 5.71 ± 1.38 ms (B); duration of the evoked response averaged 17.43 ± 2.99 ms (A) and 14.00 ± 2.58 ms (B). Filled and hollow triangles denote onset of stimulus and evoked response, respectively.

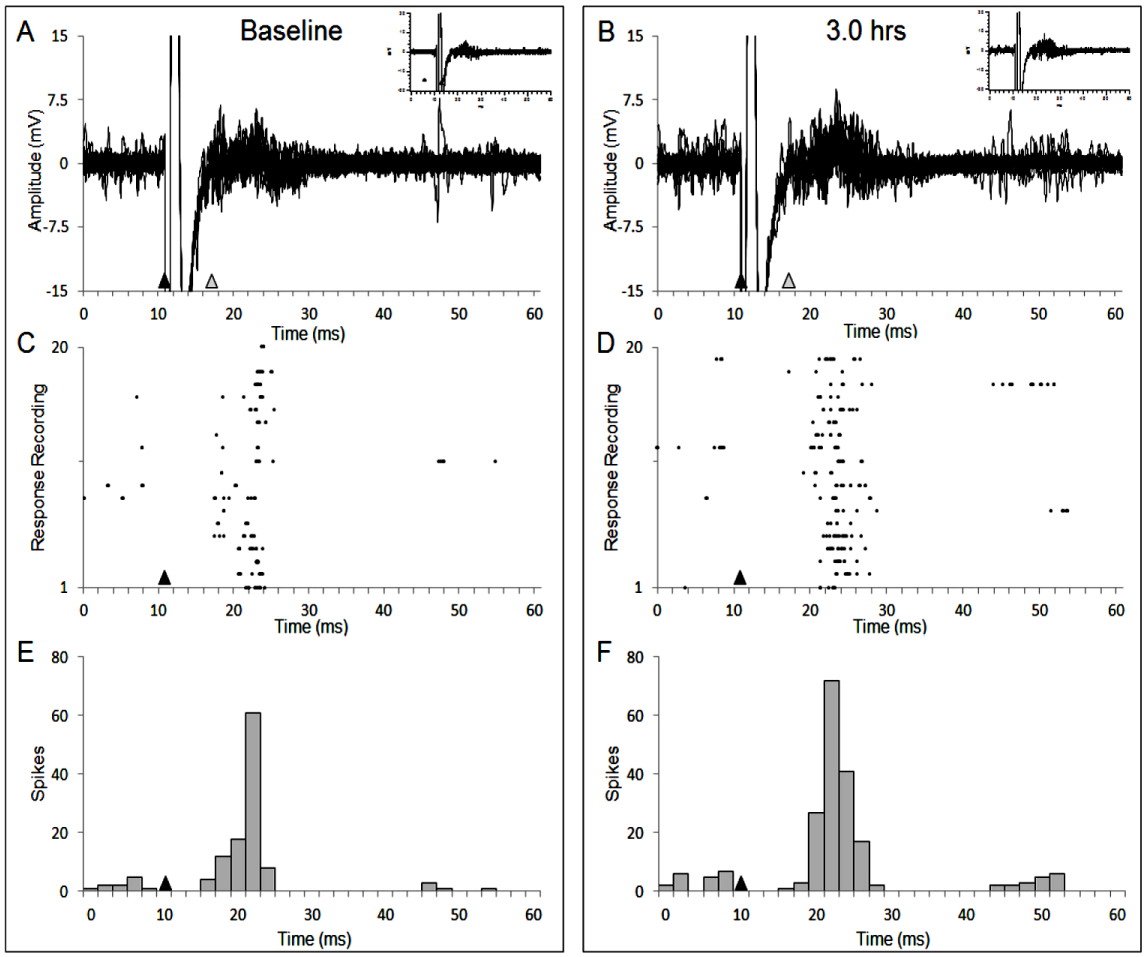

Figure 14 – Interhemispheric pathway enhancement between layer V forepaw representations in ipsilateral and contralateral SI cortices following ICMS (-30 µA, 1.0 ms pulse duration, 0.5 Hz, 3 hrs.). **A-B:** Composite of 20 response recordings before (B) and after 3.0 hrs. (B) of chronic microstimulation. **C-D:** Baseline (B) and post-ICMS (C) raster plots for the corresponding response recordings depict an increase in spike activity, taken in 2 ms time bins, concentrated in the response window of 14-40 ms. **E-F:** The number of spikes detected in response to 20 consecutive stimulations increased from 103 to 163 detected spikes (increase of 58%). Filled and hollow triangles denote onset of stimulus and evoked response, respectively. While the enhancement criterion was met following 3.0 hrs. of ICMS, the greatest amount of enhancement measured 76% increase over baseline and was observed after 1.5 hrs. of ICMS (data not presented).

0.0 hrs.) and at the end (T_{ICMS} = 3.0 hrs.) of ICMS; the insets illustrate a subset of 10 responses. Similar to the previous examples of enhancement in the wrist representation, the corresponding forepaw raster plots shown in Fig. 14C and Fig. 14D reveal the response activity increases following ICMS which was manifested as a cluster of spikes within t_{resp1} = 14-40 ms. The number of spikes detected (V_{th} = 3 mV) within the evoked response window of 14-40 ms increased from 103 spikes (Fig. 14E) to 163 spikes (Fig. 14F), an enhancement of 1.58× baseline. While the enhancement criterion was met following 3 hrs. of ICMS, the greatest amount of enhancement measured at a 76% increase over baseline was observed after 1.5 hrs. of ICMS (data not presented). The average evoked response latency ranged from 6-10 ms, averaging 7.14 ms (± 1.6 ms); duration averaged 10.6 ms (± 2.2 ms) and ranged from 8-14 ms. Filled and hollow triangles denote the onset of the stimulus artifact and the evoked response.

In 1 rat, stimulation of the interhemispheric pathway appeared to not increase responsiveness to chronic microstimulation and is shown in Fig. 15. Chronic microstimulation (-30 μA, 0.5 Hz 1.0 ms pulse duration) for 3.0 hrs. was delivered in the physiologically defined wrist representation in SI cortex at a depth of 1,300 μm, responses to which were recorded from a homotopic site in the opposite SI at a depth of 1,300 μm. Fifty consecutive responses to stimulation were gathered prior to (Fig. 15A) and following 3.0 hrs. (Fig. 15B) of ICMS. As seen in the corresponding raster plots (Fig. 15C and Fig. 15D), the concentration of spikes detected between 14-40 ms is less dense after 3.0 hrs. The peri-stimulus histograms (2ms bin) depict the number of spikes detected exceeding the voltage amplitude threshold (V_{th} = 5 mV) decreased from 93 (Fig. 15E) to 76 (Fig. 15F) which is a decrease of 18% from baseline. However, during the

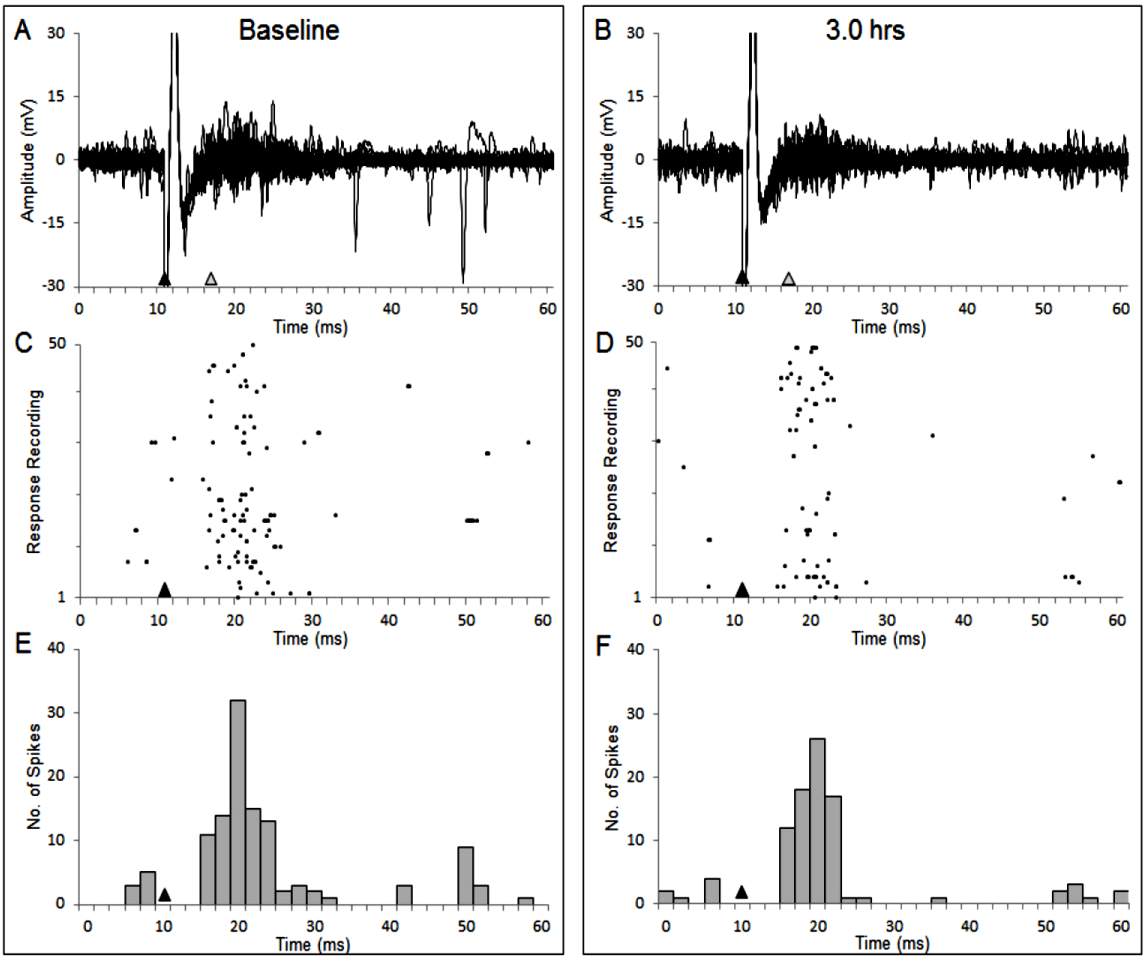

Figure 15 – Suppressed responsiveness between homotopic layer V wrist representations following ICMS (-30 µA, 1.0 ms pulse duration, 0.5 Hz, 3 hrs.). **A-B:** Composite of 50 responses recording taken prior to (A) and following 3.0 hrs. of chronic microstimulation (B) depict a decrease in responsiveness to stimulation. **C-D:** Changes in response firing rate from T_{ICMS} = 0.0 (C) to T_{CMS} = 3.0 hrs. (D) of ICMS were confined to the t_{resp} = 14-40 ms response window: **E-F:** Decrease in activity from 93 spike detected at the beginning (E) to 76 spikes detected at 3.0 hrs. (F) resulting in an 18% reduction of activity.

course of chronic stimulation, an increase in spike activity was measured to occur at 0.5 hrs. (16%) and again at 2.0 hrs. (14%). The average change in firing rate after 3.0 hrs. of ICMS was 10% under baseline. The evoked response latency in this rat was consistently measured at 6 ms and the duration of the evoked response ranged from 8 ms to 12 ms. While chronic stimulation had a suppressing effect on responsiveness to stimulation, the evoked response latency and duration were not affected.

1. Time Course for Enhancement

To assess the time course of interhemispheric pathway firing rate changes, evoked responses to ICMS were recorded before (T_{ICMS} = 0.0 hrs.), at 30 min increments (T_{ICMS} = 0.5, 1.0, 1.5, 2.0, 2. 5 hrs.), and after (T_{ICMS} = 3.0 hrs.) ICMS in all 10 rats. Response activity spike detection was performed using an amplitude voltage threshold (V_{thr}). Enhancement of the interhemispheric pathway was determined to occur when the evoked response firing rate reached or exceeded 1.5× the baseline activity; this was measured in 7 of the 9 rats experiencing a positive increase in responsiveness to chronic microstimulation. Note that in 1 rat the percent increase could not be accurately measured although evidence of an increased firing rate after 3.0 hrs. of ICMS delivery was clearly visible.

An example illustrating the time course for enhancement between homotopic forelimb representations is shown in Fig. 16. Intracortical microstimulation was delivered for 5.0 hrs. to the physiologically identified layer V (depth = 1,400 μm) wrist representation and responses to 25 consecutive stimulations were recorded from the homotopic layer V (depth = 1,400 μm) site in contralateral SI. Raster plots and peri-stimulus histograms (2 ms bins) were generated throughout the 5.0 hrs. of ICMS (-50 μA,

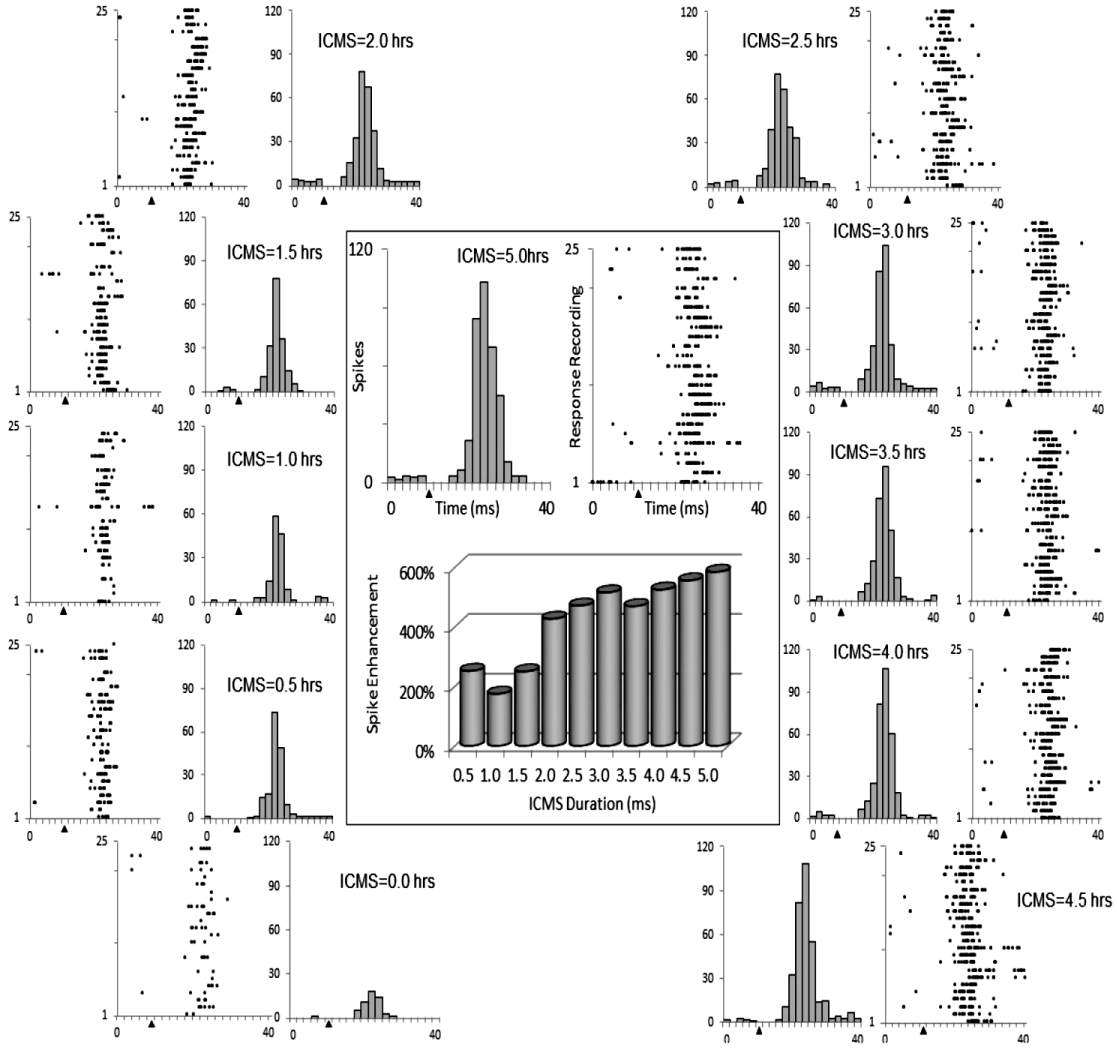

Figure 16 – Time course of interhemispheric pathway enhancement between homotopic layer V wrist representations during 5.0 hours of ICMS (-50 µA, 1.0 ms pulse duration, 0.5 Hz). Chronic microstimulation was delivered for a period of 5 hours and changes in spike activity to 25 consecutive stimulations were measured at the beginning (T_{ICMS} = 0.0), during in 30 min increments (T_{ICMS} = 0.5, 1.0, 1.5,…4.5), and at the end (T_{ICMS} = 5.0). In this rat, response activity progressively increased with ICMS duration. Enhancement was first observed at 0.5 hrs. and was retained for the full 5.0 hrs. Enhancement measured 585% at 5.0 hrs. Filled triangles denote onset of stimulus.

1.0 ms pulse duration, 0.5 Hz) in 30 minute increments. Collectively, these charts illustrate a steady progression of neural activity in response to ICMS. The number of spikes detected increased from a baseline of 52 spikes to 320 spikes after chronic microstimulation (3.0 hrs.) was delivered and after 5.0 hrs. of ICMS 356 spikes were detected. In this particular rat, the enhancement criterion of a 50% increase in spike activity was first obtained following 0.5 hrs. of stimulation where a total of 183 spikes were counted, equating to a 152% increase over baseline (161 spikes) and enhancement was retained throughout the 5.0 hrs. chronic stimulation duration. A positive correlation between the number of spikes detected and the length of chronic microstimulation was calculated at $R^2 = 0.8481$. Changes in responsiveness were confined to the t_{resp1} = 14-40 ms response window. The overall increase in evoked response firing activity measured 6.85× baseline. The average evoked response latency and duration measured 6.71 ms (± 1.38 ms) and 14.00 ms ± (2.58 ms), respectively.

Interhemispheric pathway enhancement was obtained between homotopic forepaw representations, however, the pattern of enhancement was not progressive with time and this is presented in Fig. 17. Chronic microstimulation (-30 μA, 1.0 ms pulse duration, 0.5 Hz, 3.0 hrs.) was delivered to the ventral tip of digit three (D3) and responses to 20 consecutive stimulations were collected throughout the course of ICMS delivery from the homotopic representation in the contralateral layer V site. The full raster plots and peri-stimulus time histograms of Fig. 17A show the detected spikes (V_{thr} = 2.75 mV) in 2 ms bins; filled triangles denote the stimulus onset. An increase in spike activity is apparent when comparing the baseline response (T_{ICMS} = 0.0 hrs.) to the end response (T_{ICMS} = 3.0 hrs.). However, the progression of enhancement throughout the course of ICMS delivery

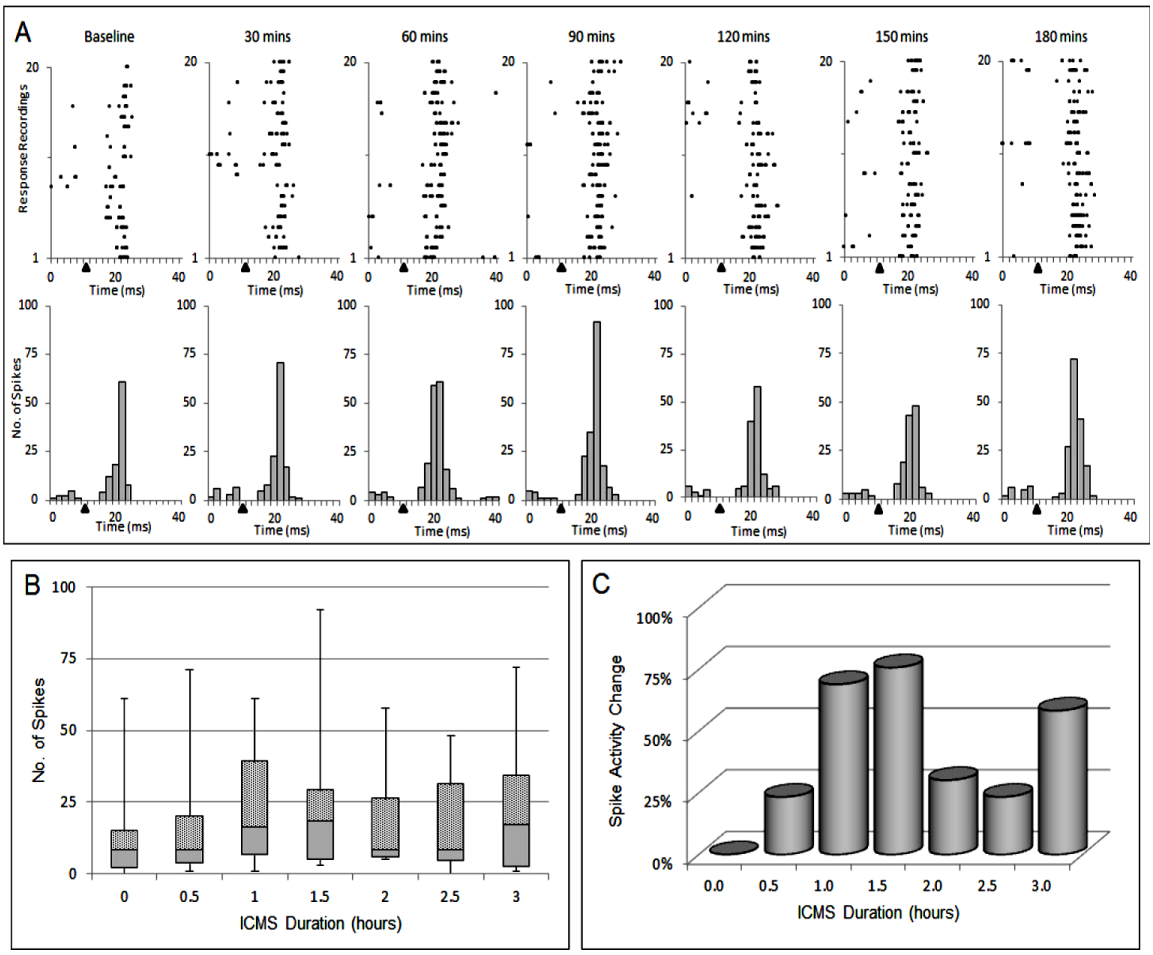

Figure 17 – Time course of interhemispheric pathway enhancement between homotopic layer V forepaw representations (D3) following ICMS (-30 µA, 1.0 ms pulse duration, 0.5 Hz, 3.0 hrs.). **A:** Chronic microstimulation (-30 µA, 1.0 ms pulse duration, 0.5 Hz) was delivered for a period of 3.0 hours and changes in spike activity to 20 consecutive stimulations were measured at the beginning (T_{ICMS} = 0.0), during in 30 min increments (T_{ICMS} = 0.5, 1.0, 1.5,…2.5), and at the end (T_{ICMS} = 3.0). Filled triangles denote onset of stimulus. **B:** Distribution of evoked response (t_{resp} = 14-40 ms) spike activity. **C:** Plasticity of transcallosal connectivity presented as a percent change over baseline. Transcallosal connectivity was strengthened compared to baseline; enhancement criterion of a 50% increase over baseline was obtained at 3.0 hrs. (58%), however, the maximal amount of enhancement was observed following 1.5 hrs. of ICMS where an increase of 76% was measured.

is not cumulative as commonly observed in the wrist representation; no correlation between the spikes detected and microstimulation duration was found ($R^2 = 0.1403$). Enhancement was confined within the t_{resp1} = 14-40 ms response window and did not affect the response latency or duration. The distribution of spike activity is summarized in the box-and-whisker plot (Fig. 17B) and shows no consistent firing pattern. For example, the median and greatest number of spikes varied throughout the course of microstimulation as did the distribution and variation of spike activity. The percent change in the number of spikes detected before (0.0 hrs.), during, and after (3.0 hrs.) chronic microstimulation is presented in Fig. 17C). In this example, the enhancement (≥1.5× baseline) was initially obtained after 1.0 hrs. of ICMS; however, a majority of the enhancement was lost after stimulating for 2.0 hrs. and regained 60 mins later. Chronic stimulation ceased after 3.0 hrs., therefore it remains undetermined if enhancement would have been retained or if response activity levels would have been further reduced.

In one rat, chronic microstimulation suppressed response activity and these results are presented in Fig. 18. Layer V wrist representation was stimulated (-30 µA, 1.0 ms pulse duration, 0.5 Hz, 3.0 hrs.) at a depth of approximately 1,300 µm and recordings from the homotopic representation were taken at the same depth. Degradation in response activity recorded following 50 consecutive stimulations can be seen in the raster plots and peri-stimulus time histograms of Fig. 18A; the stimulus onset is denoted by the filled triangle. In the baseline response a total of 93 spikes exceeded the voltage amplitude threshold of 5 mV. Firing activity of the evoked response varied between 53 and 108 detected spikes throughout the course of stimulation with no discernible pattern of activity. The box-and-whisker plot (Fig. 18 B) provides an overview of the response

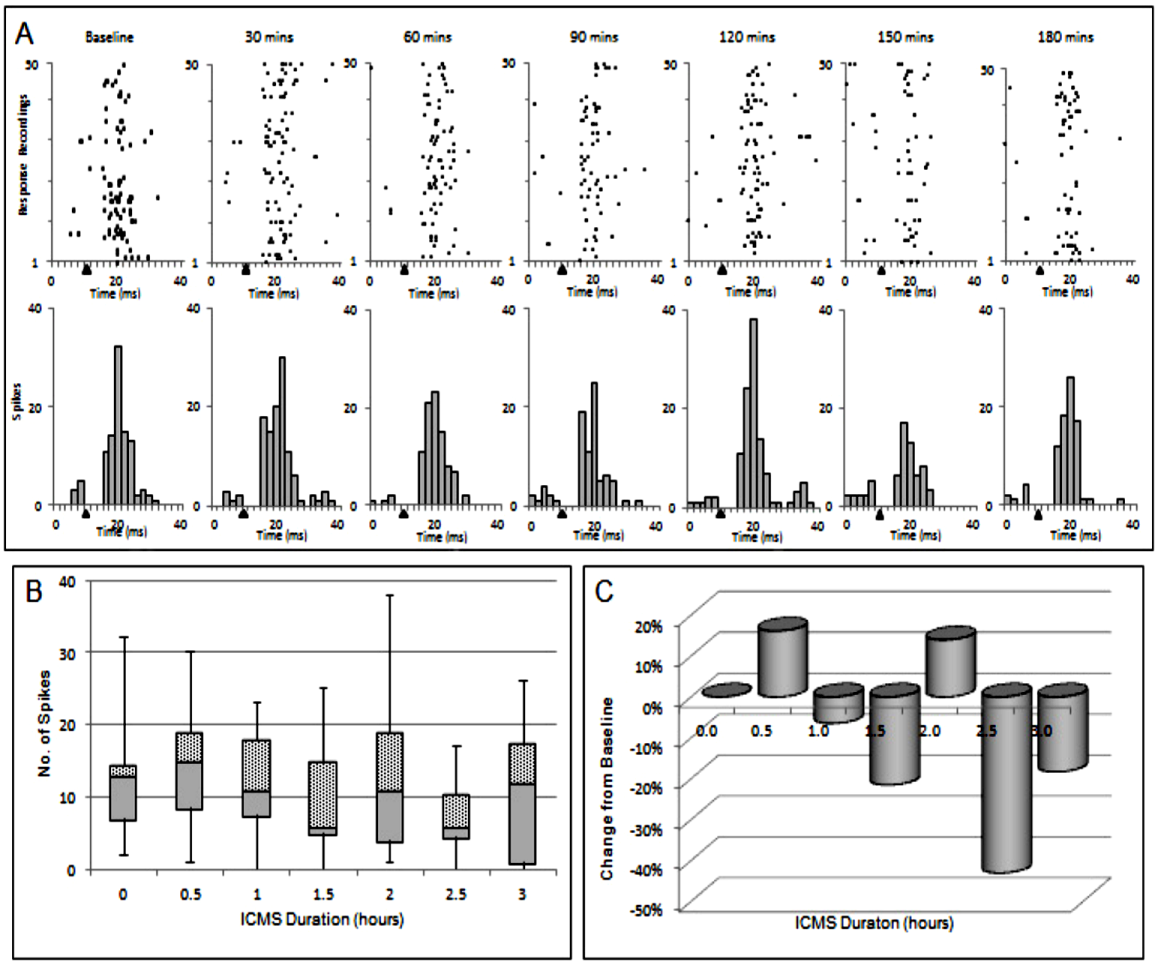

Figure 18 – Time course of interhemispheric pathway depression between homotopic layer V wrist representations following ICMS (-30 µA, 1.0 ms pulse duration, 0.5 Hz, 3.0 hrs.). **A:** Chronic microstimulation (-30 µA, 1.0 ms pulse duration, 0.5 Hz,) was delivered for a period of 3.0 hours and changes in spike activity to 50 consecutive stimulations were measured at the beginning (T_{ICMS} = 0.0), during in 30 min increments (T_{ICMS} = 0.5, 1.0, 1.5,…2.5), and at the end (T_{ICMS} = 3.0). Raster plots and corresponding peri-stimulus time histograms illustrate the change in responsiveness to chronic stimulation from 93 spikes (baseline) to 76 spikes (180 mins). Decrease in activity was concentrated between 14-40 ms. Filled and hollow triangles denote onset of stimulus and evoked response, respectively. **B:** Distribution of evoked response (t_{resp} = 14-40 ms) spike activity. **C:** Plasticity of transcallosal connectivity presented as a percent change over baseline. Spiking activity appeared to increase and decrease with no discernible or predictable pattern. Overall, a depreciation of 10% was observed.

activity distribution for t_{resp1} = 14-40 ms. In this rat, the median number of spikes varied between 6 and 15, and while the greatest variation occurred at 2.0 hrs., the most even distribution of spikes also this same time period. The percent change of response activity over baseline (Fig. 18C) shows that while activity varied from -37% to 18% throughout the course of microstimulation, at no time was enhancement achieved; the average change measured -10% after 3.0 hrs. of ICMS. This reduction in responsiveness to chronic microstimulation is presumably facilitated by an elevated activation of callosal projections terminating on inhibitory interneurons in contralateral SI. While chronic microstimulation appeared to suppress response activity, the response latency and duration were not adversely affected, averaging 6.0 ms (±0.76 ms), and 10.57 ms (± 1.51 ms), respectively.

2. Enhancement Significance

A summary of interhemispheric pathway changes in evoked response firing rate in contralateral SI cortex is presented in Fig. 19. Changes in firing activity in contralateral SI cortex following 3.0 hrs. of ICMS (n = 7) were statistically assessed for significance ($p < 0.05$) using repeated measures Analysis of Variance (ANOVA) and Student-Newman-Keuls (SNK) post-comparison tests; the remaining cases (n = 3) were omitted from statistical analysis because chronic stimulation was not measured every 30 mins for a minimum of 3.0 hrs. For the cases included in the analysis, the average number of spikes detected (20-50 stimulation samples) at the beginning, during (30 min interval), and end of ICMS is shown for t_{resp1} = 14-40 ms, t_{resp2} = 40-80 ms, and t_{resp3} = 80-120 ms is shown in Fig. 19A. Significant changes in response activity were confined to the response time period of 14-40 ms; changes in spikes detected between t_{resp2} = 40-80 ms and t_{resp3} = 80-

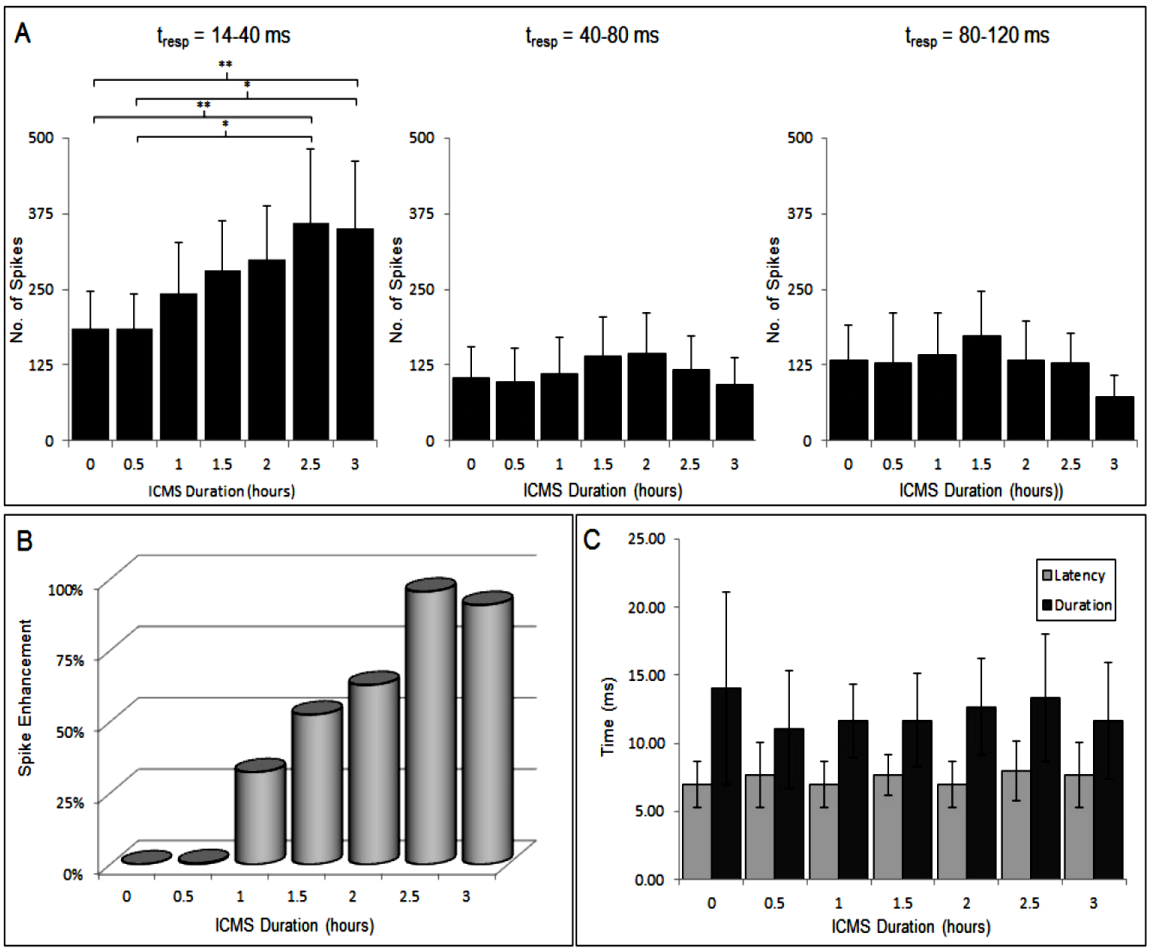

Figure 19 – Summary of interhemispheric pathway changes in evoked response firing rate in contralateral SI cortex. **A:** Distribution summary for the number of spikes detected measured in 30 min increments during the three response windows (t_{resp1} = 14-40 ms, t_{resp2} = 40-80 ms, t_{resp3} = 80-120 ms). Significant ($p < 0.05$) changes in spikes detected were restricted to the t_{resp1} = 14-40 ms response window, changes in firing activity was not significant during t_{resp2} = 40-80 ms or t_{resp3} = 80-120 ms. ANOVA and SNK revealed the number of spikes were significantly different at 2.5 hrs. and the spikes detected at baseline (0.0 hrs.) and 0.5 hrs.; significance retained at 3.0 hrs. **B:** Average spike activity presented as a percent over baseline (0.0 hrs.: 0.0%, 0.5 hrs.: 0.4%, 1.0 hrs.: 32.3%, 1.5 hrs.: 52.4%, 2.0 hrs.: 62.8%, 2.5 hrs.: 95.6%, 3.0 hrs.: 90.9%). On average, 1.5 hrs. of chronic stimulation (42.73 ± 15.55 µA) was required to meet the criterion for enhancement. C: Distribution of changes in evoked response latency and duration throughout the course of ICMS delivery. Latency and duration averaged 7.43 ± 1.15 ms and 12.29 ± 2.92 ms, respectively; changes were not found to be statistically significant as determined using a single-factor ANOVA.

120 ms were found not to be significant. SNK post comparison test revealed the evoked response was significantly enhanced following 2.5 hrs. of stimulation and remained significantly enhanced after 3.0 hrs. of chronic stimulation. Fig. 19B shows the degree of plasticity measured as a percent increase over baseline within the forepaw, wrist, and forearm representation; the collective changes in transcallosal connectivity indicate that chronic microstimulation has an overall strengthening effect and this positive increase shows the increases in responsiveness did not statically affect the response latency (7.43 ms ± 1.15 ms) nor the response duration (12.29 ms ± 2.92 ms).

B. Functional Reorganization

Functional connectivity between the ipsilateral barrel forelimb cortex and ipsilateral forelimb was established in 7 (forearm: $n = 1$, wrist: $n = 6$, forepaw: $n = 0$) out of the 9 cases where the interhemispheric pathway was strengthened. Newly delayed evoked responses to somatic stimulation of the ipsilateral forelimb were recorded with a 17.14 ± 1.95 ms latency and duration of 13.43 ± 1.90 ms. Of the interhemispheric pathways that were enhanced, functional reorganization was achieved between homotopic layer V forelimb representations that are associated with nebulous layer IV cortical regions that are devoid of barrels, these cortical regions are associated with the wrist and forearm representations. In contrast, functional reorganization was not obtained between homotopic forepaw representations, which are associated with the well-defined layer IV barrel structure of the FBS. Table 3 summaries the experimental cases; the receptive field, stimulation amount, and evoked response latency and duration are presented.

An example of functional reorganization within the wrist representation is shown in Fig. 20. Before, during, and after microstimulation was being delivered to the

Table 3 - Functional reorganization summary data. ICMS was delivered to a designated forelimb representation in SI layer V of 11 rats for a period of 1.0 – 5.0 hrs. Of these, 7 rats exhibited functional reorganization in the form of ipsilateral responsiveness. Functional reorganization manifested itself in the form of a newly evoked response to ipsilateral peripheral stimulation having an average latency of 17.14 ms ± 1.95 ms and a duration averaging 13.43 ms ± 1.90 ms. In all cases, functional reorganization was preceded by interhemispheric enhancement. However, functional reorganization was not definitive following interhemispheric enhancement between homotopic forepaw representations.

Experiment No.	Receptive Field	ICMS Duration (hrs.)	Interhemispheric Pathway Enhancement (Maximum Change)	Ipsilateral Peripheral Stimulation (μA)	Ipsilateral Responsiveness	
					Latency (ms)	Duration (ms)
CS-1	Forearm	1.5	*	200	16	12
CS-2	Wrist	3.0	134%	150	16	16
CS-3	Wrist	3.0	82%	400	20	12
CS-4	Wrist	3.0	111%	300	16	16
CS-5	Wrist	1.5	59%	165	20	14
CS-6	Wrist	3.0	-37%	100	-	-
CS-7	Forepaw	3.0	76%	300	-	-
CS-8	Wrist	1.0	23%	200	-	-
CS-9	Wrist	3.0	91%	200	16	12
CS-10	Wrist	5.0	585%	300	16	12
Mean		3.0	127%	215.91	17.14	13.43
Std Dev		1.19	178%	100.27	1.95	1.90

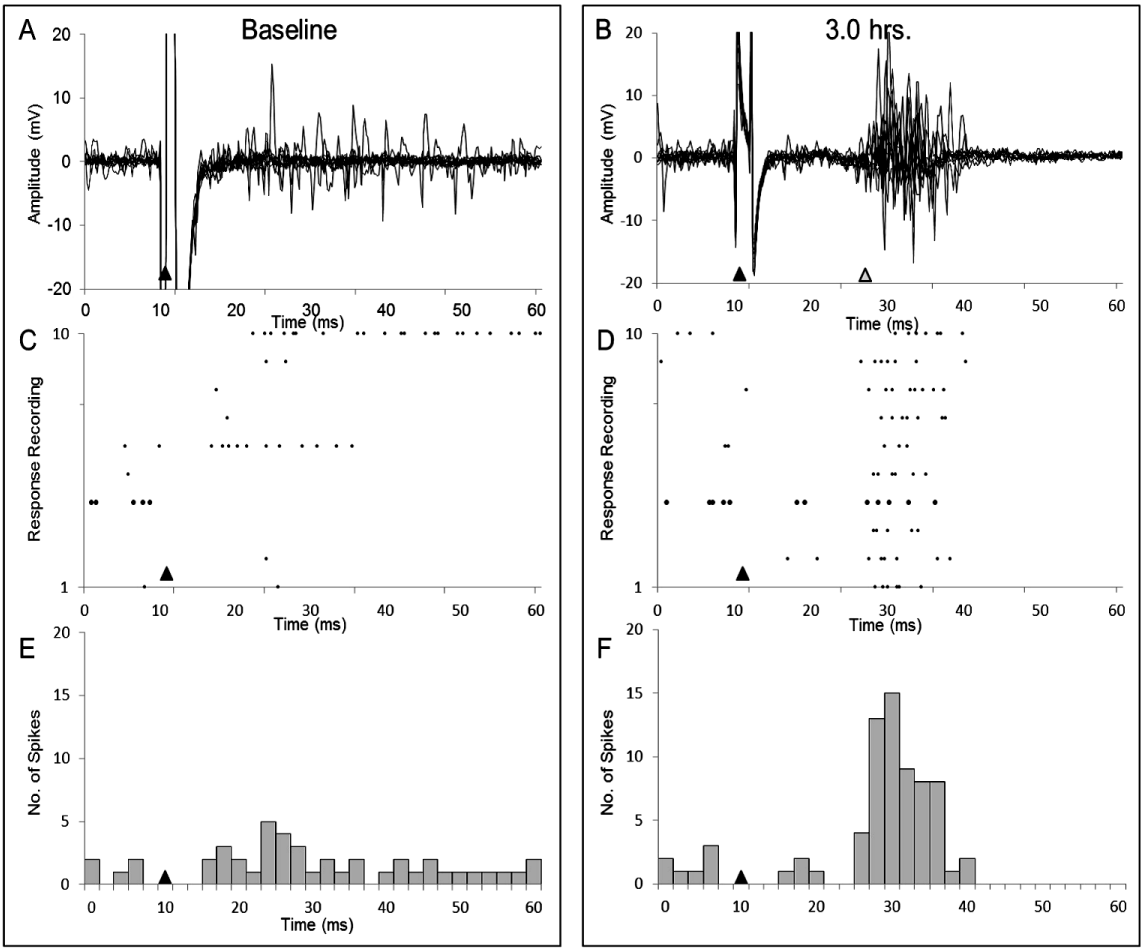

Figure 20 - Example of functional reorganization of the ulnar wrist representation after delivering 3.0 hrs. of ICMS to the interhemispheric pathway between homotopic representations. **A-B:** Composite of 10 responses recorded in ipsilateral cortex following peripheral stimulation (150 µA, 1.0 ms pulse duration, 1 Hz) applied to the ipsilateral ulnar wrist. Baseline recordings (A) show no evoked response activity, only depicts spontaneous firing; however, the recordings following 3.0 hrs. of ICMS (B) depict a delayed evoked response with a latency of approximately 16 ms. **C-D:** Raster plots for the corresponding 10 response traces illustrate no concentration of spike activity in response to ipsilateral peripheral stimulation before (C) enhancement and a newly evoked response (D) following enhancement of the interhemispheric pathway. **E-F:** Prior to enhancement no evoked response was detected (E), after enhancement (F) an evoked response with a latency of approximately 16 ms and a duration of 12-16 ms was observed. Filled and hollow triangles denote onset of stimulus and evoked response, respectively.

transcallosal connections between homotopic wrist representations, electrical stimulation (150 μA) was applied to the receptive field area on the ipsilateral wrist skin surface; a bipolar electrode was used to deliver the peripheral stimulation. Extracellular responses to peripheral stimulation were recorded from the ipsilateral barrel cortex layer V (1,100 μm) wrist representation. The composite of 10 consecutive baseline response recordings (Fig. 20A) provides evidence that the ipsilateral forelimb SI cortex was nonresponsive to ipsilateral wrist input prior to enhancement. After the interhemispheric pathway was enhanced with chronic microstimulation, ipsilateral responsiveness was obtained and is presented in Fig. 20B. The corresponding raster plots (Fig. 20C and Fig. 20D) illustrate the change in firing activity and the peri-stimulus time histograms (Fig. 20E and Fig. 20 F) depict the number of spikes detected (V_{thr} = 2mV). Prior to interhemispheric pathway enhancement, only spontaneous spike activity was detected whereas a concentration of activity was detected after enhancement. In this particular rat, the response to ipsilateral input had a latency of 15.6 ms and duration of 18 ms.

The case example where enhancement of the interhemispheric pathway did not lead to functional reorganization occurred within the forepaw representation and is shown in Fig. 21. Similar to the other experiments, peripheral stimulation was applied to the ipsilateral forepaw prior to, during, and following ICMS (3.0 hrs.). Although the pathway was enhanced at 1.59× baseline, stimulation (300 μA) of the ipsilateral forepaw failed to evoke a response in the ipsilateral barrel cortex layer V. The 40 consecutive responses to ipsilateral input taken at baseline and at 3.0 hrs. are shown in Fig. 21 A and Fig. 21B, respectively, both shows a lack of responsiveness. However, closer examination of the 3.0 hrs. responses reveals a small cluster of activity beginning to

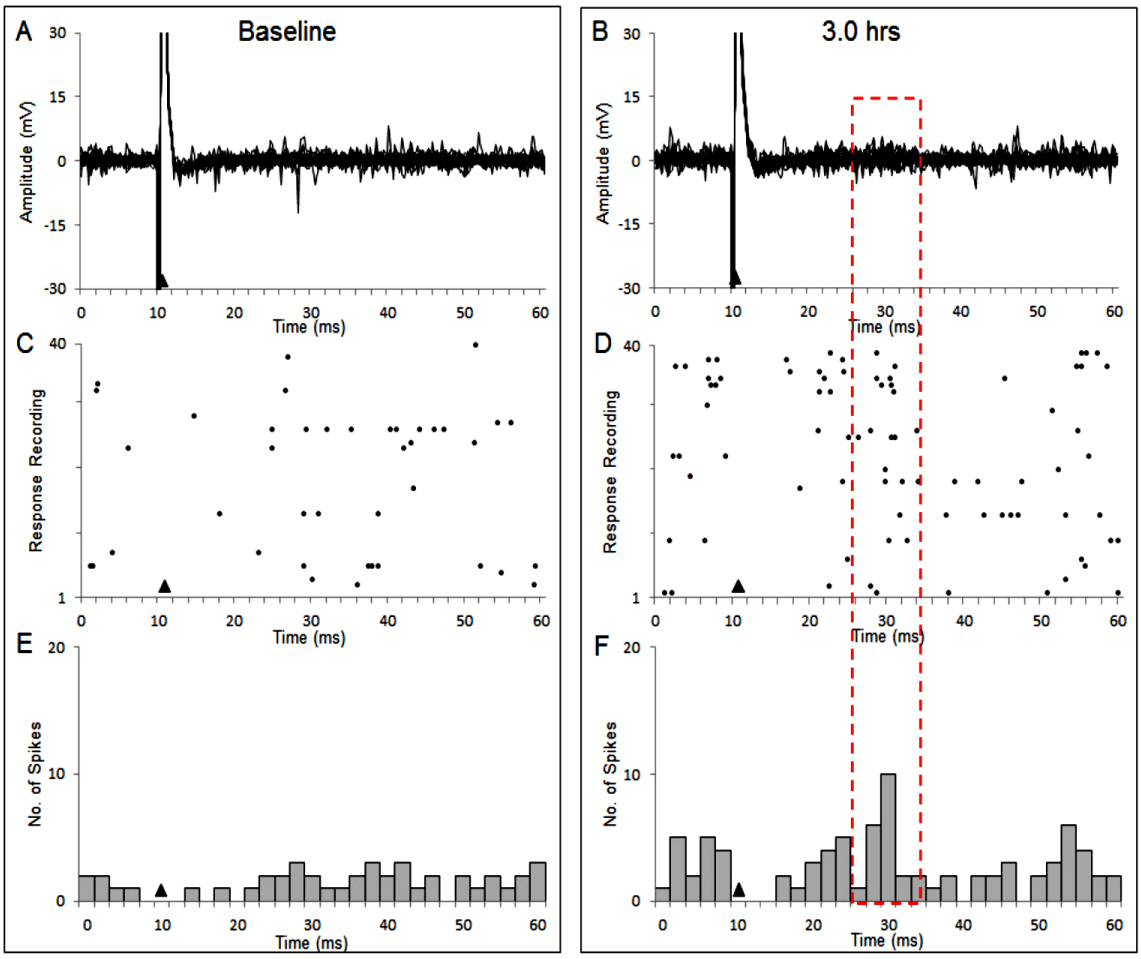

Figure 21 - Example of functional reorganization of the forepaw representation after delivering 3.0 hrs. of chronic ICMS to the interhemispheric pathway between homotopic representations. **A-B:** Composite of 40 responses recorded in ipsilateral cortex following peripheral stimulation (300 µA, 1.0 ms pulse duration, 1 Hz) applied to the ipsilateral D3. Baseline recordings (A) show no evoked response activity and minimal spontaneous firing. Similarly, ipsilateral responsiveness is readily apparent in the recordings following 3 hrs. of ICMS (B). However, close examination reveals a slight increase in response activity centered around 30 ms (black dashed outline); this could be the development of a newly evoked response. **C-D:** Raster plots for the corresponding 40 response traces illustrate no concentration of spike activity in response to ipsilateral peripheral stimulation before (C) enhancement and a slight concentration of activity at 30 ms (D) following enhancement of the interhemispheric pathway. **E-F:** Prior to enhancement no evoked response was detected (E), after enhancement (F) an evoked response was not evident, however, activity increases were observed with latencies that have previously been associated with ipsilateral responsiveness (black dashed outline). Filled triangle denotes onset of stimulus.

develop at a 20 ms latency (highlighted by red dashed box). This slight change in activity is more apparent in the examination of the raster plots (Fig. 21C and Fig. 21D) and the peri-stimulus time histograms (Fig. 21E and Fig 21F) with a voltage threshold set to 2 mV.

IV. Discussion

The present study was conducted to investigate interhemispheric pathway enhancement and functional reorganization in rat SI. Intracortical microstimulation was employed to induce firing rate changes in transcallosal connections between homotopic layer V forelimb representations and to test the hypothesis that chronic microstimulation strengthens the connectivity between the two sites. ICMS (30-90 µA, 0.5 Hz, 1.0 ms cathodal pulse duration) was delivered for up to 5 hrs. to a physiologically identified site in layer V of the forearm, wrist, or forepaw representation and responses recorded in the homotopic site in the opposite SI. Functional reorganization of the ipsilateral forelimb cortex was examined using extracellular responses to peripheral stimulation of the ipsilateral forelimb taken before, during, and after ICMS delivery. The data presented in this thesis support previous findings that repetitive ICMS can strengthen transcallosal connections and results in an increased response firing rate, they are, however, the first reported evidence *in vivo* demonstrating enhancement of interhemispheric connections between homotopic layer V forelimb representations in rodent SI and that enhancement leads to functional reorganization within rat forelimb barrel cortex. Our major findings are as follows: (1) chronic microstimulation of the interhemispheric pathway between homotopic layer V forelimb (forearm, wrist, and forepaw) representations induced changes in transcallosal connection firing rate, (2) post-ICMS changes consisted of an

increase in contralateral SI evoked response firing rate and a reduction in contralateral SI evoked response firing rate, enhanced activity is presumably facilitated by an elevated activation of callosal projections terminating on excitatory pyramidal neurons and reduced activity is presumably facilitated by an elevated activation of callosal projections terminating on inhibitory interneurons during chronic microstimulation, (3) changes in evoked response spike activity did not significantly affect the time course (latency and duration) of evoked responses, (4) enhancement within SI layer V wrist and forearm representations by chronic microstimulation led to new responsiveness to ipsilateral input from the ipsilateral wrist and forearm, respectively, (5) conversely, enhancement within the layer V forepaw representation did not lead to ipsilateral responsiveness to input from the ipsilateral forepaw; however, indications existed of an ipsilateral response developing, and (6) ipsilateral responsiveness of forelimb barrel cortex is mediated through transcallosal connections.

A. Technical Considerations

1. Interhemispheric Pathway Enhancement Site Determination

Plasticity of transcallosal connections was studied between homotopic sites in layer V forelimb barrel cortex. The bases for selecting layer V forelimb projections to test for enhancement and functional reorganization was work previously conducted in our lab and presented in abstract form (DeCosta-Fortune et al., 2010) that examined transcallosal projection patterns from layer V forelimb and shoulder representations; findings which demonstrated wrist, forearm, and shoulder SI cortex project to homotopic regions within layer V of contralateral SI and of these, projections from the wrist were consistently dense and confined to its respective homotopic site in the opposite SI. In contrast, little

evidence was found to support a homotopic relationship between forepaw cortices; rather, forepaw cortices projected primarily to neighboring cortical regions outside the contralateral FBS. As such, the forepaw representation was selected as a comparison to the effects of chronic microstimulation on homotopic projections. Clear evidence exist demonstrating layer V callosal neurons project to all cortical lamina in contralateral SI with dense connectivity occurring in layer V (Wise and Jones, 1977b; Akers and Killackey, 1978) and our work corroborated this in both wrist and forepaw barrel cortex (DeCosta-Fortune et al., 2010). Furthermore, no evidence exists of bilateral forelimb receptive field neurons in rodent SI (Shin et al., 1997), thus providing an ideal control condition from which to induce responsiveness to new input, specifically ipsilateral forelimb input.

2. Establishing an Interhemispheric Connection

In the present study, neurons with similar receptive fields were physiologically identified in layer V of both SI cortices, one served as the stimulation site while the other served as the recording site in contralateral barrel cortex. To test for callosal connectivity between the two sites, chronic microstimulation was delivered to the stimulation site and evoked responses were examined in contralateral SI from the recording electrode. A strong connection between two neurons manifests itself in form of one neuron repeatedly evoking response activity in the second neuron. As such, a strong interhemispheric connection was established when the maximum evoked response to ICMS was achieved; to achieve maximal responsiveness, slight adjustments were made to the recording electrode depth, while remaining in layer V.

3. Characterizing Enhancement

Our characterization of interhemispheric pathway enhancement as a persistent increase in evoked response firing rated is based on Hebbian theory whereby connectivity between two neurons is strengthened when the projecting neuron repeatedly contributes to the activation of the target neuron (Hebb, 1949). In the present study, enhancement was defined as an increase in neuronal firing activity of 1.5× over baseline (prior to ICMS delivery) and was examined in multiunit response recordings; an amplitude voltage threshold was established from the baseline response and employed against all subsequent response recording to detect changes in number of spikes. Increases in spikes detected may have originated from either a single neuron firing faster or the recruitment of additional neurons responding to the delivered stimulus. While a significant ($p \leq 0.05$) increase in spike activity was measured after 2.5 hours of chronic microstimulation and remained, in 1 rat, for up to 5 hrs., the enhancement criteria was reached on average after 1.5 hrs. of ICMS; significant changes to evoked response latency or duration were not observed. Long-term changes of transcallosal excitatory connections have been associated with an increase in the number and efficiency of connections (Bogdanova and Sil'kis, 2002). Since temporal aspects of responsiveness (latency and duration) were not significantly affected by chronic microstimulation, it is likely that the increase in activity is due to the recruitment of additional neurons to respond.

B. Long-Term Potentiation (LTP)

Long-term potentiation (LTP) following tetanic stimulation delivered to vertical and horizontal SI cortical synapses in rodent (Aroniadou-Anderjaska and Keller, 1995) has been accompanied by a horizontal spread of ipsilateral potentiation in layer II/III (Lee et

al., 1991), a vertical spread of ipsilateral potentiation from layer IV to layer II/III (Glazewski et al., 1998), and enhanced cortical response magnitude (Lee et al., 1991; Lee and Ebner, 1992). To induce LTP, levels of excitability need to be sufficiently elevated through an increase in *N*-methyl-D-aspartate (NMDA) receptor activation of excitatory cells or a diminished level of inhibition from a reduction in gamma-aminobutyric acid (GABA) receptor activation (Lee et al., 1991; Lee and Ebner, 1992). The threshold to induce LTP has been achieved, *in vitro* slice preparations, by reducing extracellular concentrations of Mg^{2+}, which increased activation levels of NMDA receptors (Lee et al., 1991; Lee and Ebner, 1992), and introducing low concentrations of a $GABA_A$ blocker such as biculline (BIC) to the recording site (Bindman et al., 1988; Artola et al., 1990) which disinhibited inhibition. Excitatory transcallosal connections can be induced by rhythmic stimulation (Sah and Nicoll, 1991) and provide a sufficient environment to study enhancement by elevating the activation levels of NMDA channels (Thomson, 1986). One important finding of the present study is that repetitive low frequency (0.5 Hz) ICMS of transcallosal connections between homotopic SI forelimb representations can increase responsiveness in contralateral SI; in 7 out of 10 rats, enhancement was associated with a $\geq$ 50% increase in evoked response firing rate. Note that transcallosal connections have been generally reported as being scarce in cortical regions associated with the forelimb (Wise and Jones 1976; Manzoni, 1980; Hayama and Ogawa, 1997; Henry and Catania, 2006); however this was not without exception (DeCosta-Fortune et al., 2010).

C. Long-Term Depression (LTD)

Numerous studies have indicated that high frequency stimulation induces long-term changes in rodent SI responsiveness to stimuli and these changes are generally reported as LTP (Recanzone et al., 1992b; Dinse et al., 1993; Kalarickal and Marshall, 2002). However, it has also been demonstrated that chronic microstimulation can induce long-term depression (LTD) of synaptic efficiency (Heusler et al., 2000) of both excitatory and inhibitory connections (Bogdanova and Sil'kis, 2002). It has been suggested that LTD following chronic microstimulation occurs when the pathway being stimulated has both monosynaptic excitation and disynaptic inhibition and is facilitated by an increased excitation of inhibitory interneurons (Bogdanova and Sil'kis, 2002). In rodent, following a 24 hour period of chronic whisker stimulation, a dense increase in spineous GABAergic synapses was reported in the corresponding contralateral barrel cortex and thought to have mediated the observed depressed responsiveness (Quairiaux et al., 2007). In our study, a reduction in contralateral SI evoked response firing rate was observed in 1 rat where changes in responsiveness were depressed 18% following 3.0 hours of chronic microstimulation.

D. Modulating GABAergic Inhibition

We previously demonstrated neurons in rodent forepaw barrel cortex receive short latency suprathreshold input from a principle location on the forepaw and longer latency subthreshold input from a surrounding forepaw skin surface (Li et al., 1996); other investigators have reported similar findings in rodent vibrissa barrel cortex with the displacement of a primary whisker (suprathreshold input) and adjacent whiskers (subthreshold input) (Carvell and Simons, 1988; Moore et al., 1998). Preexisting

subthreshold input can become expressed after being raised to suprathreshold levels (Calford and Tweedale, 1990; Smits et al., 1991; Li et al., 1996; Moore et al., 1998) which has been shown to occur following the release of GABAergic inhibition (Carvell and Simons, 1988; Smits et al., 1991; Moore et al., 1998; Li et al., 2002). Waters and colleagues (2002) injected a $GABA_A$ receptor blocker into the FBS and reported suppression of GABAergic inhibition was accompanied by enhanced responsiveness to stimulation from the surrounding RF which had previously provided subthreshold input.

$GABA_A$ receptors receive excitatory inputs, in part, from callosal projecting neurons (Pluto et al., 2005). In rodent SI, these neurons are pyramidal cells located primarily in layer III and layer V (Yorke and Caviness, 1975; Wise and Jones, 1976; White and DeAmicis, 1977); layer V pyramidal neurons are reported to yield sub- and surprathreshold responses (Manns et al., 2004). Also, in rabbit SI, callosal projecting neurons at cortical depths corresponding to layers II/III – V exhibited sub- and suprathreshold RF characteristics (Swadlow and Hicks, 1996). Callosal projections terminate predominately in layers III and V of the opposite SI (Wise and Jones, 1976; Akers and Killackey, 1978; Koralek and Killackey, 1990) on both excitatory pyramidal neurons and inhibitory interneurons (Pluto et al., 2005) providing direct excitation and indirect inhibition to target neurons. By modulating excitatory input callosal connections can modulate inhibition (Clarey et al., 1996; Shuler et al., 2001; Swadlow, 2003; Rema and Ebner, 2003).

E. Functional Reorganization

Cortical neurons receive both excitatory and inhibitory inputs, the combination of which determines whether a neuron's response to afferent input is sufficient to reach

firing threshold and firing rate is modulated by increasing and decreasing inhibitory transmission (Vogels et al., 2011). Barrel cortex neurons respond best to contralateral stimuli but are also influenced by ipsilateral input (Li et al., 2005). Functional reorganization, in the present study, was characterized as a functional connection between the ipsilateral forelimb barrel cortex and ipsilateral forelimb whereby evoked responses to ipsilateral input was recorded. In all 7 rats, ipsilateral responsiveness of forelimb barrel cortex accompanied interhemispheric pathway enhancement. This data suggest the appearance of new bilateral RF neurons is facilitated by strengthened transcallosal connectivity resulting from chronic stimulation modulating inhibition.

CHAPTER IV

INTERACTIVE NEURONAL STIMULATION AND RECORDING DEVICE

I. Background

Cortical reorganization in the primary somatosensory (SI) cortex is a central neurological consequence that follows limb amputation (Knecht et al., 1995, 1996; Flor et al., 1997, 1998; Borsook et al., 1998; Weiss et al., 2000) and occurs during post stroke recovery (Schaechter et al., 2006; Roiha et al., 2011); it is an innate mechanism that permits changes in the neural pathways and synaptic connectivity of cortical circuits that provides us with lifelong ability to compensate for injury. Understanding this critical mechanism is necessary for developing alternative compensation strategies and rehabilitation therapies. The ability to modulate cortical circuits to become responsive to new input is of great interest among clinicians and neuroscientists as it may indicate our ability to modulate the cortical reorganization that follows amputation and the plasticity that occurs while rehabilitating stroke patients.

Chronic microstimulation and physiological recording are fundamental techniques used in modulating cortical connections to further enable us to understand and characterize cortical plasticity (Recanzone et al., 1992b; Dinse et al., 1993; Heusler et al., 2000; Bogdanova and Sil'kis, 2002; Kalarickal and Marshall, 2002). This approach of using stimulation to induce modulation of cortical connections is based on Hebb's cell assembly theory wherein the connection between two neurons is strengthened when one cell repeated or persistently participates in the excitation and firing of the second cell (Hebb, 1949). Conventional methods of employing these techniques typically require

that the subject be sedated and/or physically tethered to the stimulating and recording devices. These constraints are minimized, if not eliminated, through the use of wireless neural interfacing systems.

In recent years, there has been much success with advances in telemetry-based neural interfacing systems for electrical stimulation (Xu et al., 2004; Thurgood et al., 2008, 2009; Arfin et al., 2009) or recording neural activity (Obeid et al., 2004; Farshchi et al., 2006; Harrison et al., 2007, 2008; Fan et al., 2011). However, few systems have demonstrated the capacity to simultaneously deliver stimulation and record response activity. Investigating cortical circuit modulation in freely behaving animals necessitates that the functional capabilities of both stimulation and recording be integrated into a cohesive system.

Fetz and colleagues (Jackson et al., 2006b, 2007) developed an autonomous microcontroller-based neural device, known as the Neurochip, which features separate circuits for stimulation and recording that can be connected. Collectively these circuits have the capacity to deliver pre-defined biphasic micro-stimuli up to 100 μA and record activity through electrodes chronically implanted in the cortex of freely moving non-human primates. After a few days of use, this device led to an artificial connection between two sites in primary motor cortex (MI) by enabling spike activity recordings from one site to trigger the stimulation of a second site. This system is limited in that it does not feature the ability to either remotely control the delivery of stimulation or monitor responses in real time; instead pre-programmed biphasic stimulation is delivered and response activity is stored on the Neurochip.

By leveraging the recording functionality of an existing wireless neural data acquisition system fabricated by Farshchi et al. (2005), Judy and colleagues developed a TelosB mote-based neural stimulator and combined their capabilities into one device (Fernando et al., 2007). This stimulator has the capacity to operate as either a constant current (0-20 mA) or constant-voltage (0-5 V) source. It features the ability to generate user-defined mono-, bi-, and pseudomonophasic pulses. However, this stimulator device does not have the capability to provide intracortical microstimulation (ICMS), which may be applied to modulate cortical circuits. While this system has been validated *in vitro* with tissue section preparations, it remains to be demonstrated *in vivo*.

Here we describe an interactive neural device that has been demonstrated *in vivo* for the controlled delivery of telemetry-based microstimulation and real-time recording of response activity. Communication between the remote device and a host computer is based on a Bluetooth to virtual serial port interface. Residing on the host computer is a custom application featuring user-definable stimulation and recording parameters that may be reprogrammed and transmitted to the remote device at any time during its operation. After receiving stimulation and recording parameters, the remote device stimulator operates autonomously; however, retrieval of recorded data requires that an open port be maintained between the remote device and host computer.

We have tested the operational performance of the system *in vivo* in anesthetized Sprague-Dawley rats. This system routinely delivered microstimulation with varying intensities and durations to a single microelectrode inserted into a layer V forelimb representation in SI. The recorder analog front end successfully recorded neural signals from a separate microelectrode inserted in a homotopic layer V forelimb site in

contralateral SI under three primary conditions: (1) in the absence of microstimulation, (2) in response to microstimulation delivered to the homotopic forelimb representation in contralateral SI, and (3) in response to manual peripheral stimulation of the contralateral forelimb. While digitized response data was effectively transmitted to the host computer and stored, signal distortion was present. This system serves as a prototype in the development of a compact microstimulation and recording device for use in freely behaving small animals to further examine cortical plasticity.

II. System Design

A single channel wireless system was developed for the controlled delivery of chronic microstimulation and real-time recording of neural signals. It represents the first phase in the fabrication of a compact neural interfacing device that can be used to induce cortical circuit modulation and examine cortical reorganization in freely moving rats. Both hardware and software aspects of this system are reconfigurable allowing for easy expansion to multiple channels, increased functionality, and minimization to a wearable backpack size.

A. System Model

The wireless stimulation and recording system consists of two main units: a base unit and a remote unit. A block diagram (Fig. 22) of the system illustrates the division between the two units and highlights their primary components. The base unit is a host computer with Bluetooth enabled capabilities; it features a custom windows-based application that provides an intuitive graphical user interface (GUI) for establishing and controlling both stimulation and recording parameters. The remote unit is a small printed circuit board (PCB) measuring 4.2 cm × 7.1 cm that contains (1) a Programmable System

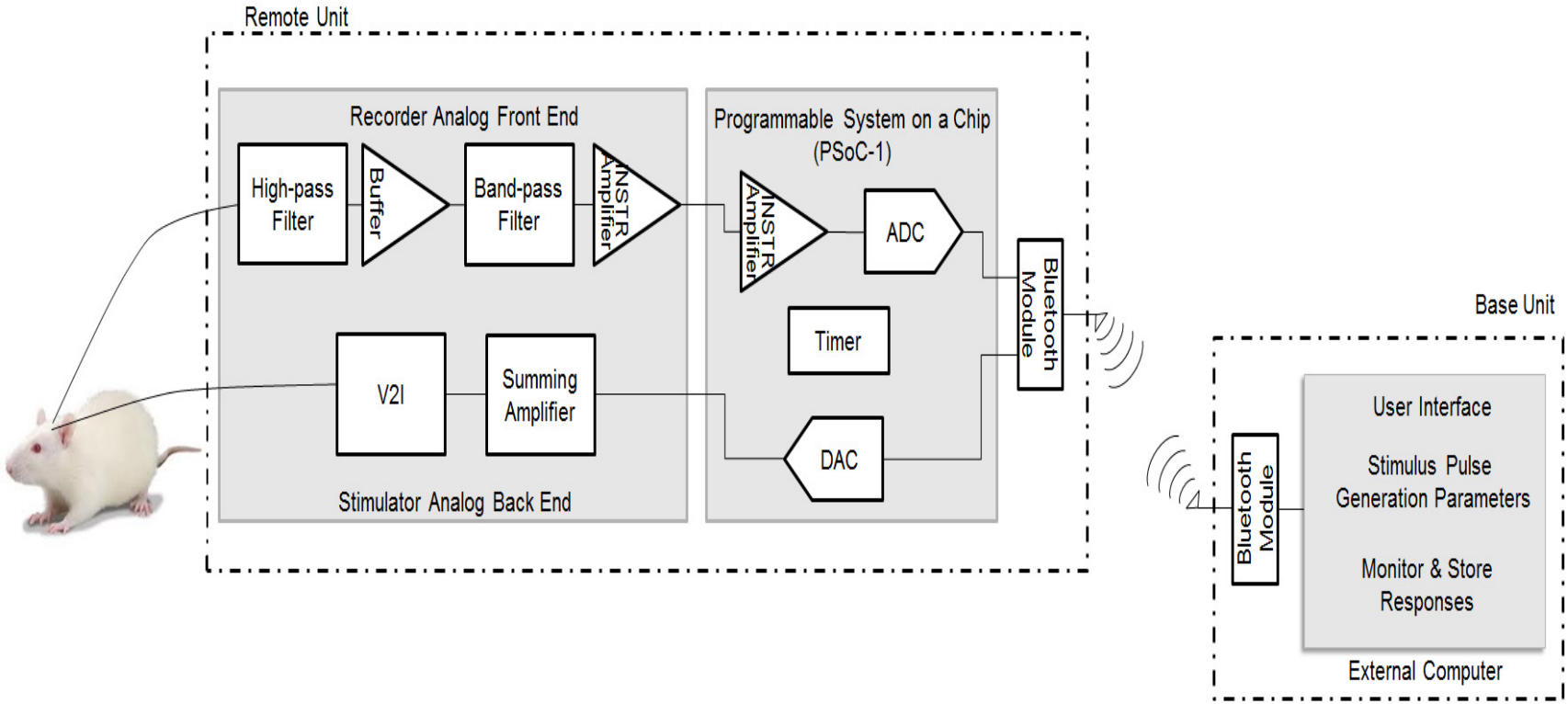

Figure 22 – Block diagram of wireless stimulating and recording system architecture. Stimulator capabilities include: Mono-, bi-, or pseudomonophasic pulse generation with user controlled amplitude, pulse width, frequency, and delay. Stimulation duration may be established for a set number of pulses (calibration mode) or for a set period of time (chronic mode). Recorder capabilities include: Record 150 ms of neuronal activity responding to a set number of consecutive stimulations at a set interval of time. Telemetric transmission: Real-time wireless transmission between base and remote unit of stimulation pulse parameters for chronic microstimulation and neural response activity for storage and off-line analysis.

on a Chip (PSoC) microcontroller that receives and executes the specific controls, (2) stimulator analog back end circuitry, (3) recorder analog front end circuitry, and (4) a Bluetooth module for wireless communication.

The stimulator can deliver mono-, bi-, and pseudomonophasic microstimulation with varying intensity (0-100 μA), duration (1-10 ms), delay (1-10 ms), and frequency (0.5 Hz or 1 Hz) to a single microelectrode (100 kΩ at 1 kHz). It is comprised of a digital front end (DFE) and an analog back end (ABE). The stimulator DFE receives and converts the digital stimulation parameters for processing by the ABE, which generates and delivers the stimulus pulses to the implanted stimulating electrode. Stimulation can be delivered as a set number of pulses (calibrate mode) or over a set period of time (chronic mode). After receiving the stimulation parameters, the stimulator operates autonomously; however, changes to the stimulation parameters can be made real-time and retransmitted to the remote device.

The recorder acquires neural signals from a separate microelectrode (100 kΩ at 1 kHz). It consists of an analog front end (AFE) and a digital back end (DBE). The ABE buffers, filters, and amplifies the transduced neural signals received prior to digitization by the DBE, which samples the first 150 ms of the recorded signal at 11 k samples per sec. The DBE transmits the recorded data in real time to the host computer for off-line storage and analysis. Two versions of the recorder AFE were developed, the differences of which are related to filtering bandwidth and system gain.

B. User Interface

Real-time interfacing with the remote device is done through a custom Windows-based application written in C# that is housed on the base unit host computer. The

custom Wireless Interactive Neuronal Stimulation and Recording (WINSR) application provides a simple and intuitive GUI that enables users to define unique stimulation and recording parameters; a screenshot of which is shown in Fig. 23. This application features the ability to remotely administer stimulation and recording, configures and controls the opening/closing of a virtual serial port, outputs stimulation and recording parameters, inputs recorded response data, and stores recorded data in .CSV format for off-line analysis.

WINSR has two modes of operation: calibrate and chronic. In calibrate mode, the user provides the number of stimulation pulses to be generated, N_oP_{ulse}, and the time interval at which they will be generated, t_{gen}. When operating in chronic mode, stimulation duration, t_{dur}, is given in addition to t_{gen}.

Users have the option to generate a mono-, bi-, or -, pseudomonophasic stimulus waveform of either negative or positive polarity. Anodic and cathodic pulse segments to generate the various waveforms are governed by user defined amplitude (A_{anodic}, $A_{cathodic}$), duration ($t_{dur\text{-}anodic}$, $t_{dur\text{-}cathodic}$), delay ($t_{del\text{-}anodic}$, $t_{del\text{-}cathodic}$), and frequency (*f*). The left picture box of Fig. 23 depicts a sample stimulus pulse annotated with parameters of interest. WINSR allows user to capture neural data by specifying the number of responses, N_oR_{esp}, to consecutive stimulations, the interval at which they will be collected, t_{rec}, and the file location where data will be saved in .CSV format; during operation, the streaming data can be viewed in the right picture box of Fig. 23. Valid stimulation and recording parameter ranges are summarized in Table 4.

A string of stimulation and recording parameters, based on user entries, is transmitted to the remote device upon opening the virtual serial port, *Open Port*, and

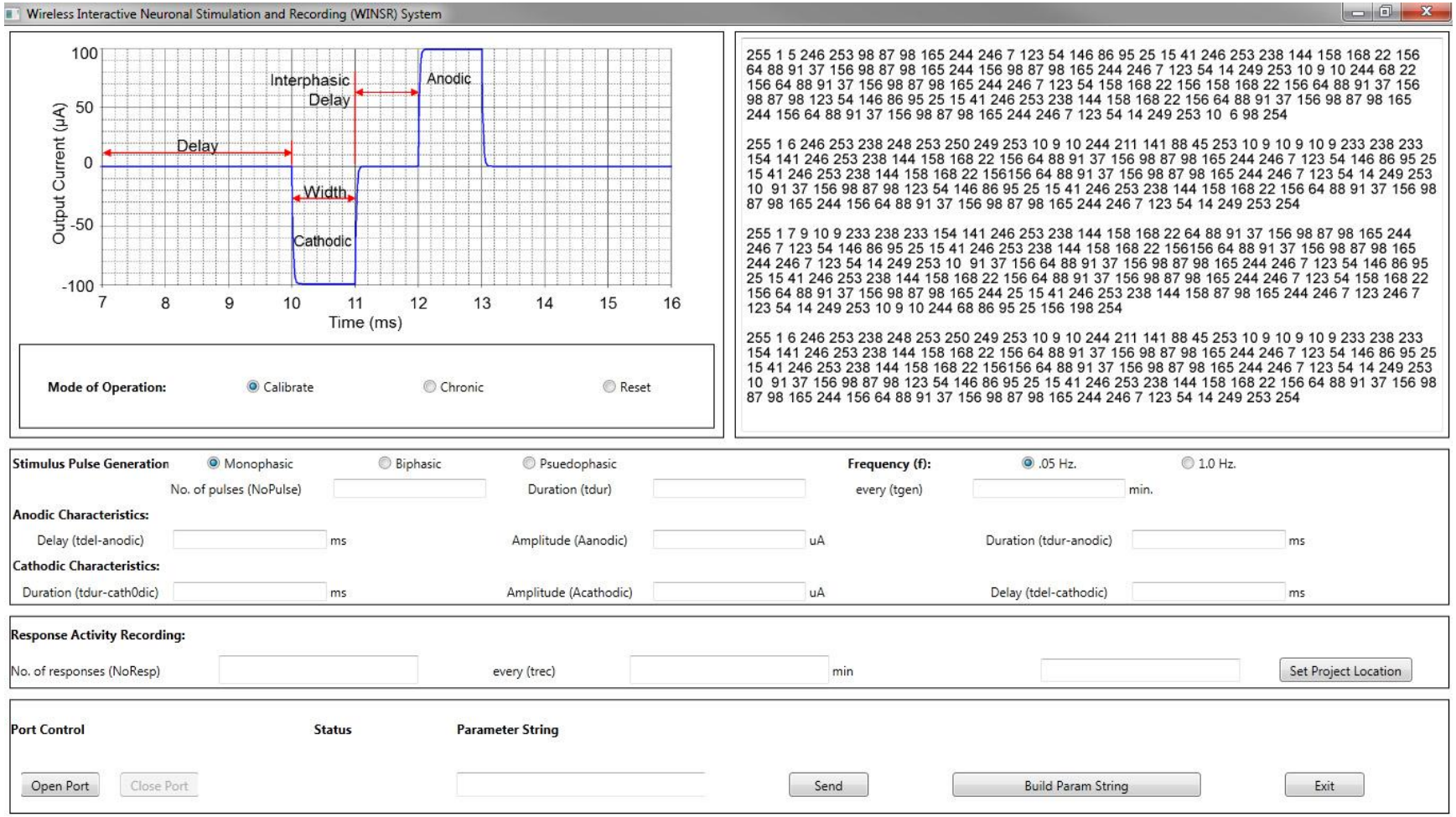

Figure 23 – Screen capture of the Wireless Interactive Neuronal Stimulation and Recording (WINSR) application residing on the host computer (base unit). It is used to interface with the remote unit PCB. Users enter specific experimental controls for stimulus pulse generation and response recording.

Table 4 – Valid stimulation and recording parameter ranges for the Wireless Interactive Neuronal Stimulation and Recording (WINSR) application.

Unit	Parameter	Variable	Value	Unit of Measure
Mode of Operation	Calibrate – Number of Pulses	N_oP_{ulse}	0-255	count
	Chronic – Stim. Duration	t_{dur}	0-1440	min
	Stimulation Interval	t_{gen}	0-1440	min
Stimulator	Amplitude (Anodic, Cathodic)	A_{anodic}, $A_{cathodic}$	0-100	µA
	Duration (Anodic, Cathodic)	$t_{dur\text{-}anodic}$, $t_{dur\text{-}cathodic}$	1-10	ms
	Delay (Anodic, Cathodic)	$t_{del\text{-}anodic}$, $t_{del\text{-}cathodic}$	0-40	ms
	Frequency	f	½ , 1	Hz
Recorder	Number of responses	N_oR_{esp}	0-255	count
	Recording Interval	t_{rec}	0-1440	min

selecting the *Send* button. The port may be closed, *Close Port*, at any time during the experiment without interrupting stimulus delivery. However, closing of the port will prohibit recorded data from being received. Adjustments to the stimulating and recording parameters can be made and re-transmitted to the remote device at any time during its operation.

C. Wireless Communication

Since numerous wireless systems are commercially available for integration into our system, it was preferable to develop a bi-directional telemetry system based on an existing platform that has been quality tested. Design of the system includes a wireless connection between two Bluetooth enabled devices, the host computer (master) and a Class 2 Bluetooth module (slave) residing on the remote unit PCB. A connection having baud rate of 115.2 kbits/sec is established over a virtual serial port. The RN-42 (Roving

Networks, Inc.) surface mount device (SMD) was selected as the slave module; it features low power consumption and offers a reported operating range of 50-60 ft. Because the Bluetooth platform requires the host computer to support the telemetry hardware (e.g. RN-42), consideration was given to the overall size and weight the slave device would add to the remote device; this Bluetooth version 2.1 +EDR device operates in the 2.414-2.484 G Hz frequency band, weighs < 0.05 oz. and measures 13.44 mm × 25.8 mm × 2 mm.

The Bluetooth circuit schematic, drawn with Cadence Allegro 16.5, is shown in Fig. 24. This system design illustrates a 500 mA peak output current linear voltage regulator (MIC5219-3.3BM5, Micrel, Inc.), Fig. 24A, was used to step down the remote unit supply voltage (V_{in}) to the 3.3 V required by the RN-42 (Fig. 24B). Data representing the stimulation and recording parameters (WINSR_Output) and recorded action potentials (WINSR_Input) are received and transmitted, respectively, by the RN-42 using a virtual serial port on the host computer. Device size 0603 was used for passive and active components, size D for tantalum capacitor (C3), and Small Outline Transistor (SOT) 23-5 for the regulator; component sizes are provided in Appendix A.

D. Programmable System on a Chip (PSoC)

Design of the remote unit was based on the Programmable System on a Chip (PSoC) architecture (Cypress Semiconductor Corp.); its features include the ability to integrate a microcontroller, memory, and configurable peripheral (analog and digital) functions onto a single chip. The PSoC architecture is available on three platforms: PSoC-1, PSoC-3, and PSoC-5. Requirements for our neural device were met using the PSoC-1 platform, which can readily be migrated to either the PSoC-3 or -5 platforms.

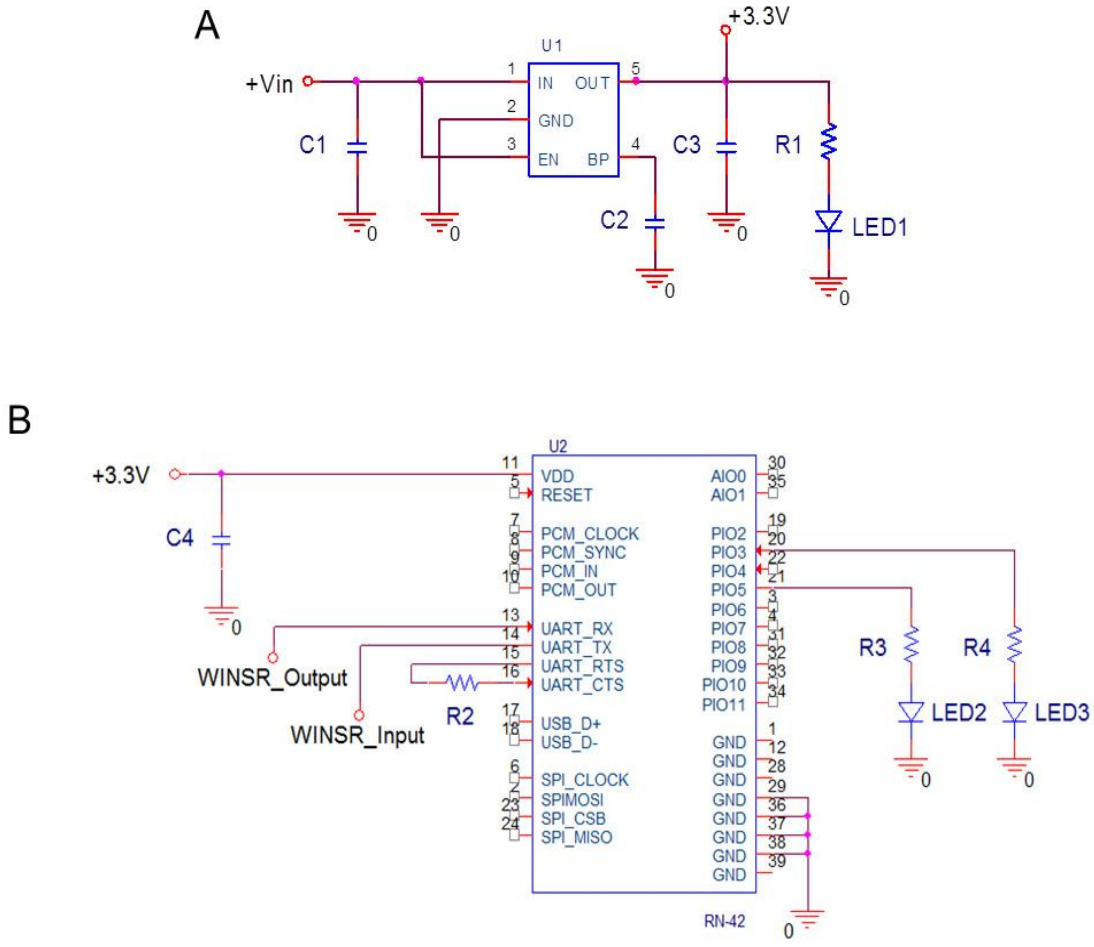

Figure 24 – Circuit schematic for wireless communication between base and remote units. This design guarantees regulated supply voltage (A) and utilizes the RN-42 (B). V_{in} is provided from an external power supply. WINSR_Output and WINSR_Input connect to the PSoC for receiving stimulation parameters and transmitting response potentials, respectively.

The PSoC-1 chip (CY8C28452-24PVXI) used in our design is powered by a proprietary 8-bit M8C central processing unit (CPU) core and presents 12 analog blocks, 8 digital blocks, and 24 general purpose input/output pins (GPIOs). Custom programming and configuration was accomplished using the PSoC Designer 5.2 Software Development Suite provided by Cypress Semiconductor Corp. This development environment contains a variety of pre-characterized analog and digital hardware peripherals, each with a specific set of application protocol interfaces (APIs). All additional programming was developed in the Suite's application editor and written in C.

After receiving the stimulation parameters from WINSR, two independent 9-bit digital-to-analog converters (DACs) are used to generate two positive voltage signals that are proportional to the stimulus amplitude; one output signal corresponds to the anodic pulse segment and the other to the cathodic pulse segment. These signals serve as the inputs to the stimulator ABE for processing and pulse delivery to the stimulating electrode. Stimulus pulse timing includes pulse delay, duration, and frequency. For each stimulus pulse generated, the PSoC produces a separate 5.0 V pulse at t = 0 ms that can be used as an external trigger delivered to an independent data acquisition system; use of the external trigger pulse allows for pre-stimulus response activity to be recorded.

Furthermore, the PSoC receives, amplifies (variable gain of 2.0-16.0×), and digitizes (11 ksps, 8-bit analog-to-digital converter [ADC]) neural data processed by the recorder AFE. For tracking purposes, the PSoC assigns a response trace and timing interval number to each recorded response data segment. The PSoC operates on a 5.0 V 24 MHz system clock and timing of the remote unit functionality is controlled by two general purpose timers, an 8-bit timer (stimulator) and a 16-bit timer (recorder).

E. Stimulator Analog Back End Circuitry

The stimulator ABE is comprised of a single channel with two processing stages: a differential amplifier and a voltage-to-current (V2I) converter; the circuit schematic shown in Fig. 25 was drawn with Cadence Allegro 16.5. The ABE is driven by an active PSoC that generates two analog voltage signals corresponding to the anodic and cathodic pulse segments (V_{anodic}, $V_{cathodic}$), which serve as inputs to the differential amplifier. A compliance voltage of ± 20 V was governed by the requirement to deliver a 100 μA biphasic stimulus pulse to a 100 kΩ load. As such, two voltage regulator circuits (Fig. 25A) were developed to step down the supply voltage and generate the ± 12 V for the differential amplifier (AMP1). Fig. 25B presents the schematic for the single channel stimulator. Design of the stimulator ABE allows for easy expansion to multiple channels. All components are commercial off-the-shelf and readily available; specific device values used are provided in Appendix A.

1. Differential Amplifier (AMP1)

The first stage of the stimulator ABE is a differential amplifier, inputs to which are two PSoC analog output voltage signals proportional to the anodic (V_{anodic}) and cathodic ($V_{cathodic}$) stimulus pulse amplitude and duration. The differential amplifier, a Texas Instruments TL081 featurs a common mode-rejection ratio (CMRR) of 86 dB; CMRR is an indicator of the goodness of an operational amplifier as it is an measures the tendency of the amplifier to reject the input signals that are common to both inputs. AMP1 generates the desired stimulus waveform by amplifying the difference between the two

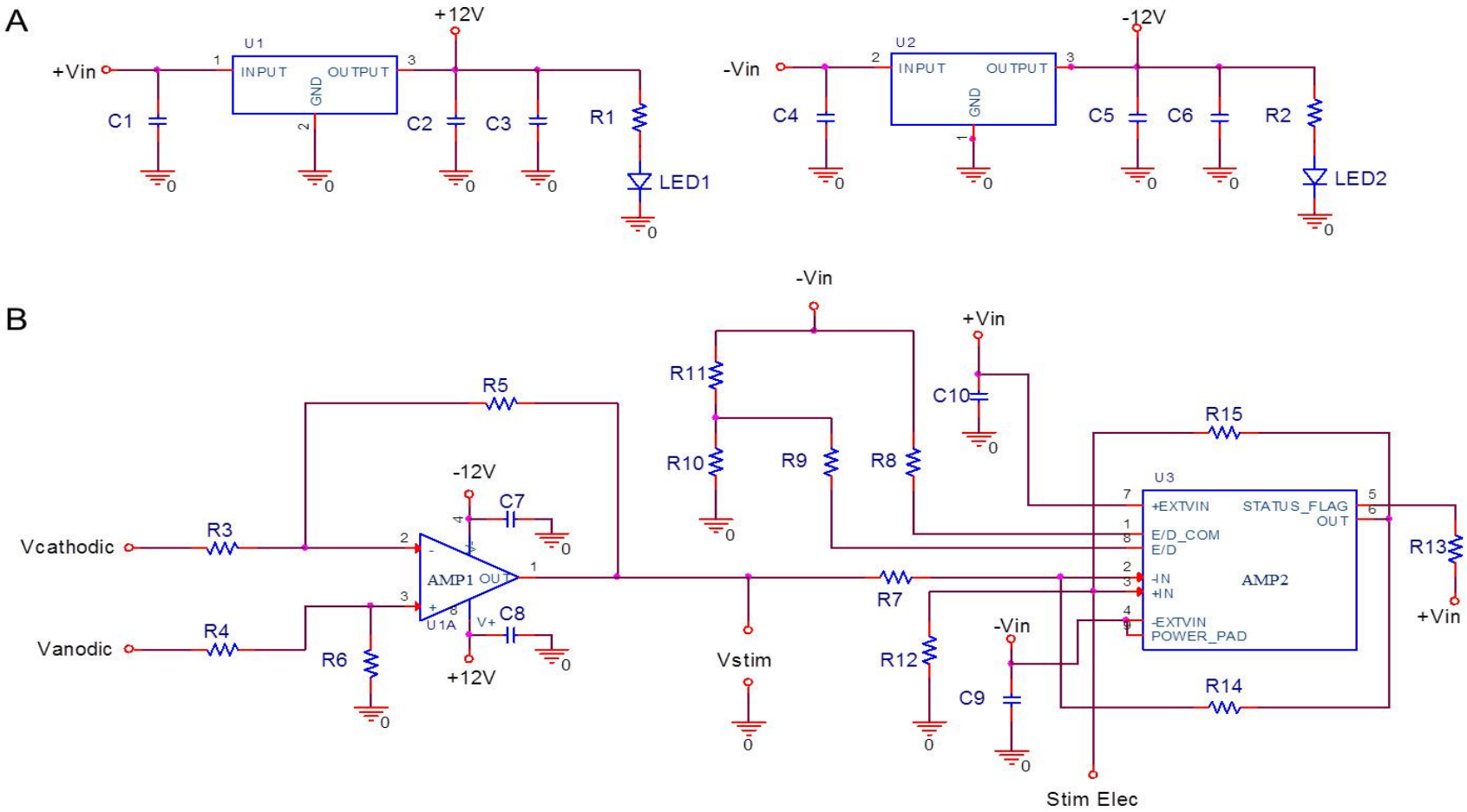

Figure 25 – Single channel stimulator analog back end circuit schematic. **A:** Positive and negative power regulation. $+V_{in}$ and $-V_{in}$ are connected to positive and negative power supplies. **B:** Single channel stimulator analog back end circuit schematic consisting of a differential amplifier acting as a subtractor and a voltage-to-current converter. The two voltage inputs, V_{anodic} and $V_{cathodic}$, are taken from the analog voltage outputs of the PSoC; V_{anodic} and $V_{cathodic}$ are the voltage output signals proportional to the user defined anodic and cathodic stimulus pulse parameters, respectively.

input voltage signals. The circuit uses balanced resistive ratios, such that R_3:R_5 is equivalent to R_4:R_6. Given that $R_3 = R_4$ and $R_5 = R_6$, the output voltage, V_{out}, is governed by Eq. 1. The differential amplifier has a fixed gain of 0.1.

$$V_{out} = \left(\frac{R_5}{R_3}\right)(V_{anodic} - V_{cathodic}) \quad (1)$$

2. Voltage to Current Converter (AMP2)

Design of the voltage-to-current converter (V2I) stage leverages a Negative Impedance Converter (NIC) circuit configuration. By setting $R_7 = R_{14}$ and $R_{12} = R_{15}$, the NIC acts as V2I that provides an output current, I_{stim}, directly proportional to the input voltage signal, V_{stim}, and is independent of the load, Z_{load} (Sedra and Smith, 1987); this holds true for voltages up to the V2I supply voltage. In the case of our design the input voltage signal, V_{stim}, is generated from the differential amplifier AMP1. The load current and transfer function for this stimulator stage are given as Eq. 2 and 3, respectively.

$$I_{stim} = \left(\frac{V_{stim}}{R_{14}}\right) \quad (2)$$

$$\frac{V_o}{V_i} = \left(\frac{-R_{15}}{R_7 R_{14}}\right) Z_{load} \quad (3)$$

A Texas Instruments OPA454 was used for AMP2; this device features a wide power supply range of ± 5 V to ± 50 V, a high current drive of 50mA, and CMRR of 88 dB.

F. Recorder Analog Front End Circuitry

During the course of this dissertation research two versions of the AFE were developed that differ with respect to filtering range and amplification. Version 1 of the recorder is described in this dissertation and only the differences pertaining to Version 2 are described where applicable.

The recorder AFE is comprised of a single channel with four processing stages: high-pass filter, voltage follower, band-pass filter, and an amplifier; all of which are consistent with standard approaches found in neural data acquisition systems. The circuit schematic for the single channel recorder AFE is shown in Fig. 26 and was drawn using Cadence Allegro 16.5. The system was designed to amplify 12,500× (82.1 dB) spike level activity (100-400 μV) within the frequency range of 510 Hz to 5250 Hz and a cut-off of 79.1 dB. The basis for our recorder AFE design was the Neurochip (Mavoori et al., 2005; Jackson et al., 2006c). Power is supplied from the two LDO ±12V regulators described previously in section E and shown in Fig. 25A. A Texas Instruments quad package chip, TL084, was used for AMP1-4, each having a maximum supply voltage of ± 15 V, CMRR of 86 dB, and an input noise voltage of 4 μV/√Hz for frequencies of 10 Hz to 10 kHz. Because neural signals are superimposed onto voltage offsets generated at the electrode-tissue interface, devices with a high CMRR were used.

The second version of the recorder AFE leverages the high-pass filter (220 Hz), has a reduced gain 8,000× (78.4 dB), an expanded frequency range (375-6425 Hz), and a

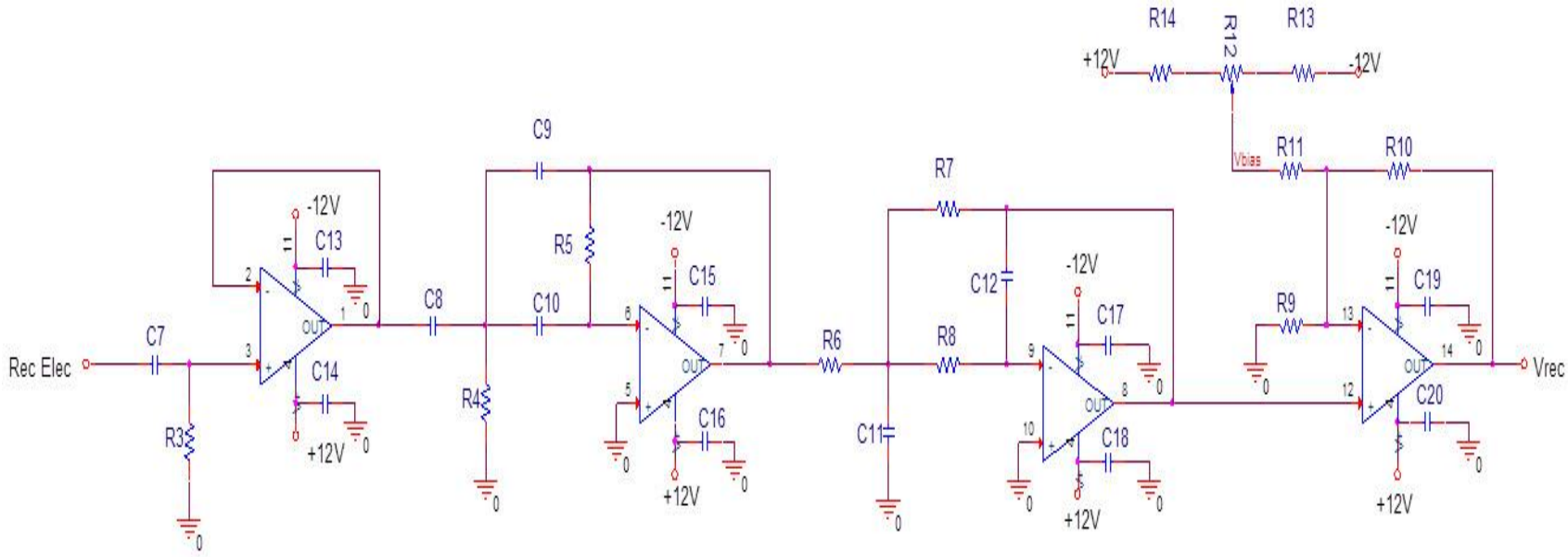

Figure 26 – Single channel recorder analog front end circuit schematic. Input potential from the inserted recording microelectrode (Rec Elec) is high-pass filtered, buffered, band-pass filtered, and amplified. The output voltage signal, Vrec, is fed to the recorder digital back end through a PSoC analog general purpose input/output pin.

75.4 dB cut off. Both versions utilized components that are commercial off-the-shelf and readily available. Device size 0603 was used for passive and active components; specific values used are provided in Appendix A.

1. High Pass Filter

The first stage of the AFE is comprised of a high pass filter (HPF) formed by C_7 and R_3. While this stage was designed into Version 1.0, it was not utilized during *in vivo* testing. However, a low frequency HPF is necessary to attenuate the low frequency voltage offsets occurring at the electrode-tissue interface (Buzsaki et al. 1996); neural spike activity is commonly superimposed onto these voltage offsets. Therefore, Version 2.0 fully executed this HPF stage with a cutoff frequency positioned at 220 Hz.

2. Voltage Follower/Buffer

A unity gain voltage follower is formed by AMP1 and serves as the second processing stage of the recorder AFE. This amplifier buffers the high input impedance source generated from the microelectrode inserted into SI cortex.

3. Band-Pass Filter

The third AFE stage is a band-pass filter that combines two Multiple Feedback (MFB) filters: a MBF high-pass filter and a MBF low-pass filter. MFB topology was used because it features a low sensitivity to component variations and the AFE design required an even number of stages to ensure the output polarity was the same as the input. The high-pass filter formed from AMP2, C_8, C_9, C_{10}, R_4, and R_5 has a high-cut-off frequency (f_{hc}) placed at 5250 Hz and cascades into the low-pass filter formed from AMP3, C_{11}, C_{12}, R_6, R_7, and R_8 that has a low cut-of frequency (f_{lc}) placed at 510 Hz; both amplifiers have gain of 30× (29.54 dB); version 2.0 expands the band-pass filtering

range to include cut-off frequencies located at 375 Hz and 6425 Hz. The transfer function for the high-pass filter is given by Eq. 4 and the transfer function for the low-pass filter is given by Eq. 5.

$$\frac{V_{out}}{V_{in}} = \frac{-s^2 C_8 C_{10}}{s^2 C_9 C_{10} + sR_5(C_8 + C_9 + C_{10}) + R_4 R_5} \tag{4}$$

$$\frac{V_{out}}{V_{in}} = \frac{R_6 R_6}{s^2 C_{11} C_{12} + sC_{12}(R_6 + R_7 + R_8) + R_7 R_8} \tag{5}$$

4. Biased Non-inverting amplifier

The last stage of the recorder AFE is a non-inverting amplifier. It is formed by AMP4, R_9, R_{10}, and R_{11}. The gain for Version 1.0 was fixed at 15× (23.5 dB) and the gain for Version 2.0 was fixed at 8× (18.0 dB). The transfer function is given as Eq. 6:

$$\frac{V_{out}}{V_{in}} = \frac{(R_{10}R_{11} + R_9 R_{11} + R_9 R_{10})}{R_9 R_{11}} \tag{6}$$

In addition, a voltage bias having a range of ± 1.5 V is introduced into this stage using a voltage divider for offset nulling. It is formed from R_{12} (potentiometer), R_{13}, and R_{14}.

G. Power Supply

This system design serves as a prototype for real-time wireless neural microstimulation and recording where portability was not a primary criterion; therefore, the power of the remote unit is supplied by an external power source that directly feeds the compliance voltage of ± 20 V to the stimulator V2I. For the remaining devices, power is supplied by four high performance low dropout voltage regulators (LDOs), which generate the ± 12 V, 5 V, and 3.3 V to operate the TL08x opamps, PSoC, and RN-42 Bluetooth device, respectively. In order to decrease power, the maximum stimulation intensity and load requirements should be reduced.

H. Physical Circuit Layout and Fabrication

A custom two-layer printed circuit board (PCB) for the remote unit was designed using CadSoft Eagle PCB Design Software v6.1.0. It measures 4.2 cm × 7.1 cm and its layout is presented in Fig. 27. The PCB layout shows all components were placed on the top layer and the bottom layer served as a grounding plane; this design approach was taken to simplify testing and troubleshooting the system. A high density board was achieved by using size 0603 (1608 metric) for passive and active components, 10 mil trace widths, and 25 mil vias with 15 mil drill holes. Considerations were given to power flow; connectivity to microelectrodes inserted in opposite SI cortices, and recorded signal preservation. The PCB was fabricated by Advanced Circuits (www.advancedcircuites.com) and all components were hand soldered.

I. Remote Unit Printed Circuit Board

The completed remote unit PCB is photographed in Fig. 28. The PSoC (1) is used as the stimulator DFE for digital-to-analog conversion of stimulation parameter and as

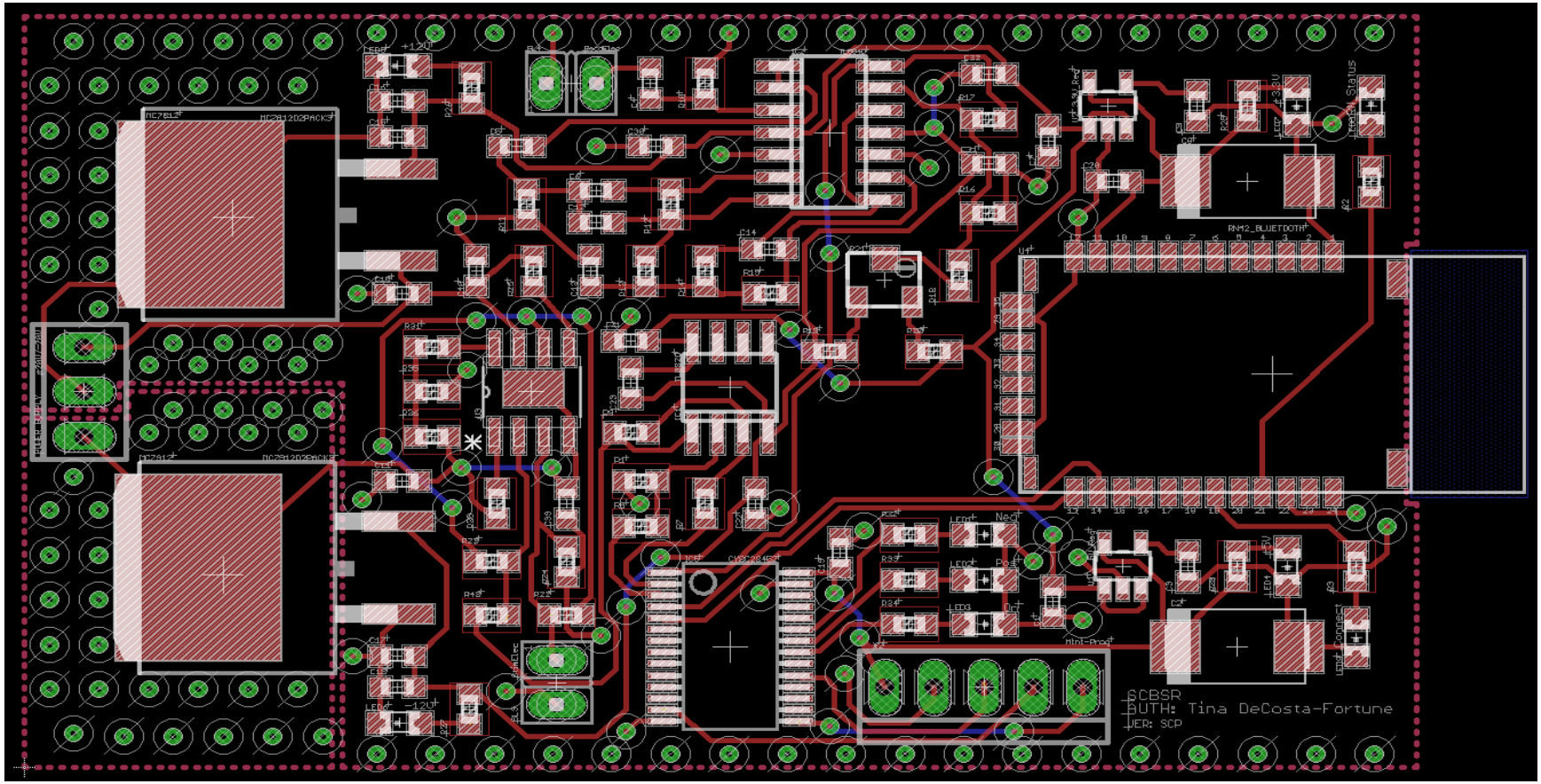

Figure 27 – Remote unit double sided printed circuit board layout measuring 4.2 cm × 7.1 cm. Power from the external supply is applied to the left side of the board and wireless transmission on the right side. The distance between the recording electrode (at top of board) and the buffer were kept to a minimum to preserve signal quality. For purposes of *in vivo* use, the stimulator electrode was placed opposite on the board (at bottom) from the recording electrode. Vias along the top and bottom side aid in noise interference whereas the vias surrounding the MC7812 and MC7912 are for heat dissipation. All components were placed on the top layer and the bottom layer was preserved for ground.

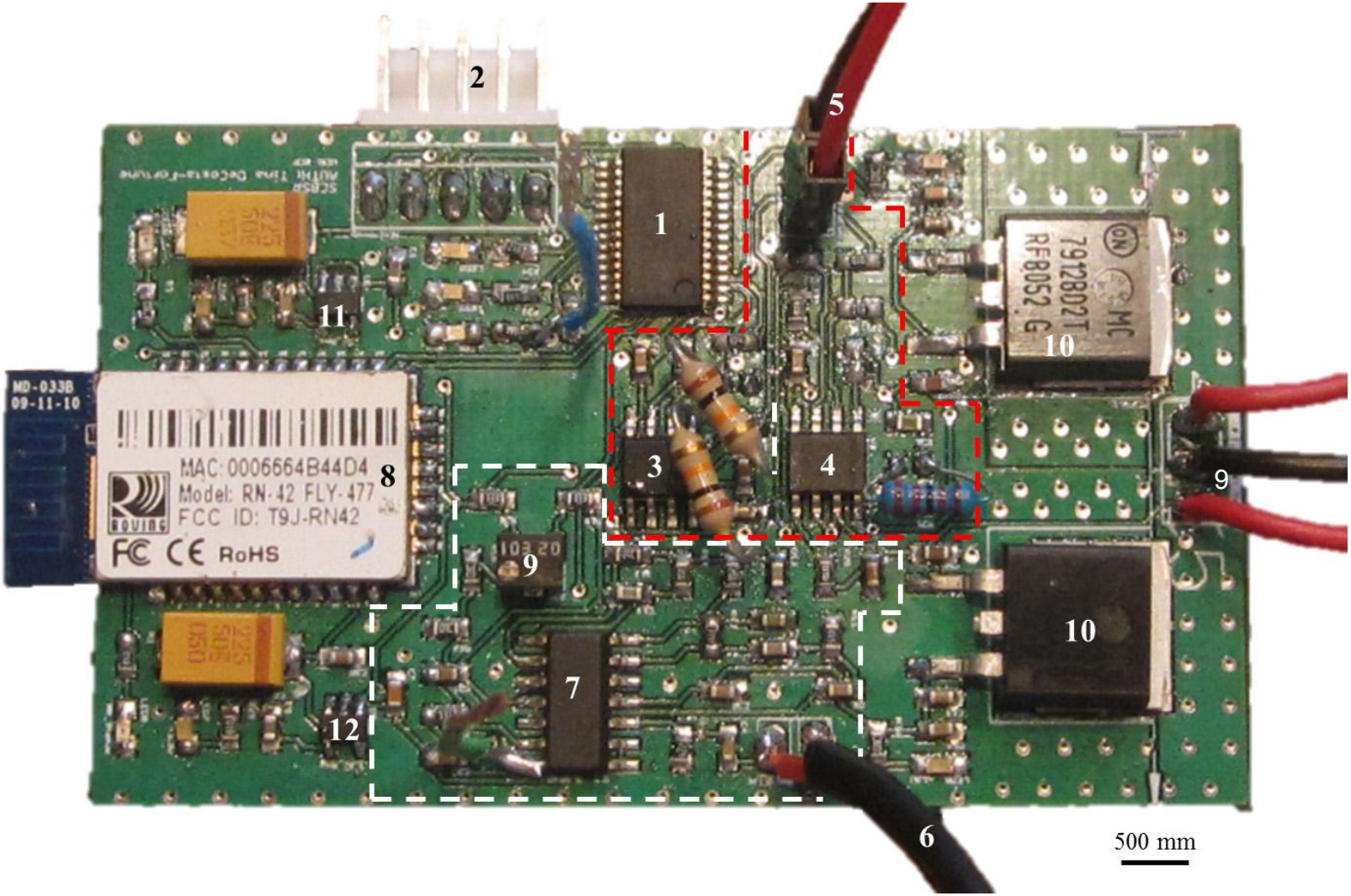

Figure 28 – Photograph of the completed remote unit for the wireless neural intracortical microstimulation and recording system.

the recorder DBE for analog-to-digital conversion of neural signals; the five pin MiniProg connector (2) is required for PSoC programming. The stimulator ABE, shown by the red dashed outline, features a differential amplifier (3), a voltage-to-current converter (4), and a two pin connector (5) that feeds the generated stimulus pulse to an implanted stimulating electrode. Neural response signals in contralateral cortex are transduced by an implanted recording electrode and fed into the recorder AFE, shown by the white dashed outline, for processing. The recorder AFE is comprised of a shielded copper electrode lead that receives the neural signals from the implanted electrode (6), and four opamps (7) used in buffering, filtering, and amplifying the analog signals. Bluetooth communication (8) is used for real-time interaction between the base and remote units. Power is provided by an external ±20 V input (9), two LDO regulators (10) that generate ±12 V, for the TL08x opamps, a 5.0 V LDO regulator (11) for the PSoC, and a 3.3 V LDO regulator (12) for the RN-42 Bluetooth device.

III. System Test and Evaluation

Design quality for the remote unit was first assessed by performing numerous P-SPICE simulation scenarios in Cadence Allegro 16.5. Next, bench-top testing of the implemented system examined the independent functionality of the stimulator, recorder, wireless communication, and graphical user interface. Saline-based solution experiments were carried out to evaluate the system's ability to simultaneously stimulate and record. Lastly, performance of the system was demonstrated *in vivo* with anesthetized Sprague-Dawley strain of rat.

A. In Vitro Functionality Verification – Stimulator

The stimulator's range of operation and its ability to generate mono-, bi-, and pseudomonophasic waveforms based on user defined parameters was assessed. P-SPICE simulations were performed followed by end-to-end bench testing. A simulation model for the PSoC was not available; two time-domain voltage sources (V_{pulse}) were used to represent the two positive output voltage signals ($V_{cathodic}$ and V_{anodic}) generated by the PSoC.

1. Range of Operation

A key functional requirement of the stimulator design was to deliver a 100 µA biphasic stimulus pulse to a 100 kΩ load. Total range of operation was first assessed by loading the stimulator with the maximum expected load and sweeping the intensity (0 µA-100 µA) of a monophasic pulse in 5 µA increments; input current was set using the WINSR software application. Output current was measured using a µCurrent meter (www.EEVblog.com) that displayed 1 mV per 1 µA onto a digital oscilloscope (Rigiol DS1052E 50 MHz 1.0 GSa/s); independent assessments were conducted for cathodic and anodic stimulus pulses. A comparison of the measured and simulated input-output characteristics of the stimulator (Fig. 29) demonstrates the system's accuracy with maximum loading (100 kΩ). Similar transfer characteristics were observed for cathodic (Fig. 29A) and anodic (Fig. 29B) stimulus pulses. The delivered stimuli intensity closely matched the simulated values.

Next, a 1.0 ms biphasic pulse with varying amplitudes ranging from 0 µA to 100 µA, in 25 µA increments, was examined under load conditions ranging from 0 kΩ to 220 kΩ; the results of which are shown in Fig. 30. The comparison plot illustrates the linear

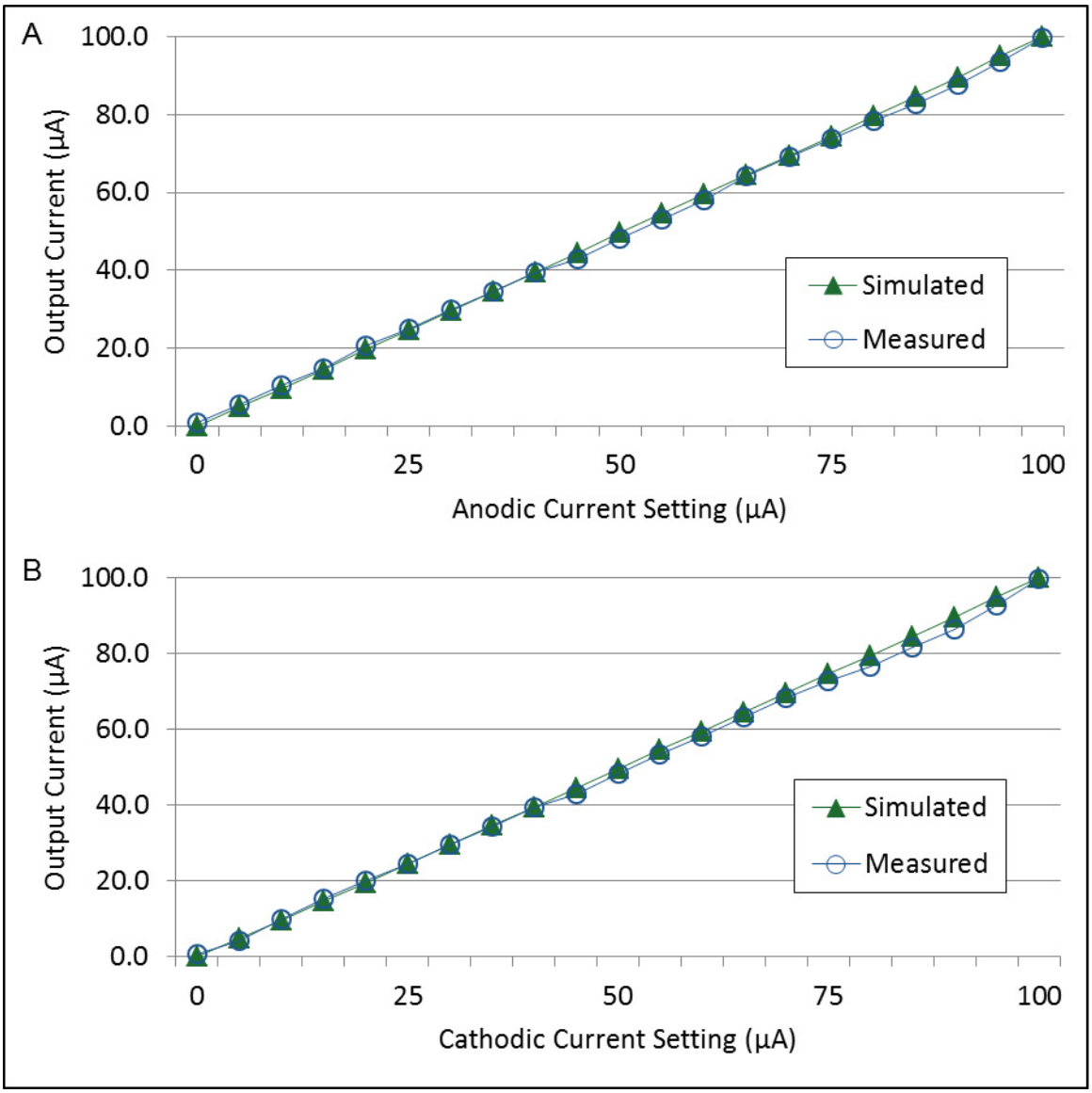

Figure 29 – Transfer characteristic of the stimulator for a 100 kΩ resistive load with varying intensities (0-100µA). **A:** Monophasic cathodic pulse with varying intensities ranging from 0µA to 100µA. **B:** Monophasic anodic pulse with varying intensities ranging from 0µA to 100µA. Input current settings were established using the custom developed WINSR software application

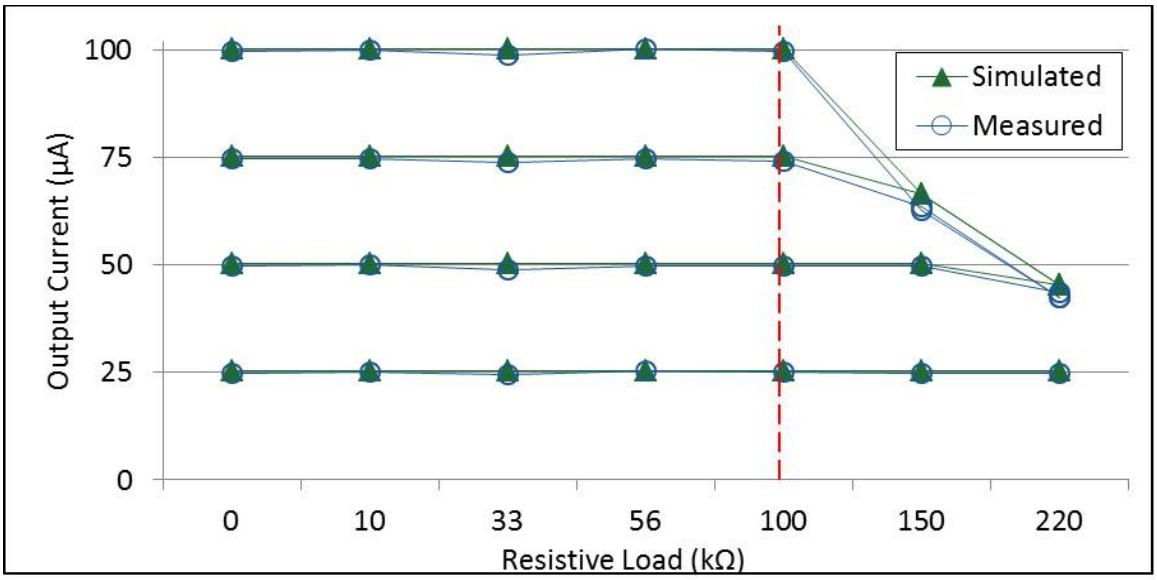

Figure 30 – Output of the stimulator under varying load conditions ranging from 0 kΩ to 220 kΩ. For biphasic stimulus intensities ranging from 60 µA to 100 µA peak-to-peak, linearity was maintained for loads up to 100 kΩ. For biphasic stimulus intensities < 60 µA peak-to-peak, linearity was maintained for loads up to 150 kΩ.

operating region of the stimulator. For biphasic stimulus intensities of up to 60 µA, linearity was maintained for loads up to 150 kΩ whereas, for intensities ranging from 60 µA to 100 µA, linearity was maintained for loads up to 100 kΩ. Note, the range of linearity may be extended (reduced) by increasing (decreasing) the V2I converter supply voltage or modifying the stimulus intensity requirements.

2. Stimulus Pulse Generation

A number of simulations and bench-top tests were performed to evaluate the ability to deliver a mono-, bi-, and pseudomonophasic waveform of either positive or negative polarity with accurate user-defined amplitude, duration, and delay. Stimulus output was measured across a resistor placed in series, which acted as a simplified electrode model; measurements were taken using the µCurrent meter previously described.

Two examples of measured output waveforms generated by the stimulator are shown in Fig. 31. A charge balanced biphasic pulse (45 µA, 1ms) with a 10 ms delay was measured using a 100 kΩ load and is depicted in Fig. 31A. Fig. 31B shows a charge balanced pseudomonophasic pulse comprised of a 1.0 ms 50 µA cathodic segment and a 2 ms 25 µA anodic segment.

B. In Vitro Functionality Verification – Recorder

P-SPICE simulations of the recorder functionality were performed with either a sinusoidal voltage source (V_{sin}) or an alternating voltage source (V_{ac}) to represent an analog input signal of spike activity from the recording electrode. Bench testing was performed by applying a sinusoidal waveform from a signal generator (Rigol DG4062 Functional/Arbitrary Waveform Generator); the output of the signal generator was connected to the first stage of the recorder AFE, a high-pass filter (220Hz), through a 10,000:1 voltage divider circuit (10 MΩ:1 kΩ).

1. Fidelity

Fidelity of the simulated and implemented recording circuitry is represented by the magnitude response curves shown in Fig. 32. The comparison plots were generated by sweeping a 300 µV peak-to-peak sinusoid from 125 Hz to 6.5 kHz. The system was designed with a gain of 12,500× (82.1 dB) and cutoff frequencies at 510 Hz and 5250 Hz. The measured gain was 82.8 dB while the 3 dB frequencies were located at 500 Hz and 5750 Hz.

Similar findings were obtained for AFE Version 2.0; to generate its magnitude response curve, the input signal frequency sweep was extended to 10 kHz. Version 2 was designed with a gain of 8,000× (78.4 dB) and cutoff frequencies at 375 Hz and 6425 Hz.

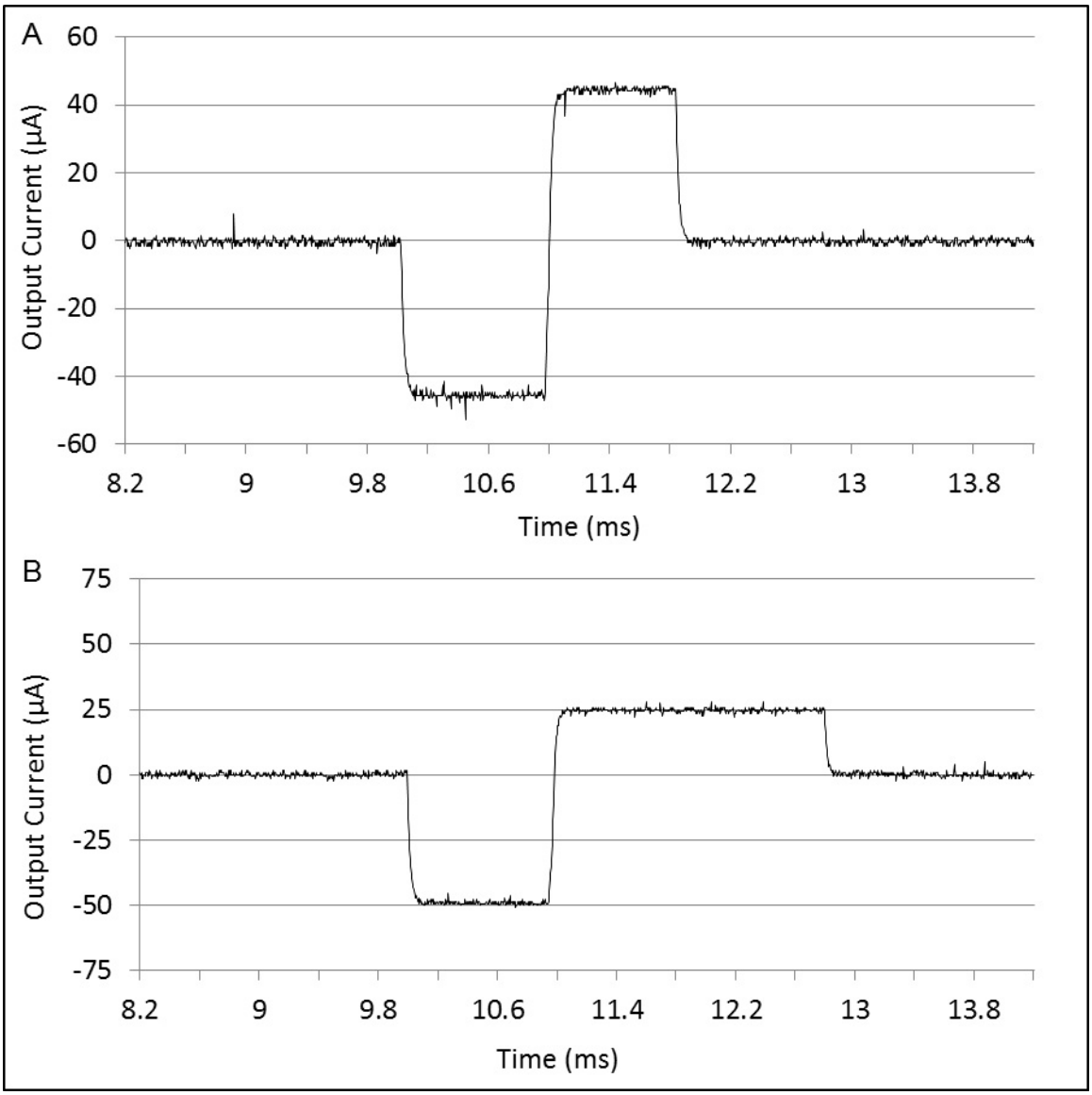

Figure 31 – Examples of charge balanced biphasic and pseudomonophasic stimuli delivered to a 100 kΩ load. **A:** Charge balanced biphasic pulse featuring a 1.0 ms 45 µA peak intensity with a 10 ms delay. **B:** A pseudomonophasic stimulus pulse with a 10 ms delay that is charge balanced by combining a 1.0 ms 50 µA peak intensity cathodic pulse segment and a 2 ms 25 µA peak intensity anodic pulse segment.

The measured gain was 78.8 dB and 3 dB frequencies were 367 Hz and 6470 Hz. Performance of each implemented system followed closely to the predicted outcome. Table 5 summarizes the fidelity results for both AFE versions.

2. Linearity

Recorder linearity was assessed by sweeping the amplitude of a 4 kHz sinusoidal input signal from 100 μV_{pp} to 500 μV_{pp}. Comparison of the simulated and measured results is shown in Fig. 33. The simulated and measure linearity were 81.5 dB and 82.7 dB.

3. Total Harmonic Distortion

Total harmonic distortion (THD) for the recorder design (Version 1) was simulated using a 300 μV sinusoidal input at 1 kHz was 1.9%. THD for Version 2 of the recorder AFE was 1.07%.

C. Power Distribution

Actual power dissipated by the remote unit depends on the frequency and intensity of the stimulation. Table 6 provides a breakdown of the dissipated power for each device operating in standby mode (P_{std}) with no stimulus taking place and the instantaneous power (P_{inst}). Standby mode power values were obtained from manufacturer's device datasheets. Instantaneous power values were obtained from system simulations using device PSPICE models for each operational amplifier (OPA454, TL081, and TL084) and a standard dc voltage source for each regulator (MC7812, MC7912, MIC5219-5.0, and MIC5219-3.3). A PSPICE model or equivalent was not available for the RN-42 or PSoC-1; as such, the RN-42 datasheet was used to determine instantaneous power.

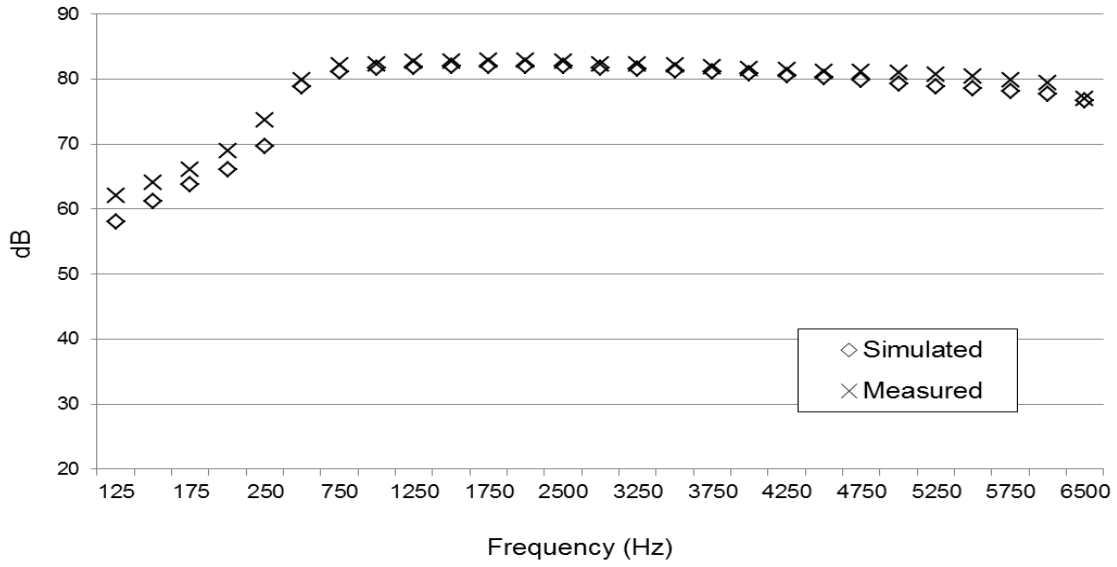

Figure 32 – Fidelity results for simulated and measured recorder AFE by sweeping a 300 µV peak-to-peak sinusoid from 125 Hz to 6.5 kHz. The designed 3 dB frequencies were located at 510 Hz and 5250 Hz; they measured at 500 Hz and 5750 Hz.

Table 5 – Summary of simulated and measured fidelity and frequency cutoff results for the recorder analog front end. Data generated by sweeping a 300 µV peak-to-peak sinusoid from 125 Hz to 6.5 kHz (Version 1) and 125 Hz to 10 kHz (Version 2).

Recorder AFE	Test Environment	Gain (dB)	HPF (Hz)	LPF (Hz)
Version 1	Simulated	82.1	510	5250
	Measured	82.8	500	5750
Version 2	Simulated	78.4	375	6425
	Measured	78.8	367	6470

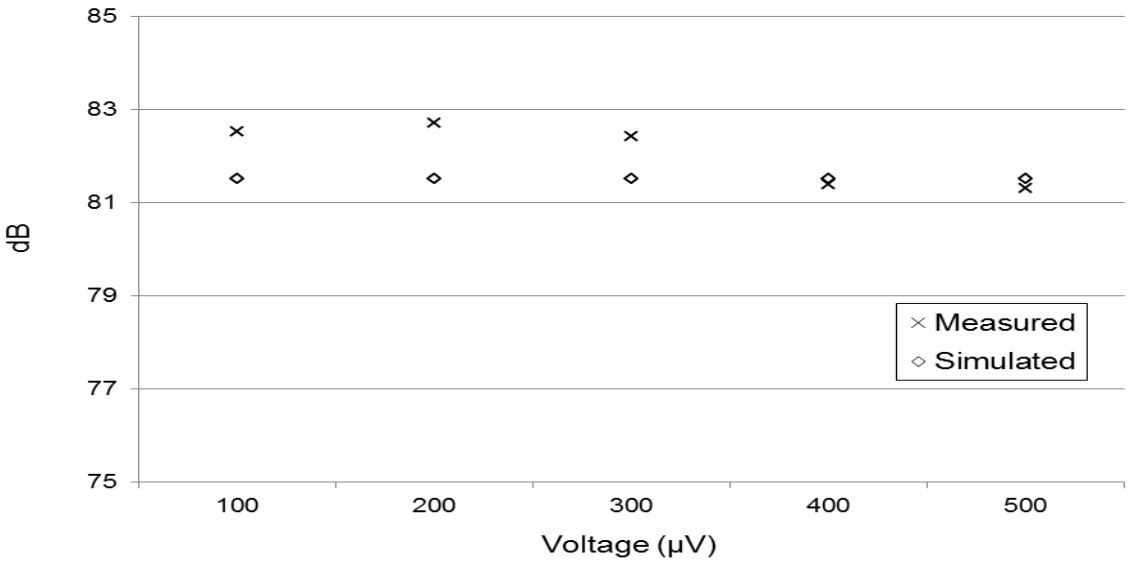

Figure 33 – Linearity results for simulated and measured recorder AFE by sweeping a 4 kHz sinusoidal input voltage signal from 100 µV to 500 µV. Simulated and measure linearity were 81.5 dB and 82.7 dB, respectively.

PSoC power consumption was estimated by calculating the total current for each stimulating and recording device configured on the CPU (Cypress Application Note 2216). All device aspects of the PSoC were configured to operate at medium-power, if reconfigured to operate at high power, the PSoC power consumption increases to 159.24 mW with a quiescent current (I_Q) of 31.85 mA. If configured at low power, the PSoC power consumption drops to 47.87 mW with I_Q = 9.87 mA.

Design of the system was primarily focused on functionality of the stimulator ABE and recorder AFE, constraints of using the RN-42 platform, and developing the PSOC-1 architecture. As a result, the system has not been fully optimized for low-power operation. Evidence of this is the voltage compliance of ±20 V and the use of linear regulators to generate the supply voltages for the various devices.

Table 6 - Breakdown of the dissipated power in standby mode (P_{std}) and the instantaneous power (P_{inst}) for each remote unit device. Power dissipated is presented for the system in standby mode and the power dissipated is dependent on the frequency and intensity of stimulation. Standby mode power values were obtained from manufacturer's device datasheets. Instantaneous power values were obtained from system simulations; when PSPICE models were not available device datasheets were used to calculate power consumption.

	Quiescent Current (I_Q) [mA]	Standby Mode Power (P_{std}) [mW]	Instantaneous Power (P_{inst}) [mW]
20 V components			
OPA454	3.20	66.00	130.40
MC7812	3.40	68.00	71.78
MC7912	3.40	68.00	93.53
12 V Components			
TL081	1.40	16.80	109.78
TL084	5.6	67.20	439.12
MIC5219-5.0	0.008	0.072	881.90
MIC5219-3.3	0.008	0.072	881.90
5 V Components			
PSoC-1	13.995	69.97	69.97
3 V Components			
RN-42	3.00	9.00	9.00
Total	23.79 mA	276.61 mW	2.68 W

D. Simultaneous Stimulation and Recording

To demonstrate the performance of simultaneous stimulation and recording, system capabilities were first evaluated in saline-based solution experiments. Next, operation of the system interfacing with biological tissue was validated by performing *in vivo* testing in anesthetized rat models

1. Saline-based Experiments

An experiment environment modeling biological-tissue response to electrical stimulation was established using a 0.9% saline-based solution and two tungsten microelectrodes (Fredrick Haer and Company). Each electrode was attached to an independent stereotaxically mounted microdrive and lowered into the saline solution. The distance between the two electrodes measured approximately 8 mm, which is representative of the distance between homotopic forelimb representations in rat SI cortices; a bare silver microwire placed in the saline solution served as the reference electrode. Stimulus pulses of varying amplitudes and durations were delivered to one electrode (StimElec) while potential changes in the saline solution were measured from the second electrode (RecElec). An example of a 50 μA biphasic stimulus pulse having a 1.0 ms duration and its recorded artifact is shown in Fig. 34A and Fig. 34B, respectively. In this experiment set-up, the device showed an output dc offset of approximately 3 V. Fortunately this offset did not limit the ability to record the stimulus artifact.

2. *In vivo* Examination

After evaluating the system on a bench-top and in saline-based experimental models, its capabilities were demonstrated *in vivo* with an anesthetized adult Sprague-Dawley rat model. All surgical and experimental procedures were approved by the

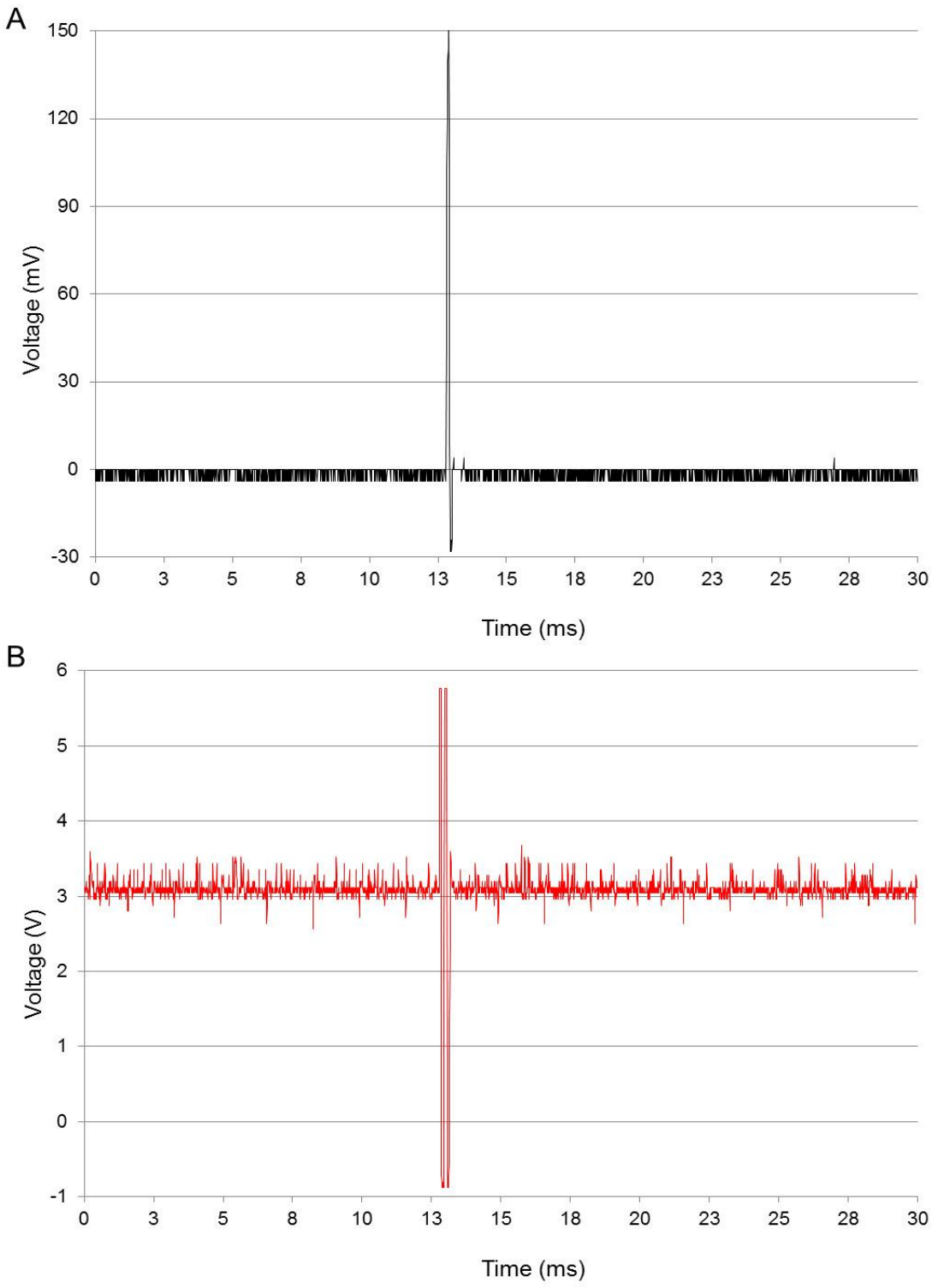

Figure 34 – Simultaneous stimulation and recording using saline-based solution experiment model and band-pass frequencies of 500-5750Hz. **A:** biphasic ±50 µA, 1.0 ms stimulus pulse duration. **B:** Recorded stimulus artifact of pulse presented in A; in this example a dc offset of approximately 3 V was measured.

University of Tennessee Health Science Center (UTHSC) Institutional Animal Care Committee (IACUC). Two electrodes were inserted into physiologically identified homotopic forelimb sites in SI as described in Chapter II – Intracortical Microstimulation Study. Briefly, bilateral craniotomies, approximately 4 mm × 4 mm, were made over the presumptive SI regions representing the forelimb, the dura was incised and reflected back exposing the cortical surface, and the brain surface was covered with silicon fluid to prevent drying. An electrode attached to a stereotaxically mounted microdrive was lowered to a depth of 700μm (layer IV) and the receptive field was identified. Once a desired forelimb receptive field was mapped, the electrode was advanced to a depth corresponding to layer V (depth = 1,100 μm to 1,400 μm) where the receptive field was reexamined. This procedure was repeated in the contralateral SI. After homotopic forelimb receptive fields were identified and an interhemispheric connection was established, the remote device hardware was connected to the implanted electrodes. A Bluetooth enabled Vaio laptop (VPCSB, Sony Corporation) running WINSR served as the host computer for interfacing with the remote device.

A number of different stimulation configurations were successfully delivered to the stimulating site, as monitored on a digital oscilloscope, and its artifact recorded in a homotopic site in contralateral forelimb barrel cortex. The stimulator repeatedly generated mono-, bi-, and pseudomonophasic stimulus pulses corresponding to the user-defined controls for intensity and duration. An example of a ±50 μA biphasic stimulus artifact recorded in layer V (depth = 1,100 μm) forepaw representation is presented in Fig. 35; a dc offset of 25 mV was observed. Adjustments were made in WINSR to one or more stimulus attributes and retransmitted to the remote unit during its operation. In

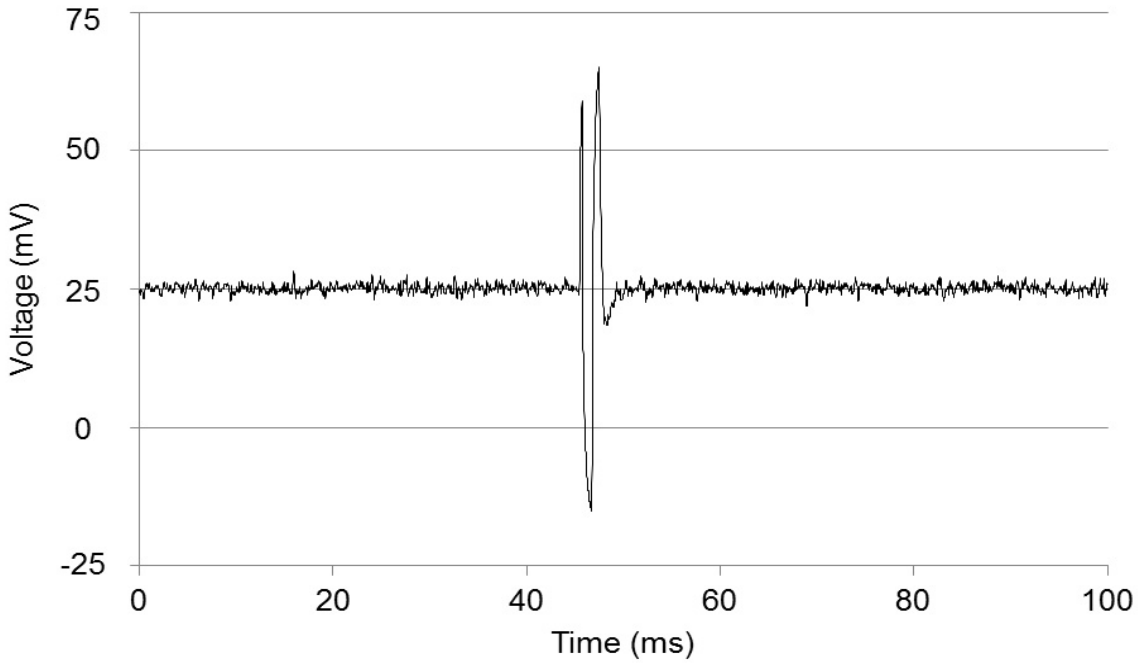

Figure 35 – Recorded stimulus artifact in layer V forepaw representation at a depth of approximately 1,100 µm. Artifact was generated from a 50 µA, 1.0 ms biphasic stimulus pulse delivered to the homotopic forepaw representation in contralateral SI.

addition, an external trigger pulse successfully triggered an independent data acquisition program (IGOR Pro 6.20, Wavemetrics Inc.). The stimulator performed as expected while under each operating mode (calibrate and chronic).

Real-time response activity from an electrode inserted in the contralateral forelimb barrel cortex was successfully acquired (n = 2) and processed by the recorder AFE; signals were transmitted to an external data analysis system (IGOR Pro 6.20, Wavemetrics Inc.) and viewed on an analog oscilloscope. Digitized response data was successfully (n = 1) transmitted to the host computer and stored. However, during the experiment an increased level of noise was present while the Bluetooth port remained opened and analysis of the digitized response trace revealed spike level activity could not be easily distinguished.

Three categories of real-time response activity were processed by the recorder AFE (1) spontaneous activity in the absence of microstimulation, (2) evoked responses to manual stimulation of the contralateral periphery, and (3) evoked responses following microstimulation of the homotopic site in contralateral forelimb barrel cortex. An example of a single spontaneous activity trace recorded in SI layer V dorsal wrist representation at a depth of 1,000 μm is shown in Fig. 36. This extracellular response recording depicts multiple neurons firing in the absence of stimulation. The difference in response amplitude is an indicator of the firing neuron's distance from the recording electrode. The closer the firing neuron is to the recording electrode, the larger the response amplitude will be; the farther away the firing neuron is from the recording electrode, the smaller the response amplitude will be. In this experiment a frequency range of 425 Hz to 6400 Hz was used and the analog response recording was transmitted to an independent analysis system running IGOR Pro 6.20 (Wavemetrics, Inc.). The recording revealed a 175 mV dc offset; fortunately this offset did not prevent recording response activity.

Following successful analog processing of spontaneous activity in the absence of stimulation, evoked responses to peripheral stimulation of the contralateral forelimb was demonstrated. Evoked response activity to peripheral stimulation recorded in SI layer V dorsal wrist representation at a depth of 1,000 μm is presented in Fig. 37. Fig. 37A shows an example of a single evoked response and Fig. 37B shows a composite of 4 evoked responses to peripheral stimulation (-70 μA) of the right dorsal wrist. Evoked response activity occurred with an 8-10 ms latency and the data was collected within the frequency range of 425 Hz to 6400 Hz.

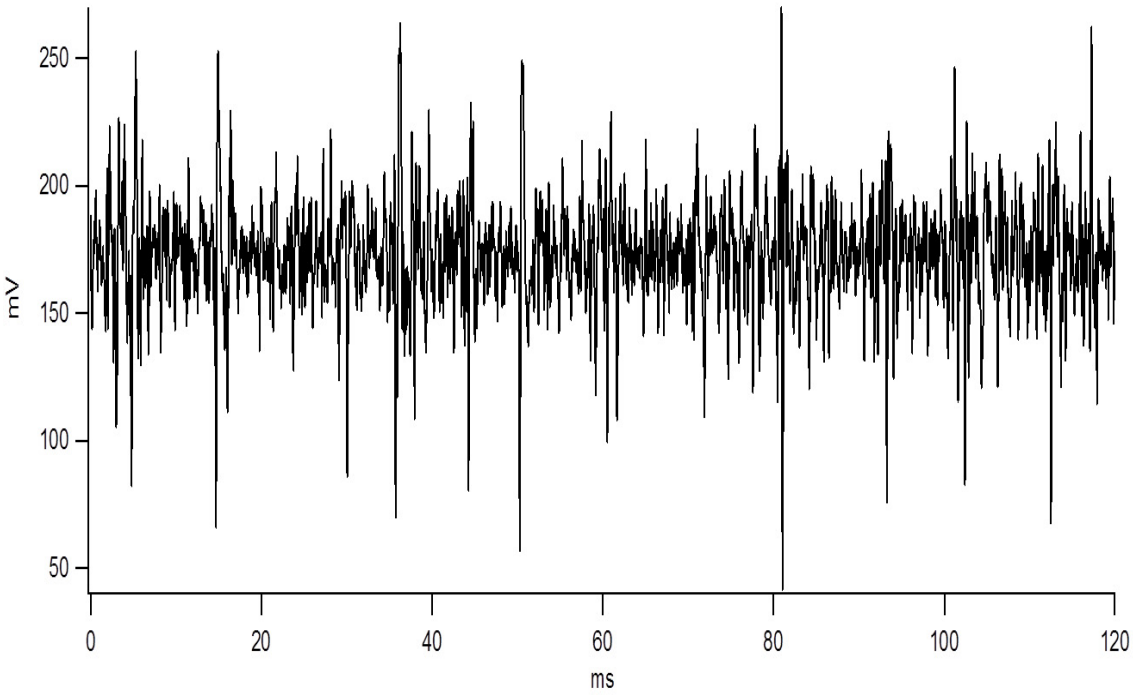

Figure 36 – Real-time spontaneous spike activity recorded in SI layer V (depth = 1,000 μm) dorsal wrist representation.

Lastly, real-time recording of evoked responses to cortical microstimulation was demonstrated. A monophasic (-75 μA, 1.0 ms duration, 1 Hz) stimulation pulse was delivered to the layer V dorsal wrist representation. Response activity following cortical microstimulation was recorded from the homotopic layer V representation in contralateral SI and sample activity processed by the recorder AFE is shown in Fig. 38. An example of a single evoked response with a latency of 8 ms is depicted in Fig. 38A. Fig. 38B shows a composite of 5 evoked response recordings having a latency of 8-10ms and duration of approximately 14 ms. Data was collected within 425 Hz to 6400 Hz frequency band.

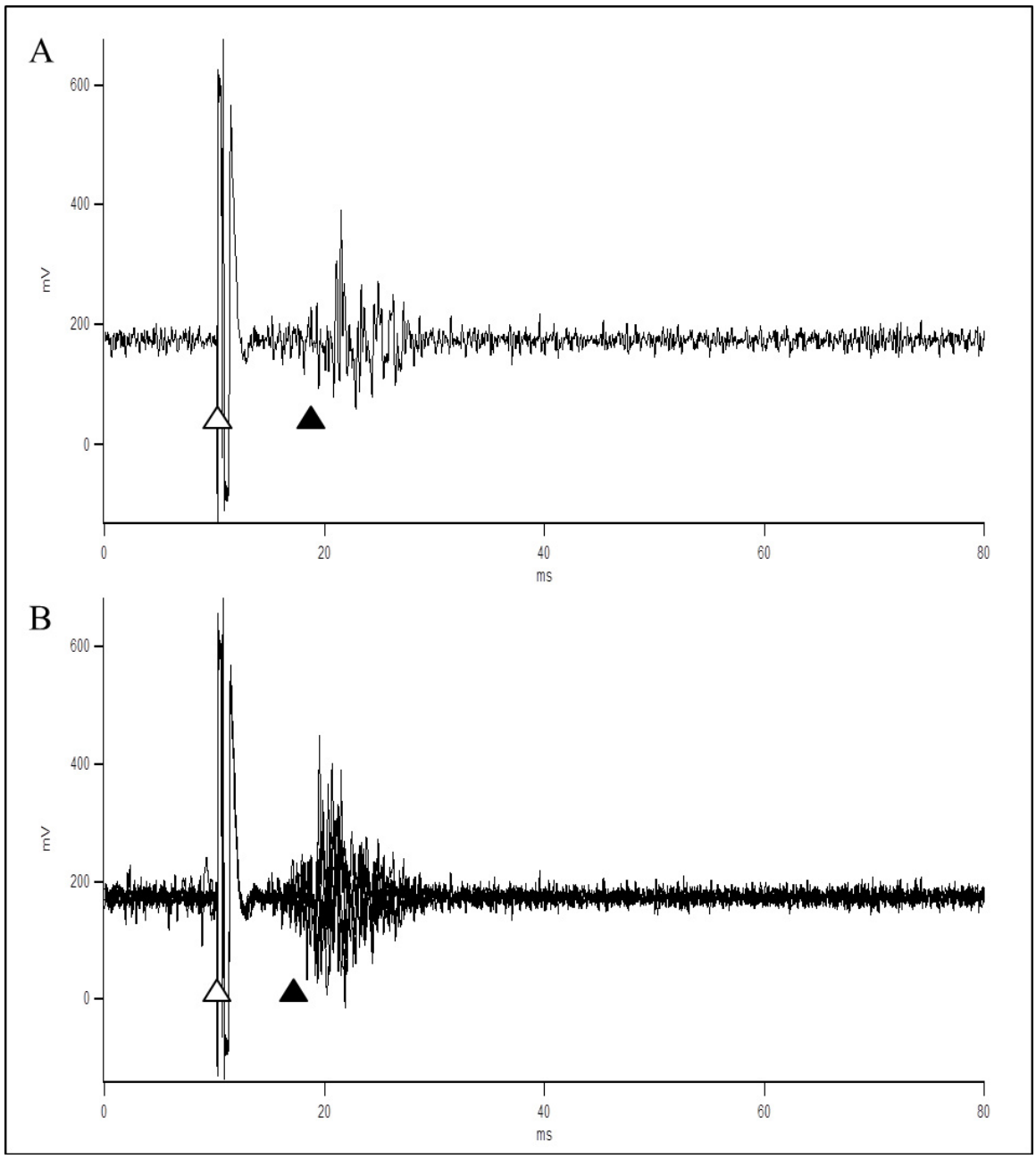

Figure 37 – Real-time responses recorded in SI layer V (depth = 1,000 μm) dorsal wrist representation to peripheral stimulation (-70 μA, 1.0 ms duration, 1 Hz) of the contralateral dorsal wrist. **A:** Single evoked response. **B:** Composite of 4 evoked responses. The open and filled triangles denote the onset of the stimulus pulse and evoked response, respectively.

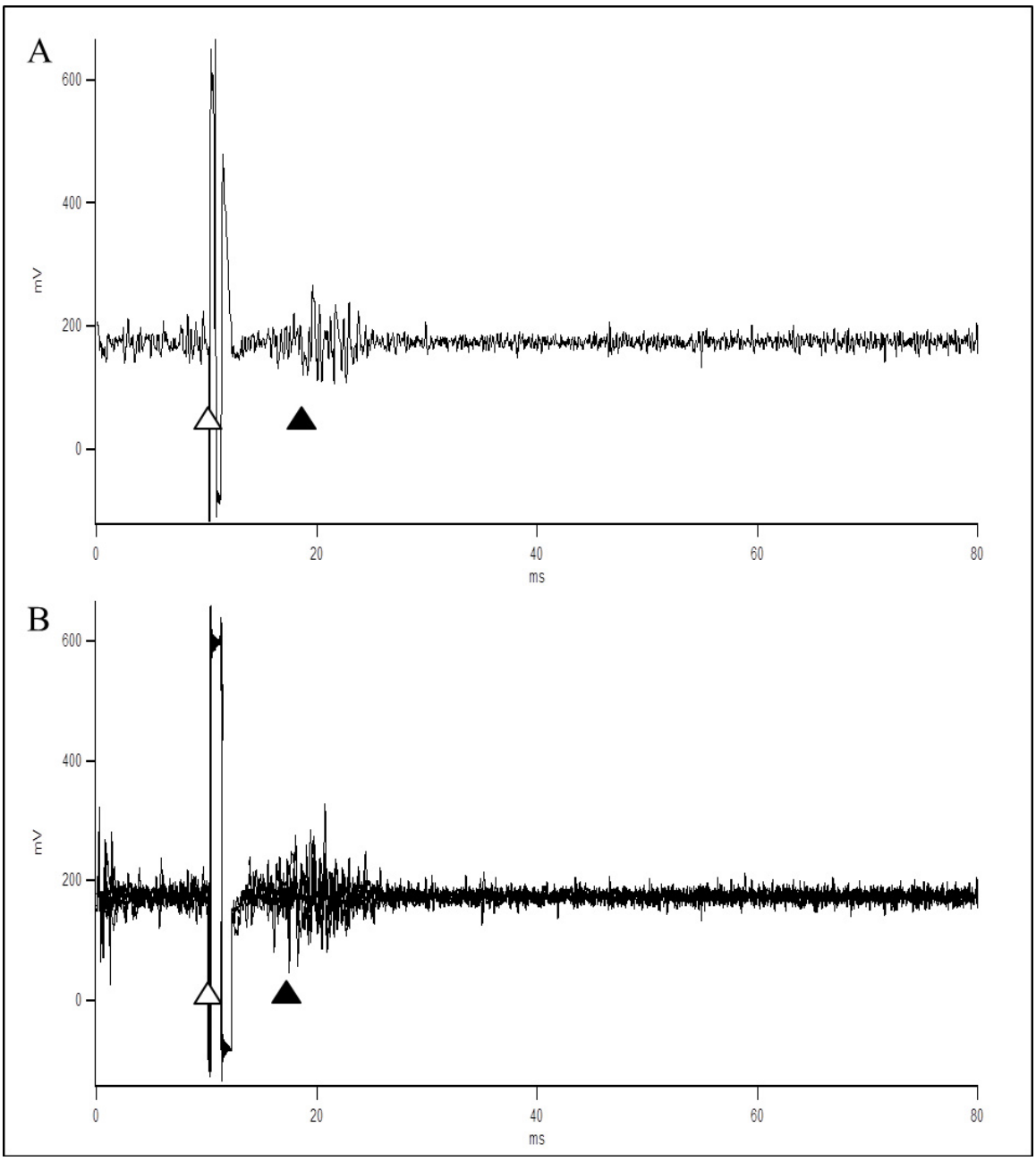

Figure 38 – Real-time response activity between physiologically identified layer V dorsal wrist representations in ipsilateral and contralateral SI following a -75 µA monophasic stimulus pulse (1.0 ms duration). **A:** Single evoked response. **B:** Composite of 5 evoked responses. The open and filled triangles denote the onset of the stimulus pulse and evoked response, respectively.

Overall, the system allowed for the controlled delivery of telemetry-based intracortical microstimulation as defined by the operator. Stimulation parameters were faithfully modified and retransmitted in real-time to the remote device. Real-time response recordings in the absence of microstimulation (spontaneous activity), in response to peripheral stimulation, and in response to cortical microstimulation were successfully processed by the recorder analog circuitry and transmitted to an independent analysis system. Analog response recordings were digitized and successfully transmitted to the host computer; however the data could not be accurately analyzed due to signal distortion.

IV. Discussion

An interactive neural interface device for the controlled delivery of telemetry based microstimulation and real-time recording was developed. It was built to serve as a prototype of an eventual system that will be fully optimized and sized to fit on the back of a freely behaving rat. All components of the remote device circuitry are available off the shelf and may be hand soldered; the printed circuit board design can be fabricated at any number of board houses. Custom programming of the user interface, WINSR, and the PSoC was written in C# and C, respectively. As designed, this system can be implemented with minimal costs and provides a platform to further investigate of cortical circuit modulation for enhancing the interhemispheric pathway and inducing functional reorganization. While the studies conducted in our lab have focused primarily on the connectivity between similar SI representations in each hemisphere, which require a

single channel system, it is conceivable that a higher degree of flexibility may be desired to examine connectivity between multiple sites simultaneously, which would require multiple channels.

A. Electrode-Tissue-Interface

The neural interface device was designed for use *in vivo* where the environment created by the electrode and surrounding cortical tissue, known as the electrode-tissue interface, has a number of characteristic features that motivate specific design requirements for chronic microstimulation and extracellular response recording.

1. Electrode Impedance

Introduction of an electrode for stimulating or recording *in vivo* initiates a series of cellular responses known collectively as the foreign body reaction composed of macrophages in the surrounding tissue attempting to remove the object or isolate it from the remaining tissue (Anderson et al., 2008); this reaction can significantly affect the performance of the electrode. For stimulation and recording, an electrode is the last and first piece of hardware in the signal processing pathway, respectively; it is the point where current from the electrode is transduced into ionic charge in the surrounding tissue (stimulation) and where ionic charge from the surrounding tissue is transduced into current (recording).

Electrode impedance at the electrode-tissue interface plays an important role in both neural stimulation and recording. It is typically measured at 1 kHz in saline and can range from the order of kilo- to mega- ohms; factors contributing to its value include material, signal frequency, cross sectional area (tip diameter), and the electrode-tissue interface. Impedance of the surrounding tissue varies due to cellular reactions at the

electrode-tissue interface and the electrode impedance magnitude at 1 kHz can vary significantly; an increase from a range of 75-125 kΩ to a range of 200-375 kΩ was reported following 7 days of implantation (Williams et al., 2007).

To minimize tissue damage, low impedance is necessary for neural stimulation (Franks et al., 2005); however with low impedance the electrode tip diameter is larger. Efforts to reduce the high input impedance levels of chronically implanted electrodes without increasing electrode size include increasing stimulation frequency and minimizing the distance between the stimulating and reference electrodes. During data acquisition, a high electrode impedance source makes microvolt level neural signals susceptible to external noise generated by ionic-based electrical fluctuations (Franks et al., 2005); however, high impedance electrodes allow for recording of single isolated cells. Multiunit recordings necessitate placing a buffer as close to the recording electrode as possible prior to being processed by the recorder AFE.

2. Stimulation Charge Distribution

An important factor contributing to the distribution of charge during stimulation of excitable tissue (e.g. cortex) is the stimulus waveform; ideally the stimulus pulse would produce a net zero charge injected into the tissue. Chronic monophasic stimulation, which delivers constant current in one direction (either cathodic or anodic) for a specific period of time can cause unrecoverable charge injected into the tissue that can result in electrode corrosion and/or tissue damage. This is avoidable by using charge balanced biphasic stimulation in which current is delivered in two equally charged phases: stimulating and reversal. During the stimulation phase, current is delivered in one direction (typically cathodic) for a period of time to elicit an action potential and then

during the reversal phase current is delivered in the reverse direction (typically anodic), for an equal period of time and intensity to minimize the electrochemical reactions that can occur at the electrode-tissue interface during the stimulation phase. A disadvantage of biphasic stimulation is that a higher threshold is required for initiating action potentials (Rubinstein et al., 2001). However, low threshold stimulation with minimal electrochemical reaction is obtainable using a pseudomonophasic stimulus pulse (Van Wieringen et al., 2005), which is a biphasic pulse where the intensity and duration of the two phases are different but remain charge balanced.

A fundamental range for electrical stimulation of excitable tissue is known as the water-window. It is the potential region at which water oxidizes (anodically) to form oxygen and water reduces (cathodically) to form hydrogen (Merrill et al. 2004). Evoked responses are typically obtained with currents ranging from 10 μA to 1 mA (Tehovnik, 1996); microstimulation currents typically range up to 250 μA (Thurgood et al., 2009).

3. Electrode Offset

Due to differences in half-cell potentials between the recording and reference electrodes, large DC to low frequency offsets are common ranging from 100 mV (Chapin and Moxon, 2001) to 1-2V (Ferris, 1978). These voltage offsets pose a challenge in recording microvolt level neural signals that are typically superimposed on them (Chandran et al., 1999); this necessitates attenuating the offset prior to amplification. A common approach is to use a high pass filter with a low cutoff frequency between 100-300 Hz (Harrison, 2003) when measuring extracellular spike activity. Spike activity has been reported to contain frequencies ranging from 500 Hz to 5 kHz (Buzsáki et al., 1996) and from 300 Hz to 7 kHz (Najafi and Wise, 1986).

B. Stimulator Analog Processing

A major challenge when designing the stimulator was the need to deliver chronic microstimulation of 100 µA to an impedance load of up to 100 kΩ. While an average stimulation intensity of -50 µA was found to initiate an evoked response in contralateral SI, the increased design range to 100 µA provides flexibility and assurance that the required intensity will be available. Furthermore, during experiments with anesthetized rats, higher intensity stimulation is required to strengthen transcallosal connections within a matter of hours. However, the higher intensity requirement drives the amount of power required by the remote unit. A high impedance load was utilized in our design to accommodate for load variations that may result from the electrodes used, distances between the stimulating and reference electrodes, and tissue impedance. Furthermore, cell damage and scar tissue development around the electrode may contribute to increased changes in impedance during chronic stimulation.

The design approach to address this challenge was to use a high power precision op amp for the voltage to current converter that resulted in a stimulator system having a ±20 V compliance voltage. The drawback to this approach is the amount of power consumed. To optimize power, consideration should be given to reducing the stimulator range expectations.

C. Recorder Analog Processing

Neural data acquisition systems are designed to measure microvolt level signals. A major design challenge of these systems exists as a result of the low level neural signals being superimposed onto large DC or low frequency voltage offsets that occur at the electrode-tissue interface (Buzsáki et al., 1996). These offsets are due to half-cell

potentials at the electrode-tissue interface between the working and reference electrode; slight movements of the electrode can lead to offset variations. Rejecting the large offsets while preserving spike activity requires a high pass filter with a low corner frequency positioned at the input of the recorder; this system filters at 220 Hz followed immediately by a buffer.

For this system, two versions of the recorder AFE were developed. Both versions band-pass filtered response activity using a Multiple Feed Back HPF that cascades into a Multiple Feed Back LPF. However, the first stage HPF was executed in Version 2.0. The versions differed in gain and frequency range; Version 1.0 has a measured fidelity of 82.8 dB and a 3 dB bandwidth of 500-5750 Hz whereas Version 2.0 has a fidelity of 78.8 dB and a 3 dB bandwidth of 367-6470 Hz. Both systems performed close to their predicted outcomes and were able to record responses from an implanted electrode.

D. WINSR System Application

The primary purpose of WINSR was the ability to remotely administer and control microstimulation and recording characteristics in real-time. This ability greatly enhances the system's flexibility. Thru WINSR, users have the ability to stop and restart stimulation as well as make modifications to each of the stimulation pulse parameters including polarity, waveform, amplitude, duration, delay, and frequency at any time during the device operation. Users also have the ability to dictate the number of response recordings to be transferred to the base unit and saved for off-line analysis. Having these features designed into the system allows consideration to be given to habituating freely

moving rats to the remote device prior to conducting a study. This system application can be improved upon by incorporating spike detection algorithms for real-time spike analysis.

E. Information Transmission

Practicality of the system is demonstrated, in part, by its autonomous stimulator. This ability allows for chronic stimulation to occur over an extended period of time without continuous data transmission between the remote and base units. Recorder capabilities, however, require continuous connectivity to the host computer for storing of raw response data in real-time. A completely autonomous neural device is obtainable by storing the spike data on a secure digital card mounted to the PCB, this however will increase the overall footprint and weight of the final remote device.

Stimulating and recording parameters were routinely transmitted using Bluetooth communication from the host computer to the remote device without issue. However when the port was kept open to allow for digitized response recordings to be transmitted to the host computer, an increased level of noise was observed; after closing the port, the distortion was no longer apparent. Although digitized response activity was successfully transmitted and stored, responses could not be easily distinguished. This observation was made in both bench-top testing and *in vivo*.

F. Expansion to Multiple Channels

By virtue of the modular design employed for the stimulation and recording systems, additional off-the shelf components can be utilized to increase the number of stimulating and/or recording channels. There are three possible approaches that can be used to accomplish this: (1) adding multiplexors for stimulation and demultiplexors for

recording, (2) duplicating the entire channel, and (3) procuring a fully integrated multi-channel biopotential microchip. By using analog multiplexors and/or demultiplexors, the first approach enables the stimulator to deliver stimuli to different sites and/or the recorder to acquire data from different sites; however this approach does not support multiple active channels for stimulating or recording. To enable multiple concurrent stimulation and/or recording channels, the entire channel must be replicated; the PSoC 1 architecture restricts expandability to a total of 3 channels which can consist of any combination of stimulating and recording channels. However, PSoC 3 and PSoC 5 architectures provide an environment for greater expansion and the PSoC 1 program is easily converted to operate on either of these platforms. Duplicating entire channels, however, increases the overall footprint of the remote device and may restrict the amount of miniaturization that can ultimately be achieved. To enable multiple stimulating and recording channels while maintaining an optimal footprint size, procurement of a fully integrated multiple channel biopotential microchip should be considered. Such products are currently available from Intan Technologies, LLC (www.intantech.com) and are priced around $300 per chip. The chip can be used independently for recording neural signals and in conjunction with a PSoC 3 or PSoC 5 for stimulation.

G. Portability and Miniaturization

While this prototype operates wirelessly, the system is not portable due to the stimulator ±20 V compliance voltage. As such, an external power supply was used to provide the required supply-voltage. This necessitated the use of large footprint regulators to generate the required lower level voltages to for the PSoC, Bluetooth device, and the remaining operational amplifiers. To make the system portable and

significantly smaller and thus more suitable for freely moving rats, consideration should be given to lowering the stimulation intensity required and enhancing the interhemispheric pathway over a period of days as opposed to a period of hours; enhancement of the interhemispheric pathway and inducing functional reorganization in anesthetized animal models must be accomplished within a matter of hours and dictates the higher stimulation intensities.

Functional capabilities of the system were made easier to examine by leveraging a two layer PCB layout. The remote unit printed circuit board could be reduced in size by designing a 4-layer PCB that uses 0402 size components on the top and bottom layers while using the middle two layers for ground and power planes.

CHAPTER V

SUMMARY

I. Dissertation Research Goals

The goal of my dissertation research was to provide additional insight into cortical reorganization in rat primary somatosensory (SI) cortex; this was accomplished by enhancing transcallosal circuitry in forelimb barrel cortex (FBC) by chronic microstimulation and inducing FBC neurons to respond to new input from the ipsilateral forelimb. To begin, I used retrograde and anterograde track tracking techniques to characterize interhemispheric connectivity and identified a differential pattern between homotopic layer V forelimb representations in rat barrel field cortex. This differential pattern of connectivity suggests that interhemispheric circuits in the wrist, forearm, and shoulder regions may be more readily modulated to induce ipsilateral responsiveness given the presence of reciprocal connections with their respective sites in contralateral SI. However, cortical circuits in the forepaw region may be more difficult to modulate due to the lack of homotopic projections to the contralateral forepaw representation. This study was followed by an examination to enhance the interhemispheric pathway using chronic intracortical microstimulation (ICMS) and determining if enhancement leads to functional reorganization. My findings revealed that chronic microstimulation induces changes in evoked response firing rate of transcallosal connections between homotopic layer V forelimb representations, which included forepaw, wrist, and forearm sites. Strengthened connectivity between homotopic wrist and forearm representations led to newly evoked responses to ipsilateral input whereas no clear evidence of ipsilateral responsiveness was found in forepaw cortex. The results from this second study provided

proof of principle that an interhemispheric pathway between SI cortices can be enhanced and the enhancement leads to functional reorganization. The third experimental study contributed to the development of an interactive neural device for the controlled delivery of telemetry-based microstimulation and real-time activity recording. This system can deliver mono-, bi-, and pseudomonophasic microstimulation to a single implanted electrode with user-controlled intensity, duration, delay, and frequency. The device can also acquire neural action potentials from a separate implanted electrode whereby neural signals are band-passed filtered and amplified. The main board measures 4.2 cm × 7.1 cm and interfaces with a custom application used for real-time control of stimulation and recording. Its operational performance has been successfully demonstrated *in vivo* with an anesthetized rat. The interactive neural device presented in this dissertation serves as a prototype of an eventual system that can be used to further examine interhemispheric pathway enhancement and functional reorganization in freely behaving small animals.

II. Review of Experimental Results

A. Experiment One – Anatomical Tract Tracing Study

Experiment One focused on characterizing the regional and laminar distribution patterns of transcallosal projections between homotopic layer V neurons in forelimb barrel field cortex. This was accomplished by making independent focal injections of retrograde or anterograde anatomical tracer into layer V forepaw, wrist, forearm, or shoulder representation. Using the retrograde tracer cholera toxin-B subunit (CT-B), I identified retrogradely labeled callosal projecting neurons in contralateral SI that terminate in layer V barrel cortex. Use of the anterograde racer biotinylated dextran

amine (BDA) provided insight as to where layer V projecting neurons terminate in contralateral barrel cortex. Tissue sectioned in the tangential and coronal planes enabled examination of the regional and laminar distribution patterns, respectively.

Following a small volume injection of CT-B or BDA into one or two independent physiologically identified layer V forelimb representations, homotopic projections exist between the wrist, forearm, and shoulder representation and their respective sites in the contralateral barrel cortex. However, projections from the highly organized forepaw representation terminated in cortical regions bordering the contralateral presumptive FBS. Additionally, the lamina distribution pattern revealed layer V barrel cortex receives input from transcallosal projecting neurons distributed across all cortical lamina in contralateral SI and layer V callosal projecting neurons terminate in all cortical lamina in contralateral barrel cortex; the highest degree of connectivity was observed in layer V and III while layer IV received sparse projections from contralateral layer V.

The absence of dense populations of transcallosal connections within the forepaw barrel cortex suggest that if the forepaw representation sends input to a homotopic forepaw site in contralateral SI, it musts do so via an indirect disynaptic pathway. This is in contrast to the direct monosynaptic pathway from wrist, forearm, and shoulder representations to their homotopic representations in contralateral SI cortex. These findings may provide an indication of the ability to enhance the interhemispheric pathway between homotopic forelimb representations and induce neurons to respond to new input from the ipsilateral forelimb.

Modulation of cortical circuitry requires a thorough grounding of the underlying anatomical connectivity. The regional and laminar distribution patterns characterized in

Experiment One supplied the data necessary to identify an optimal site in layer V forelimb barrel cortex for strengthening transcallosal connections and inducing functional reorganization. Based on the consistency of dense localized populations of transcallosal connections, the interhemispheric pathway connecting homotopic layer V wrist representations in SI cortex was selected as the primary site for enhancement in Experiment Two. Provided that little evidence was found to support a homotopic relationship between forepaw cortices, the forepaw representation was selected as a comparison to the effects of chronic microstimulation on homotopic projections.

B. Experiment Two – Chronic Microstimulation Study

The primary goal of Experiment Two was to demonstrate that the interhemispheric pathway can be strengthened by chronic microstimulation and that the newly enhanced interhemispheric pathway leads to functional reorganization. This was accomplished using intracortical microstimulation (ICMS) to enhance the interhemispheric pathway and peripheral stimulation of the ipsilateral forelimb was used to test for functional reorganization. The following results were obtained:

1. Repeated low frequency (0.5-1 Hz) chronic microstimulation of the interhemispheric pathway between homotopic layer V forelimb (forearm, wrist, and forepaw) representations induced changes in contralateral SI firing rate.

2. Post-ICMS changes consisted predominately of an increase in evoked response activity (n = 9); this increase in firing rate is presumably facilitated by an elevated activation of callosal projections terminating on excitatory pyramidal neurons.

3. In one case, stimulation of the interhemispheric pathway reduced responsiveness in contralateral SI cortex; this decrease in evoked response firing rate is presumably facilitated by an elevated activation of callosal projections terminating on inhibitory interneurons.

4. Strengthened interhemispheric connections had a significant effect on the firing rate of evoked responses to chronic microstimulation; however, the time course of evoked response latency and duration were not significantly affected. The increases in spike activity may be a result of additional neurons being recruited to respond or from neurons firing at a faster rate.

5. Enhancement of the interhemispheric pathway between homotopic wrist and forearm representations led to new responsiveness to input from the ipsilateral wrist and forearm, respectively; ipsilateral responsiveness is likely mediated by the interhemispheric pathways.

6. In contrast, new responses to input from the ipsilateral forepaw were not evident following enhancement of the interhemispheric pathway between homotopic forepaw representations; however, indications of ipsilateral responsiveness developing were present. The absence of a direct monosynaptic pathway between FBS cortices may impact the time and stimulation intensity conditions necessary to induce functional reorganization in the forepaw barrel cortex.

These data indicate that intracortical microstimulation strengthens interhemispheric connections and leads to functional reorganization in rat FBC. Transcallosal projections terminate on both excitatory pyramidal neurons and inhibitory interneurons; interhemispheric pathway enhancement is likely mediated by an increased

activation of transcallosal projecting neurons terminating on excitatory pyramidal neurons. Prior to enhancement of the interhemispheric pathway, neurons in rat forelimb barrel field cortex were nonresponsive to input from the ipsilateral forelimb; however new ipsilateral responsiveness became apparent following enhancement, indicating that responses to ipsilateral input is mediated through the corpus callosum.

C. Experiment Three – Interactive Neuronal Stimulation and Recording Device

The results from Experiment Two provided proof of principle that an interhemispheric pathway between SI cortices can be enhanced and the enhancement leads to functional reorganization. The third experimental study contributed to the development of an interactive neural device that can be used for the controlled delivery of telemetry-based microstimulation and real-time activity recording. The system consists of two major components: a remote device and a host computer. The remote device incorporates stimulator circuitry capable of providing constant current microstimulation to a cortically inserted microelectrode and recorder circuitry capable of acquiring responses from a separate microelectrode in contralateral cortex; all circuitry is housed on a single printed circuit board measuring 4.2 cm × 7.1 cm. The principal design requirement for this system was the ability to simultaneously deliver biphasic stimulation with a maximum intensity of 100 μA and record response activity from loads of up to 100 kΩ with real-time control of microstimulation and recording. It includes the following features:

1. Stimulator analog back end (ABE) circuitry for the generating mono-, bi-, and pseudomonophasic current stimulus pulses with variable intensity (0-100 μA), pulse width (1-10 ms), and delay (0-40 ms).

2. The capacity to deliver a as a set number of stimulation pulses (calibrate mode) or over stimulate for a set period of time (chronic mode).

3. Recorder analog front end (AFE) circuitry that attenuates the low frequency offsets generated at the electrode-tissue interface, band-pass filters, and amplifies acquired spike activity.

4. A Programmable System on a Chip (PSoC) that maintains stimulus pulse generation and digitizes 150 ms of processed neural data at 11 k sps.

5. Bluetooth communication configured with a baud rate of 115.2 k bps for wireless interaction between the remote device and a Bluetooth enabled laptop or desktop computer.

6. A custom application, Wireless Interactive Stimulation and Recording (WINSR), that provides an intuitive graphical user interface for controlling microstimulation delivery and recording response data.

Operational performance of the system was demonstrated *in vivo* in anesthetized adult Sprague-Dawley rats. The system successfully delivered microstimulation of various configurations to a physiologically identified layer V forelimb representation in SI and recorded response activity from the homotopic site in contralateral SI. This device serves as a prototype for developing a compact neural device that can be used to investigate interhemispheric enhancement and functional reorganization in freely moving rats.

III. Conclusion

The material presented in this dissertation contributes to furthering our understanding of cortical reorganization in rat SI cortex. The data suggest that chronic

microstimulation strengthens the firing rate of transcallosal connections in forelimb cortex such that neurons can be induced to respond to new sensory input from the ipsilateral forelimb through an enhanced connection between contralateral and ipsilateral forelimb cortices. Furthermore, I designed and built an interactive embedded system for the controlled delivery of telemetry-based microstimulation and real-time response recoding; this device can be further optimized to study interhemispheric enhancement and functional reorganization in freely moving rats.

The results obtained and the neural interface device presented in these studies also raise new experimental questions that should be addressed to enable a more complete understanding of modulating cortical reorganization. (1) Provided the sparse callosal projections between forepaw representations, what effect do non-homotopic projections have on cortical circuit modulation? (2) How is the activation of callosal projections terminating onto excitatory pyramidal neurons preferentially elevated by chronic microstimulation as opposed to the activation of callosal projections terminating on inhibitory interneurons? (3) How long can enhancement of interhemispheric pathway and functional reorganization remain? (4) How is the time course required for strengthening transcallosal connections and inducing functional reorganization affected in freely moving rats? (5) Is the increased firing rate observed following interhemispheric enhancement a result of additional neurons being recruited to respond or from neurons firing at a faster rate? (6) What are the consequences of chronic operation of the neural interface device? Answers to these questions could provide valuable information relative to cortical plasticity in the primary somatosensory cortex as well as overall brain function to both basic science and clinical communities.

This dissertation research provides a unique insight into the role transcallosal connections and chronic microstimulation may have in cortical reorganization. This work demonstrates the ability to modulate cortical circuits and induce functional reorganization in rat forelimb barrel cortex, which may indicate our ability to modulate cortical reorganization that occurs following limb amputation and during post-stroke recovery.

LIST OF REFERENCES

Akers RM, Killackey HP (1978) Organization of corticocortical connections in the parietal cortex of the rat. Journal of Comparative Neurology 181:513–537 Available at: http://www.ncbi.nlm.nih.gov/pubmed/690276.

Anderson JM, Rodriguez A, Chang DT (2008) Foreign body reaction to biomaterials. Seminars in Immunology 20:86–100 Available at: http://www.pubmedcentral.nih.gov/articlerender.fcgi?artid=2327202&tool=pmcentrez&rendertype=abstract.

Angel A, Banks D (1983) The functional organization of the forepaw sensorimortor cortex in the adult rat. Proc. J. Physiol (Lond):70.

Angel A, Lemon RN (1975) Sensorimotor cortical representation in the rat and the role of the cortex in the production of sensory myoclonic jerks. The Journal of physiology 248:465–88 Available at: http://www.pubmedcentral.nih.gov/articlerender.fcgi?artid=1309532&tool=pmcentrez&rendertype=abstract [Accessed March 6, 2013].

Arfin SK, Long MA, Fee MS, Sarpeshkar R (2009) Wireless Neural Stimulation in Freely Behaving Small Animals. Journal of Neurophysiology:598 – 605.

Armstrong-James M, Fox K, Das-Gupta A (1992) Flow of excitation within rat barrel cortex on striking a single vibrissa. Journal of Neurophysiology 68:1345–1358 Available at: http://www.ncbi.nlm.nih.gov/pubmed/1432088.

Armstrong-James M, George MJ (1988) Bilateral receptive fields of cells in rat Sm1 cortex. Experimental brain research. Experimentelle Hirnforschung. Expérimentation cérébrale 70:155–65 Available at: http://www.ncbi.nlm.nih.gov/pubmed/3402562 [Accessed September 17, 2011].

Armstrong-James M, Millar J (1979) Carbon fibre microelectrodes. Journal of Neuroscience Methods 1:279–287 Available at: http://www.ncbi.nlm.nih.gov/pubmed/544972.

Arnold PB, Li CX, Waters RS (2001) Thalamocortical arbors extend beyond single cortical barrels: an in vivo intracellular tracing study in rat. Experimental Brain Research 136:152–168 Available at: http://www.springerlink.com/openurl.asp?genre=article&id=doi:10.1007/s002210000570 [Accessed July 12, 2011].

Aroniadou-Anderjaska V, Keller A (1995) LTP in the barrel cortex of adult rats. Neuroreport 6:2297–300 Available at: http://www.ncbi.nlm.nih.gov/pubmed/8747140 [Accessed October 29, 2011].

Artola A, Bröcher S, Singer W (1990) Different voltage-dependent thresholds for inducing long-term depression and long-term potentiation in slices of rat visual cortex. Nature 347:69–72 Available at: http://www.ncbi.nlm.nih.gov/pubmed/1975639 [Accessed March 6, 2013].

Barbaresi P, Fabri M, Conti F, Manzoni T (1987) D-[3H]aspartate retrograde labelling of callosal and association neurones of somatosensory areas I and II of cats. The Journal of Comparative Neurology 263:159–78 Available at: http://www.ncbi.nlm.nih.gov/pubmed/3667974 [Accessed November 5, 2012].

Bernardo KL, McCasland JS, Woolsey TA, Strominger RN (1990) Local intra- and interlaminar connections in mouse barrel cortex. The Journal of comparative neurology 291:231–55 Available at: http://www.ncbi.nlm.nih.gov/pubmed/2298933 [Accessed November 10, 2012].

Bindman LJ, Murphy KP, Pockett S (1988) Postsynaptic control of the induction of long-term changes in efficacy of transmission at neocortical synapses in slices of rat brain. Journal of neurophysiology 60:1053–65 Available at: http://www.ncbi.nlm.nih.gov/pubmed/2845015 [Accessed March 6, 2013].

Bogdanova OG, Sil'kis IG (2002) Post-tetanic modification of the efficiency of excitatory transmission in neural networks including interhemispheric connections. Neuroscience and behavioral physiology 32:15–24 Available at: http://www.ncbi.nlm.nih.gov/pubmed/11838551 [Accessed October 29, 2011].

Borsook D, Becerra L, Fishman S, Edwards a, Jennings CL, Stojanovic M, Papinicolas L, Ramachandran VS, Gonzalez RG, Breiter H (1998) Acute plasticity in the human somatosensory cortex following amputation. Neuroreport 9:1013–7 Available at: http://www.ncbi.nlm.nih.gov/pubmed/9601659.

Brodmann K (1909) Vergleichende Localisationslehre der Grosshirnrinde in ihren Principien dargestellt auf Grund des Zellenbaues Barth, ed. J A Barth.

Brooks VB, Rudomin P, Slayman CL (1961)(a) Peripheral Receptive Fields of Neurons in the Cat's Cerebral Cortex. Methods:302–325.

Brooks VB, Rudomin P, Slayman CL (1961)(b) Sensory Activation of Neurons in the Cat's Cerebral Cortex. Methods:286–301.

Buzsáki G, Penttonen M, Nádasdy Z, Bragin A (1996) Pattern and inhibition-dependent invasion of pyramidal cell dendrites by fast spikes in the hippocampus in vivo. Proceedings of the National Academy of Sciences of the United States of America 93:9921–5 Available at: http://www.pubmedcentral.nih.gov/articlerender.fcgi?artid=38530&tool=pmcentrez&rendertype=abstract.

Calford MB, Tweedale R (1988) Immediate and Chronic Changes in Responses of Somatosensory Cortex in Adult Flying-Fox After Digit Amputation. Nature 332:446–448 Available at: http://eutils.ncbi.nlm.nih.gov/entrez/eutils/elink.fcgi?dbfrom=pubmed&id=3352742&retmode=ref&cmd=prlinks.

Calford MB, Tweedale R (1990) Interhemispheric transfer of plasticity in the cerebral cortex. Science (New York, N.Y.) 249:805–7 Available at: http://www.ncbi.nlm.nih.gov/entrez/query.fcgi?cmd=Retrieve&db=PubMed&dopt=Citation&list_uids=2389146.

Carvell GE, Simons DJ (1988) Membrane potential changes in rat SmI cortical neurons evoked by controlled stimulation of mystacial vibrissae. Brain Research 448:186–191 Available at: http://dx.doi.org/10.1016/0006-8993(88)91118-3 [Accessed September 18, 2011].

Chandran AP, Najafi K, Wise KD (1999) A new dc baseline stabilization scheme for neural recording microprobes In Proceedings of the First Joint BMES/EMBS Conference. 1999 IEEE Engineering in Medicine and Biology 21st Annual Conference and the 1999 Annual Fall Meeting of the Biomedical Engineering Society (Cat. No.99CH37015) IEEE, p. 386. Available at: http://ieeexplore.ieee.org/xpls/abs_all.jsp?arnumber=802463’ escapeXml='false'/> [Accessed March 4, 2013].

Chapin JK, Lin CS (1984) Mapping the body representation in the SI cortex of anesthetized and awake rats. Journal of Comparative Neurology 229:199–213 Available at: http://www.ncbi.nlm.nih.gov/pubmed/6438190.

Chapin JK, Moxon KA (2001) Neural Prostheses for Restoration of Sensory and Motor Function, Methods and New Frontiers in Neuroscience J. K. Chapin & K. A. Moxon, eds. Boca raton: CRC Press. Available at: http://books.google.com/books/about/Neural_Prostheses_for_Restoration_of_Sen.html?id=zKx_hSJAMpgC [Accessed March 4, 2013].

Chapin JK, Sadeq M, Guise JL (1987) Corticocortical connections within the primary somatosensory cortex of the rat. Journal of Comparative Neurology 263:326–346 Available at: http://www.ncbi.nlm.nih.gov/entrez/query.fcgi?cmd=Retrieve&db=PubMed&dopt=Citation&list_uids=2822774.

Chmielowska J, Carvell GE, Simons DJ (1989) Spatial organization of thalamocortical and corticothalamic projection systems in the rat SmI barrel cortex. Journal of Comparative Neurology 285:325–338 Available at: http://www.ncbi.nlm.nih.gov/entrez/query.fcgi?cmd=Retrieve&db=PubMed&dopt=Citation&list_uids=2547850 [Accessed November 10, 2012].

Clarey JC, Tweedale R, Calford MB (1996) Interhemispheric modulation of somatosensory receptive fields: evidence for plasticity in primary somatosensory cortex. Cerebral cortex (New York, N.Y. : 1991) 6:196–206 Available at: http://www.ncbi.nlm.nih.gov/pubmed/8670650.

Conti F, Fabri M, Manzoni T (1986) Bilateral receptive fields and callosal connectivity of the body midline representation in the first somatosensory area of primates. Somatosensory research 3:273–89 Available at: http://www.ncbi.nlm.nih.gov/pubmed/3775151 [Accessed February 11, 2012].

Dawson DR, Killackey HP (1987) The organization and mutability of the forepaw and hindpaw representations in the somatosensory cortex of the neonatal rat. Journal of Comparative Neurology 256:246–256 Available at: http://www.ncbi.nlm.nih.gov/entrez/query.fcgi?cmd=Retrieve&db=PubMed&dopt=Citation&list_uids=3558880.

DeCosta-Fortune T, Li CX, Vemulapalli S, DeJongh-Curry A, Waters RS (2010) Pattern of Interhemispheric Connections Between Forelimb Representations in Rat Barrel Field Cortex In Program No. 377.10 2010 Neuroscience Meeting Planner San Diego, CA: Society for Neuroscience, 2010. Online. Available at: http://www.abstractsonline.com/Plan/start.aspx.

DeCosta-Fortune T, Yang Q, Tyagi N, DeJongh-Curry A, Li C-X, Waters RS (2009) Functional Modulation of Interhemispheric Forelimb Connectins in Rat In Program No. 363.21. 2009 Neuroscience Meeting Planner. Chicago, IL: Society for Neuroscience, 2009. Online. Available at: http://www.abstractsonline.com/Plan/start.aspx.

DeVries I (1911) De Cellulaire Bouw der Groote Hersenschors van de Muis en de Veranderingen daarin na Doornijding van het Corpus Callosum. De Waal, Groningen.

Diamond ME, Armstrong-James M, Ebner FF (1993) Experience-dependent plasticity in adult rat barrel cortex. Proceedings of the National Academy of Sciences of the United States of America 90:2082–6 Available at: http://www.ncbi.nlm.nih.gov/pubmed/12514235.

Dinse HR, Recanzone GH, Merzenich MM (1993) Alterations in correlated activity parallel ICMS-induced representational plasticity. Neuroreport 5:173–6 Available at: http://www.ncbi.nlm.nih.gov/pubmed/8111006 [Accessed March 4, 2013].

Dreyer DA, Loe PR, Metz CB, Whitsel BL (1975) Representation of Head and Face in Postcentral Gyrus of the Macaque. Journal of neurophysiology 38:714–33 Available at: http://www.ncbi.nlm.nih.gov/pubmed/1127463 [Accessed February 11, 2012].

Ebner FF, Myers RE (1965) Distribution of corpus callosum and anterior commissure in cat and raccoon. The Journal of Comparative Nurology 124:353–65 Available at: http://www.ncbi.nlm.nih.gov/pubmed/5861718 [Accessed November 5, 2012].

Elbert T, Flor H, Birbaumer N, Knecht S, Hampson S, Larbig W, Taub E (1994) Extensive reorganization of the somatosensory cortex in adult humans after nervous system injury. Neuroreport 5:2593–7 Available at: http://www.ncbi.nlm.nih.gov/pubmed/7696611.

Fan D, Rich D, Holtzman T, Ruther P, Dalley JW, Lopez A, Rossi M a, Barter JW, Salas-Meza D, Herwik S, Holzhammer T, Morizio J, Yin HH (2011) A wireless multi-channel recording system for freely behaving mice and rats. PloS one 6:e22033 Available at: http://www.ncbi.nlm.nih.gov/pubmed/21765934 [Accessed July 21, 2011].

Farshchi S, Nuyujukian PH, Pesterev A, Mody I, Judy JW (2006) A TinyOS-enabled MICA2-based wireless neural interface. IEEE transactions on bio-medical engineering 53:1416–24 Available at: http://www.ncbi.nlm.nih.gov/pubmed/16830946.

Favorov O V, Diamond ME (1990) Demonstration of discrete place-defined columns--segregates--in the cat SI. The Journal of comparative neurology 298:97–112 Available at: http://www.ncbi.nlm.nih.gov/pubmed/23027250.

Favorov O V, Diamond ME, Whitsel BL (1987) Evidence for a mosaic representation of the body surface in area 3b of the somatic cortex of cat. Proceedings of the National Academy of Sciences of the United States of America 84:6606–10 Available at: http://www.pubmedcentral.nih.gov/articlerender.fcgi?artid=299128&tool=pmcentrez&rendertype=abstract [Accessed July 12, 2011].

Favorov O V, Whitsel BL, Chiu JS, Tommerdahl M (2006) Activation of cat SII cortex by flutter stimulation of contralateral vs. ipsilateral forepaws. Brain research 1071:81–90 Available at: http://www.ncbi.nlm.nih.gov/pubmed/16412394 [Accessed July 12, 2011].

Favorov O, Whitsel BL (1988) Spatial organization of the peripheral input to area 1 cell columns. I. The detection of "segregates". Brain research 472:25–42 Available at: http://www.ncbi.nlm.nih.gov/pubmed/3342334.

Feldmeyer D (2012) Excitatory neuronal connectivity in the barrel cortex. Frontiers in neuroanatomy 6:24 Available at: http://www.pubmedcentral.nih.gov/articlerender.fcgi?artid=3394394&tool=pmcentrez&rendertype=abstract [Accessed November 5, 2012].

Fernando NX, Macklin DN, Hsu MY, Judy JW (2007) An Embedded Wireless Neural Stimulation and Recording System In 2007 3rd International IEEE/EMBS Conference on Neural Engineering IEEE, p. 333–336. Available at: http://ieeexplore.ieee.org/xpls/abs_all.jsp?arnumber=4227283' escapeXml='false'/> [Accessed March 1, 2013].

Ferris CD (1978) Introduction to Bioinstrumentation. Clifton, NJ: Humana. Available at: http://books.google.com/books/about/Introduction_to_Bioinstrumentation.html?id=0RR6M66EwDIC [Accessed March 1, 2013].

Flor H, Braun C, Elbert T, Birbaumer N (1997) Extensive reorganization of primary somatosensory cortex in chronic back pain patients. Neuroscience letters 224:5–8 Available at: http://www.ncbi.nlm.nih.gov/pubmed/9132689.

Flor H, Elbert T, Mühlnickel W, Pantev C, Wienbruch C, Taub E (1998) Cortical reorganization and phantom phenomena in congenital and traumatic upper-extremity amputees. Experimental brain research. Experimentelle Hirnforschung. Expérimentation cérébrale 119:205–12 Available at: http://www.ncbi.nlm.nih.gov/pubmed/9535570.

Florence SL, Jain N, Pospichal MW, Beck PD, Sly DL, Kaas JH (1996) Central reorganization of sensory pathways following peripheral nerve regeneration in fetal monkeys. Nature 381:69–71 Available at: http://dx.doi.org/10.1038/381069a0 [Accessed January 28, 2012].

Florence SL, Kaas JH (1995) Large-scale reorganization at multiple levels of the somatosensory pathway follows therapeutic amputation of the hand in monkeys. The Journal of neuroscience : the official journal of the Society for Neuroscience 15:8083–95 Available at: http://www.ncbi.nlm.nih.gov/pubmed/8613744.

Franks W, Schenker I, Schmutz P, Hierlemann A (2005) Impedance characterization and modeling of electrodes for biomedical applications. IEEE transactions on bio-medical engineering 52:1295–302 Available at: http://www.ncbi.nlm.nih.gov/pubmed/16041993.

Glazewski S, Herman C, McKenna M, Chapman PF, Fox K (1998) Long-term potentiation in vivo in layers II/III of rat barrel cortex. Neuropharmacology 37:581–92 Available at: http://www.ncbi.nlm.nih.gov/pubmed/9704999 [Accessed October 29, 2011].

Harrison RR (2003) A low-power integrated circuit for adaptive detection of action potentials in noisy signals. Proceedings of the 25th Annual International Conference of the IEEE Engineering in Medicine and Biology Society (IEEE Cat. No.03CH37439):3325–3328 Available at: http://ieeexplore.ieee.org/lpdocs/epic03/wrapper.htm?arnumber=1280856.

Harrison RR, Kier RJ, Kim S, Rieth L, Warren DJ, Ledbetter NM, Clark GA, Solzbacher F, Chestek CA, Gilja V, Nuyujukian P, Ryu SI, Shenoy K V, Design C (2008) A Wireless Neural Interface for Chronic Recording. IEEE:125–128.

Harrison RR, Watkins PT, Kier RJ, Lovejoy RO, Black DJ, Greger B, Solzbacher F (2007) A Low-Power Integrated Circuit for a Wireless 100-Electrode Neural Recording System. IEEE Journal of Solid-State Circuits 42:123–133 Available at: http://ieeexplore.ieee.org/xpls/abs_all.jsp?arnumber=4039585' escapeXml='false'/> [Accessed March 1, 2013].

Hattox AM, Nelson SB (2007) Layer V neurons in mouse cortex projecting to different targets have distinct physiological properties. Journal of neurophysiology 98:3330–40 Available at: http://www.ncbi.nlm.nih.gov/pubmed/17898147 [Accessed November 4, 2012].

Hayama T, Ogawa H (1997) Regional differences of callosal connections in the granular zones of the primary somatosensory cortex in rats. Brain Research Bulletin 43:341–347 Available at: http://www.ncbi.nlm.nih.gov/pubmed/9227846.

Hebb DO (1949) The organization of behavior. Wiley.

Henry EC, Catania KC (2006) Cortical, callosal, and thalamic connections from primary somatosensory cortex in the naked mole-rat (Heterocephalus glaber), with special emphasis on the connectivity of the incisor representation. The anatomical record Part A Discoveries in molecular cellular and evolutionary biology 288:626–645.

Herron P, Johnson JI (1987) Organization of intracortical and commissural connections in somatosensory cortical areas I and II in the raccoon. The Journal of comparative neurology 257:359–71 Available at: http://www.ncbi.nlm.nih.gov/pubmed/3558894 [Accessed November 5, 2012].

Heusler P, Cebulla B, Boehmer G, Dinse HR (2000) A repetitive intracortical microstimulation pattern induces long-lasting synaptic depression in brain slices of the rat primary somatosensory cortex. Experimental brain research. Experimentelle Hirnforschung. Expérimentation cérébrale 135:300–10 Available at: http://www.ncbi.nlm.nih.gov/pubmed/11146808 [Accessed February 14, 2012].

Hoeflinger BF, Bennett-Clarke CA, Chiaia NL, Killackey HP, Rhoades RW (1995) Patterning of local intracortical projections within the vibrissae representation of rat primary somatosensory cortex. The Journal of comparative neurology 354:551–63 Available at: http://www.ncbi.nlm.nih.gov/pubmed/7541807 [Accessed November 10, 2012].

Hubel DH, Wiesel TN (1977) Functional architecture of macaque monkey visual cortex. Society 198:1–59 Available at: http://www.ncbi.nlm.nih.gov/pubmed/20635.

Hubel DH, Wiesel TN, LeVay S (1977) Plasticity of ocular dominance columns in monkey striate cortex. Philosophical Transactions of the Royal Society of London - Series B: Biological Sciences 278:377–409 Available at: http://www.ncbi.nlm.nih.gov/pubmed/19791.

Innocenti GM (1986) General organization of callosal connections in the cerebral cortex In E. G. Jones & A. Peters, eds. Cerebral Cortex Plenum Press, p. 291–353. Available at: http://130.203.133.150/showciting;jsessionid=D4F2D80A03128A640BFF1BBA30F2CA8E?cid=5467485 [Accessed December 14, 2012].

Innocenti GM, Manzoni T, Spidalieri G (1973) Relevance of the callosal transfer in defining the peripheral reactivity of somesthetic cortical neurones. Archives italiennes de biologie 111:187–221 Available at: http://www.ncbi.nlm.nih.gov/pubmed/18843823 [Accessed September 17, 2011].

Ivy GO, Killackey HP (1981) The ontogeny of the distribution of callosal projection neurons in the rat parietal cortex. Journal of Comparative Neurology 195:367–89 Available at: http://www.ncbi.nlm.nih.gov/pubmed/6205722.

Iwamura Y (2000) Bilateral receptive field neurons and callosal connections in the somatosensory cortex. Philosophical transactions of the Royal Society of London. Series B, Biological sciences 355:267–73 Available at: http://www.pubmedcentral.nih.gov/articlerender.fcgi?artid=1692728&tool=pmcentrez&rendertype=abstract.

Iwamura Y, Iriki A, Tanaka M (1994) Bilateral hand representation in the postcentral somatosensory cortex. Nature 369:554–6 Available at: http://www.ncbi.nlm.nih.gov/pubmed/8202155 [Accessed June 18, 2011].

Iwamura Y, Iriki A, Tanaka M, Taoka M, Toda T (1996) Bilateral receptive field neurons in the postcentral gyrus: two hands meet the midline In T. Ono, B. L. McNaughton, S. Molotchnikoff, E. T. Rolls, & H. Nishijo, eds. Pergamon studies in neuroscience. Perception, mempory and emotion: fortier in neuroscience Oxford, UK: Elsevier, p. 33–44.

Iwamura Y, Tanaka M, Iriki a, Taoka M, Toda T (2002) Processing of tactile and kinesthetic signals from bilateral sides of the body in the postcentral gyrus of awake monkeys. Behavioural brain research 135:185–90 Available at: http://www.ncbi.nlm.nih.gov/pubmed/12356449.

Iwamura Y, Taoka M, Iriki A (2001) Bilateral activity and callosal connections in the somatosensory cortex. The Neuroscientist : a review journal bringing neurobiology, neurology and psychiatry 7:419–29 Available at: http://www.ncbi.nlm.nih.gov/pubmed/11597101 [Accessed November 6, 2012].

Jackson A, Baker SN, Fetz EE (2006)(a) Tests for presynaptic modulation of corticospinal terminals from peripheral afferents and pyramidal tract in the macaque. Society 1:107–120.

Jackson A, Mavoori J, Fetz EE (2006)(b) Long-term motor cortex plasticity induced by an electronic neural implant. Nature 444:56–60 Available at: http://www.ncbi.nlm.nih.gov/pubmed/17057705 [Accessed June 29, 2011].

Jackson A, Mavoori J, Fetz EE (2007) Correlations between the same motor cortex cells and arm muscles during a trained task, free behavior, and natural sleep in the macaque monkey. Journal of neurophysiology 97:360–74 Available at: http://www.ncbi.nlm.nih.gov/pubmed/17021028 [Accessed June 30, 2010].

Jackson A, Moritz CT, Mavoori J, Lucas TH, Fetz EE (2006)(c) The Neurochip BCI: towards a neural prosthesis for upper limb function. IEEE transactions on neural systems and rehabilitation engineering : a publication of the IEEE Engineering in Medicine and Biology Society 14:187–90 Available at: http://www.ncbi.nlm.nih.gov/pubmed/16792290.

Jensen KF, Killackey HP (1987)(a) Terminal Arbors of Axons Projecting to the Somatosensory Cortex of the Adult Rat. II. The Altered Morphology of Thalamocortical Afferents Following Neonatal Infraorbital Nerve Cut. The Journal of neuroscience : the official journal of the Society for Neuroscience 7:3544–53 Available at: http://www.ncbi.nlm.nih.gov/pubmed/3316525.

Jensen KF, Killackey HP (1987)(b) Terminal arbors of axons projecting to the somatosensory cortex of the adult rat. I. The normal morphology of specific thalamocortical afferents. The Journal of neuroscience : the official journal of the Society for Neuroscience 7:3529–43 Available at: http://www.ncbi.nlm.nih.gov/pubmed/3316525.

Jones E (1985) The thalamus. New York: Plenum Press.

Kalarickal GJ, Marshall JA (2002) Rearrangement of receptive field topography after intracortical and peripheral stimulation: the role of plasticity in inhibitory pathways. Network (Bristol, England) 13:1–40 Available at: http://www.ncbi.nlm.nih.gov/pubmed/11873840 [Accessed March 1, 2013].

Kalaska J, Pomeranz B (1979) Chronic paw denervation causes an age-dependent appearance of novel responses from forearm in “paw cortex” of kittens and adult cats. Journal of Neurophysiology 42:618–633 Available at: http://www.ncbi.nlm.nih.gov/entrez/query.fcgi?cmd=Retrieve&db=PubMed&dopt=Citation&list_uids=422979.

Kelahan AM, Ray RH, Carson L V, Massey CE, Doetsch GS (1981) Functional reorganization of adult raccoon somatosensory cerebral cortex following neonatal digit amputation. Brain Research 223:152–159

Kerr AL, Cheng S-Y, Jones TA (2011) Experience-dependent neural plasticity in the adult damaged brain. Journal of Communication Disorders 44:538–548 Available at: http://www.ncbi.nlm.nih.gov/pubmed/21620413.

Knecht S, Henningsen H, Elbert T, Flor H, Höhling C, Pantev C, Birbaumer N, Taub E (1995) Cortical reorganization in human amputees and mislocalization of painful stimuli to the phantom limb. Neuroscience letters 201:262–4 Available at: http://www.ncbi.nlm.nih.gov/pubmed/8786855.

Knecht S, Henningsen H, Elbert T, Flor H, Höhling C, Pantev C, Taub E (1996) Reorganizational and perceptional changes after amputation. Brain : a journal of neurology 119 (Pt 4:1213–9 Available at: http://www.ncbi.nlm.nih.gov/pubmed/8813284.

Koralek KA, Killackey HP (1990) Callosal projections in rat somatosensory cortex are altered by early removal of afferent input. Proceedings of the National Academy of Sciences of the United States of America 87:1396–400 Available at: http://www.pubmedcentral.nih.gov/articlerender.fcgi?artid=53482&tool=pmcentrez&rendertype=abstract.

Koralek KA, Olavarria J, Killackey HP (1990) Areal and laminar organization of corticocortical projections in the rat somatosensory cortex. The Journal of Comparative Nurology 299:133–50 Available at: http://www.ncbi.nlm.nih.gov/pubmed/2172324 [Accessed September 15, 2011].

Korvenoja A, Wikstrom H, Huttunen J, Virtanan J, Laine P, Aronen HJ, Seppalainen AM, Ilmoniemi RJ (1995) Activation of ipsilateral primary sensorimotor cortex by median nerve stimulation. Neuroreport 6:2589–93 Available at: http://www.ncbi.nlm.nih.gov/pubmed/8741769 [Accessed September 17, 2011].

Land PW, Buffer SA, Yaskosky JD (1995) Barreloids in adult rat thalamus: three-dimensional architecture and relationship to somatosensory cortical barrels. Journal of Comparative Neurology 355:573–588 Available at: http://www.ncbi.nlm.nih.gov/pubmed/7636032.

Ledoux MS, Whitworth RH, Gould HJ (1987) Interhemispheric connections of the somatosensory cortex in the rabbit. The Journal of comparative neurology 258:145–57 Available at: http://www.ncbi.nlm.nih.gov/pubmed/3571535 [Accessed November 6, 2012].

Lee KS (1982) Sustained enhancement of evoked potentials following brief, high-frequency stimulation of the cerebral cortex in vitro. Brain research 239:617–23 Available at: http://www.ncbi.nlm.nih.gov/pubmed/6284309 [Accessed March 6, 2013].

Lee SM, Ebner FF (1992) Induction of high frequency activity in the somatosensory thalamus of rats in vivo results in long-term potentiation of responses in SI cortex. Experimental brain research. Experimentelle Hirnforschung. Expérimentation cérébrale 90:253–61 Available at: http://www.ncbi.nlm.nih.gov/pubmed/1397139 [Accessed October 29, 2011].

Lee SM, Weisskopf MG, Ebner FF (1991) Horizontal long-term potentiation of responses in rat somatosensory cortex. Brain research 544:303–10 Available at: http://www.ncbi.nlm.nih.gov/pubmed/1828185 [Accessed October 29, 2011].

Li CX, Callaway JC, Waters RS (2002) Removal of GABAergic inhibition alters subthreshold input in neurons in forepaw barrel subfield (FBS) in rat first somatosensory cortex (SI) after digit stimulation. Experimental brain research. Experimentelle Hirnforschung. Expérimentation cérébrale 145:411–28 Available at: http://www.ncbi.nlm.nih.gov/pubmed/12172653 [Accessed June 17, 2011].

Li CX, Waters RS (1996) In vivo intracellular recording and labeling of neurons in the forepaw barrel subfield (FBS) of rat somatosensory cortex: possible physiological and morphological substrates for reorganization. Neuroreport 7:2261–72 Available at: http://www.ncbi.nlm.nih.gov/pubmed/8951838 [Accessed October 19, 2011].

Li CX, Waters RS, McCandlish CA, Johnson EF (1996) Electrical stimulation of a forepaw digit increases the physiological representation of that digit in layer IV of SI cortex in rat. Neuroreport 7:2395–400 Available at: http://www.ncbi.nlm.nih.gov/pubmed/8951859 [Accessed August 23, 2011].

Li L, Rema V, Ebner FF (2005) Chronic suppression of activity in barrel field cortex downregulates sensory responses in contralateral barrel field cortex. Journal of neurophysiology 94:3342–56 Available at: http://www.ncbi.nlm.nih.gov/pubmed/16014795 [Accessed August 23, 2011].

Liepert J, Bauder H, Miltner WHR, Taub E (2009) Treatment-Induced Cortical Reorganization After Stroke in Humans. Stroke.

Lipton ML, Fu K-MG, Branch C a, Schroeder CE (2006) Ipsilateral hand input to area 3b revealed by converging hemodynamic and electrophysiological analyses in macaque monkeys. The Journal of neuroscience : the official journal of the Society for Neuroscience 26:180–5 Available at: http://www.ncbi.nlm.nih.gov/pubmed/16399685 [Accessed July 12, 2011].

Lorente De No R (1922) La corteza cerebral del raton. Trab Lab Invest Bio 20:41–78 .

Lübke J, Egger V, Sakmann B, Feldmeyer D (2000) Columnar organization of dendrites and axons of single and synaptically coupled excitatory spiny neurons in layer 4 of the rat barrel cortex. The Journal of neuroscience : the official journal of the Society for Neuroscience 20:5300–11 Available at: http://www.ncbi.nlm.nih.gov/pubmed/10884314.

MacIver K, Lloyd DM, Kelly S, Roberts N, Nurmikko T (2008) Phantom limb pain, cortical reorganization and the therapeutic effect of mental imagery. Brain : a journal of neurology 131:2181–91 Available at: http://www.pubmedcentral.nih.gov/articlerender.fcgi?artid=2494616&tool=pmcentrez&rendertype=abstract [Accessed June 15, 2011].

Mann MD (1979) Sets of neurons in somatic cerebral cortex of the cat and their ontogeny. Brain research 180:3–45 Available at: http://www.ncbi.nlm.nih.gov/pubmed/385112 [Accessed March 6, 2013].

Manns ID, Sakmann B, Brecht M (2004) Sub- and suprathreshold receptive field properties of pyramidal neurones in layers 5A and 5B of rat somatosensory barrel cortex. The Journal of physiology 556:601–22 Available at: http://www.pubmedcentral.nih.gov/articlerender.fcgi?artid=1664944&tool=pmcentrez&rendertype=abstract [Accessed November 5, 2012].

Manzoni T (1997) The callosal connections of the hierarchically organized somatosensory areas of primates. Journal of neurosurgical sciences 41:1–22 Available at: http://www.ncbi.nlm.nih.gov/pubmed/9273853 [Accessed November 6, 2012].

Manzoni T, Barbaresi P, Bellardinelli E, Caminiti R (1980) Callosal projections from the two body midlines. Experimental Brain Research 39:1–9 Available at: http://www.springerlink.com/index/P51K27M250237920.pdf [Accessed September 17, 2011].

Manzoni T, Barbaresi P, Conti F, Fabri M (1989) The callosal connections of the primary somatosensory cortex and the neural bases of midline fusion. Experimental Brain Research 76:251–266 Available at: http://www.ncbi.nlm.nih.gov/entrez/query.fcgi?cmd=Retrieve&db=PubMed&dopt=Citation&list_uids=2670598.

Martin JH (1989) Neuroanatomy Text and Atlas 4th ed. Elsevier Science Publishing Co., Inc.

Mavoori J, Jackson A, Diorio C, Fetz E (2005) An autonomous implantable computer for neural recording and stimulation in unrestrained primates. Journal of neuroscience methods 148:71–7 Available at: http://www.ncbi.nlm.nih.gov/pubmed/16102841.

McCandlish CA, Li CX, Waters RS, Howard EM (1996) Digit removal leads to discrepancies between the structural and functional organization of the forepaw barrel subfield in layer IV of rat primary somatosensory cortex. Experimental Brain Research 108:417–426 Available at: http://www.ncbi.nlm.nih.gov/pubmed/8801121.

Merzenich MM, Kaas JH, Wall J, Nelson RJ, Sur M, Felleman D (1983) Topographic reorganization of somatosensory cortical areas 3b and 1 in adult monkeys following restricted deafferentation. Neuroscience 8:33–55 Available at: http://www.ncbi.nlm.nih.gov/pubmed/6835522.

Meyer HS, Schwarz D, Wimmer VC, Schmitt AC, Kerr JND, Sakmann B, Helmstaedter M (2011) Inhibitory interneurons in a cortical column form hot zones of inhibition in layers 2 and 5A. Proceedings of the National Academy of Sciences of the United States of America 108:16807–12 Available at: http://www.pubmedcentral.nih.gov/articlerender.fcgi?artid=3189020&tool=pmcentrez&rendertype=abstract [Accessed November 10, 2012].

Meyer HS, Wimmer VC, Oberlaender M, Kock CPJ de, Sakmann B, Helmstaedter M (2010) Number and laminar distribution of neurons in a thalamocortical projection column of rat vibrissal cortex. Cerebral cortex (New York, N.Y. : 1991) 20:2277–86 Available at: http://www.pubmedcentral.nih.gov/articlerender.fcgi?artid=2936806&tool=pmcentrez&rendertype=abstract [Accessed November 4, 2012].

Moore CI, Nelson SB, Cam J Le, Estebanez L, Jacob V, Shulz DE, Roy NC, Bessaih T, Contreras D (1998) Spatio-temporal subthreshold receptive fields in the vibrissa representation of rat primary somatosensory cortex. Journal of Neurophysiology 80:2882–2892 Available at: http://www.ncbi.nlm.nih.gov/pubmed/9862892.

Morris RG (1999) D.O. Hebb: The Organization of Behavior, Wiley: New York; 1949. Brain research bulletin 50:437 Available at: http://www.ncbi.nlm.nih.gov/pubmed/10643472 [Accessed March 6, 2013].

Mountcastle VB (1957) Modality and topographic properties of single neurons of cat's somatic sensory cortex. Journal of Neurophysiology 20:408–434 Available at: http://jn.physiology.org.

Mountcastle VB (1978) An organizing principle for cerebral function In G. Edelman & V. B. Mountcastle, eds. The Mindful Brain MIT Press, p. 7–50.

Mountcastle VB (1997) The columnar organization of the neocortex. Brain : a journal of neurology 120 (Pt 4:701–22 Available at: http://www.ncbi.nlm.nih.gov/pubmed/9153131.

Mountcastle VB, Berman AL, Davies PW (1955) Topographic organization and modality representation in first somatic area of cat's cerebral cortex by method of single unit analysis. American Journal of Physiology 183:464.

Mountcastle VB, Davies PW, Berman a L (1957) Response properties of neurons of cat's somatic sensory cortex to peripheral stimuli. Journal of neurophysiology 20:374–407 Available at: http://www.ncbi.nlm.nih.gov/pubmed/13439409.

Murphy TH, Corbett D (2009) Plasticity during stroke recovery: from synapse to behaviour. Nature reviews. Neuroscience 10:861–72 Available at: http://www.ncbi.nlm.nih.gov/pubmed/19888284 [Accessed March 1, 2013].

Najafi K, Wise K (1986) Implantable multielectrode array with on-chip signal processing In 1986 IEEE International Solid-State Circuits Conference. Digest of Technical Papers Institute of Electrical and Electronics Engineers, p. 98–99. Available at: http://ieeexplore.ieee.org/xpls/abs_all.jsp?arnumber=1157002' escapeXml='false'/> [Accessed March 1, 2013].

Nolte J (2009) The human brain: an introduction to its functional anatomy 6th ed. Philadelphia: Mosby Inc./Elsevier Inc. Available at: http://books.google.com/books/about/The_human_brain.html?id=0ytfPgAACAAJ [Accessed July 18, 2011].

Obeid I, Nicolelis MAL, Wolf PD (2004) A multichannel telemetry system for single unit neural recordings. Journal of neuroscience methods 133:33–8 Available at: http://www.ncbi.nlm.nih.gov/pubmed/14757342 [Accessed March 1, 2013].

Ogawa H, Ito S, Nomura T (1989) Oral cavity representation at the frontal operculum of macaque monkeys. Neuroscience Research 6:283–298 Available at: http://www.ncbi.nlm.nih.gov/entrez/query.fcgi?cmd=Retrieve&db=PubMed&dopt=Citation&list_uids=2725988.

Olavarria J, Sluyters RC Van, Killackey HP (1984) Evidence for the complementary organization of callosal and thalamic connections within rat somatosensory cortex. Brain Research 291:364–8 Available at: http://www.ncbi.nlm.nih.gov/pubmed/6697197.

Pearson PP, Li CX, Waters RS (1999) Effects of large-scale limb deafferentation on the morphological and physiological organization of the forepaw barrel subfield (FBS) in somatosensory cortex (SI) in adult and neonatal rats. Experimental Brain Research 128:315–331 Available at: http://www.ncbi.nlm.nih.gov/entrez/query.fcgi?cmd=Retrieve&db=PubMed&dopt=Citation&list_uids=10501804.

Pearson PP, Oladehin A, Li CX, Johnson EF, Weeden AM, Daniel CH, Waters RS (1996) Relationship between representation of hindpaw and hindpaw barrel subfield (HBS) in layer IV of rat somatosensory cortex. NeuroReport 7:2317–2323 Available at: http://www.ncbi.nlm.nih.gov/entrez/query.fcgi?cmd=Retrieve&db=PubMed&dopt=Citation&list_uids=8951845.

Pidoux B, Verley R (1979) Projections on the cortical somatic I barrel subfield from ipsilateral vibrissae in adult rodents. Electroencephalography and clinical neurophysiology 46:715–26 Available at: http://www.ncbi.nlm.nih.gov/pubmed/87318 [Accessed September 17, 2011].

Pluto CP, Chiaia NL, Rhoades RW, Lane RD (2005) Reducing contralateral SI activity reveals hindlimb receptive fields in the SI forelimb-stump representation of neonatally amputated rats. Journal of neurophysiology 94:1727–32 Available at: http://www.ncbi.nlm.nih.gov/pubmed/15800076 [Accessed June 18, 2011].

Powell TP, Mountcastle VB (1959) Some aspects of the functional organization of the cortex of the postcentral gyrus of the monkey: a correlation of findings obtained in a single unit analysis with cytoarchitecture. Bulletin of the Johns Hopkins Hospital 105:133–62 Available at: http://www.ncbi.nlm.nih.gov/pubmed/14434571 [Accessed July 12, 2011].

Quairiaux C, Armstrong-James M, Welker E (2007) Modified sensory processing in the barrel cortex of the adult mouse after chronic whisker stimulation. Journal of neurophysiology 97:2130–47 Available at: http://www.ncbi.nlm.nih.gov/pubmed/17122325 [Accessed June 15, 2011].

Quiroga RQ, Nadasdy Z, Ben-Shaul Y (2004) Unsupervised spike detection and sorting with wavelets and superparamagnetic clustering. Neural computation 16:1661–87 Available at: http://www.ncbi.nlm.nih.gov/pubmed/15228749.

Ranck JB (1975) Which elements are excited in electrical stimulation of mammalian central nervous system: a review. Brain research 98:417–40 Available at: http://www.ncbi.nlm.nih.gov/pubmed/1102064 [Accessed March 7, 2013].

Recanzone GH, Merzenich MM, Dinse HR (1992)(a) Expansion of the cortical representation of a specific skin field in primary somatosensory cortex by intracortical microstimulation. Cerebral cortex (New York, N.Y. : 1991) 2:181–96 Available at: http://www.ncbi.nlm.nih.gov/pubmed/1511220.

Recanzone GH, Merzenich MM, Dinse HR (1992)(b) Expansion of the cortical representation of a specific skin field in primary somatosensory cortex by intracortical microstimulation. Cerebral Cortex 2:181–196 Available at: http://www.ncbi.nlm.nih.gov/pubmed/1511220.

Rema V, Armstrong-James M, Jenkinson N, Ebner FF (2006) Short exposure to an enriched environment accelerates plasticity in the barrel cortex of adult rats. Neuroscience 140:659–672 Available at: http://www.ncbi.nlm.nih.gov/pubmed/16616426.

Rema V, Ebner FF (2003) Lesions of mature barrel field cortex interfere with sensory processing and plasticity in connected areas of the contralateral hemisphere. The Journal of neuroscience : the official journal of the Society for Neuroscience 23:10378–87 Available at: http://www.ncbi.nlm.nih.gov/pubmed/14614097.

Roiha K, Kirveskari E, Kaste M, Mustanoja S, Mäkelä JP, Salonen O, Tatlisumak T, Forss N (2011) Reorganization of the primary somatosensory cortex during stroke recovery. Clinical Neurophysiology 122:339–345 Available at: http://www.ncbi.nlm.nih.gov/pubmed/20673646.

Rubinstein JT, Miller CA, Mino H, Abbas PJ (2001) Analysis of monophasic and biphasic electrical stimulation of nerve. IEEE transactions on bio-medical engineering 48:1065–70 Available at: http://www.ncbi.nlm.nih.gov/pubmed/11585029 [Accessed March 4, 2013].

Rutishauser U, Schuman EM, Mamelak AN (2006) Online detection and sorting of extracellularly recorded action potentials in human medial temporal lobe recordings, in vivo. Journal of neuroscience methods 154:204–24 Available at: http://www.ncbi.nlm.nih.gov/pubmed/16488479 [Accessed June 10, 2011].

Sah P, Nicoll RA (1991) Mechanisms underlying potentiation of synaptic transmission in rat anterior cingulate cortex in vitro. The Journal of physiology 433:615–30 Available at: http://www.pubmedcentral.nih.gov/articlerender.fcgi?artid=1181391&tool=pmcentrez&rendertype=abstract [Accessed March 6, 2013].

Salinas E, Sejnowski TJ (2001) Correlated neuronal activity and the flow of neural information. Nature reviews. Neuroscience 2:539–50 Available at: http://www.pubmedcentral.nih.gov/articlerender.fcgi?artid=2868968&tool=pmcentrez&rendertype=abstract [Accessed March 7, 2013].

Schaechter JD, Moore CI, Connell BD, Rosen BR, Dijkhuizen RM (2006) Structural and functional plasticity in the somatosensory cortex of chronic stroke patients. Brain : a journal of neurology 129:2722–33 Available at: http://www.ncbi.nlm.nih.gov/pubmed/16921177 [Accessed July 18, 2011].

Schwarz DW, Fredrickson JM (1971) Tactile direction sensitivity of area 2 oral neurons in the rhesus monkey cortex. Brain research 27:397–401 Available at: http://www.ncbi.nlm.nih.gov/pubmed/4994681 [Accessed March 6, 2013].

Sedra A, Smith KC (1987) Microelectronic Circuits 2nd ed. Orlando: The Dryden Press.

Shin H-CC, Won C-KK, Jung S-CC, Oh S, Park S, Sohn J-HH (1997) Interhemispheric modulation of sensory transmission in the primary somatosensory cortex of rats. Neuroscience letters 230:137–139 Available at: http://dx.doi.org/10.1016/S0304-3940(97)00486-2 [Accessed December 19, 2012].

Shuler MG, Krupa DJ, Nicolelis MA (2001) Bilateral integration of whisker information in the primary somatosensory cortex of rats. Journal of Neuroscience 21:5251–5261 Available at: http://www.ncbi.nlm.nih.gov/pubmed/11438600.

Smits E, Gordon DC, Witte S, Rasmusson DD, Zarzecki P (1991) Synaptic potentials evoked by convergent somatosensory and corticocortical inputs in raccoon somatosensory cortex: substrates for plasticity. Journal of neurophysiology 66:688–95 Available at: http://www.ncbi.nlm.nih.gov/pubmed/1753280 [Accessed September 18, 2011].

Squire LR, Berg D, Bloom FE, Lac S du, Ghosh A, Spitzer NC (2008) Somatosensory System In Fundamental Neuroscience, 3rd ed. Elsevier Inc, p. 581–608.

Swadlow HA (2003) Fast-spike interneurons and feedforward inhibition in awake sensory neocortex. Cerebral cortex (New York, N.Y. : 1991) 13:25–32 Available at: http://www.ncbi.nlm.nih.gov/pubmed/12466212 [Accessed March 6, 2013].

Swadlow HA, Hicks TP (1996) Somatosensory cortical efferent neurons of the awake rabbit: latencies to activation via supra--and subthreshold receptive fields. Journal of neurophysiology 75:1753–9 Available at: http://www.ncbi.nlm.nih.gov/pubmed/8727411 [Accessed November 8, 2012].

Taoka M, Toda T, Iriki A, Tanaka M, Iwamura Y (1999) Bilateral representation of the hindlimb in the postcentral somatosensory cortex of awake macaque monkeys. Soc. Neurosci Abstr:2196.

Taoka M, Toda T, Iwamura Y (1998) Representation of the midline trunk, bilateral arms, and shoulders in the monkey postcentral somatosensory cortex. Experimental brain research. Experimentelle Hirnforschung. Expérimentation cérébrale 123:315–22 Available at: http://www.ncbi.nlm.nih.gov/pubmed/9860270.

Tehovnik EJ (1996) Electrical stimulation of neural tissue to evoke behavioral responses. Journal of neuroscience methods 65:1–17 Available at: http://www.ncbi.nlm.nih.gov/pubmed/8815302.

Thomson AM (1986) A magnesium-sensitive post-synaptic potential in rat cerebral cortex resembles neuronal responses to N-methylaspartate. The Journal of physiology 370:531–49 Available at: http://www.pubmedcentral.nih.gov/articlerender.fcgi?artid=1192695&tool=pmcentrez&rendertype=abstract [Accessed March 6, 2013].

Thurgood BK, Ledbetter NM, Warren DJ, Clark GA, Harrison RR (2008) Wireless Integrated Circuit for 100-Channel Neural Stimulation. IEEE:129–132.

Thurgood BK, Warren DJ, Ledbetter NM, Clark GA, Harrison RR (2009) A Wireless Integrated Circuit for 100-Channel Charge-Balanced Neural Stimulation. IEEE Transactions on Biomedical Circuits and Systems 3:405–414 Available at: http://ieeexplore.ieee.org/xpls/abs_all.jsp?arnumber=5335875' escapeXml='false'/> [Accessed March 1, 2013].

Toda T, Taoka M, Iwamura Y (1996) Trancallosal connections of the upperarm/shoulder region of the monkey postcentral somatosensory cortex. Fap. F. Physiol:S159.

Tommerdahl M, Simons SB, Chiu JS, Favorov O, Whitsel BL (2006) Ipsilateral input modifies the primary somatosensory cortex response to contralateral skin flutter. The Journal of neuroscience : the official journal of the Society for Neuroscience 26:5970–7 Available at: http://www.ncbi.nlm.nih.gov/pubmed/16738239 [Accessed August 23, 2011].

Tortora GJ, Anagnostakos NP (1990) The Sensory, Motor, and Integrative Systems In Principles of Anatomy and Physiology Biological Sicences Textbooks, Inc., A&P Textbooks, Inc., and Elis-Sparta, Inc., p. 426–436.

Van Der Loos H, Woolsey TA (1973) Somatosensory cortex: structural alterations following early injury to sense organs. Science 179:395–398 Available at: http://www.ncbi.nlm.nih.gov/pubmed/4682966.

Vogels TP, Sprekeler H, Zenke F, Clopath (2011) Inhibitory plasticity balances excitation and inhibition in sensory pathways and memory networks. Science (New York, N.Y.) 334:1569–73 Available at: http://www.ncbi.nlm.nih.gov/pubmed/22075724.

Wang X, Merzenich MM, Sameshima K, Jenkins WM (1995) Remodelling of hand representation in adult cortex determined by timing of tactile stimulation. Nature 378:71–75 Available at: http://web1.johnshopkins.edu/xwang/Publications_files/Wang_Nature1995.pdf.

Waters RS, McCandlish CA, Li CX (1995)(a) Relationship between the organization of the forepaw barrel subfield and the representation of the forepaw in layer IV of rat somatosensory cortex. E. G. Jones & I. T. Diamond, eds. Experimental Brain Research 103:183–197 Available at: http://www.ncbi.nlm.nih.gov/entrez/query.fcgi?cmd=Retrieve&db=PubMed&dopt=Citation&list_uids=7789426.

Waters RS, McCandlish CA, Li CX (1995)(b) Organization and Development of the Forepaw Representation in Forepaw Barrel Subfield in Somatosensory Cortex in Rat In E. G. Jones & I. T. Diamond, eds. Cerebral Cortex New York: Plenum Press, p. 183–197. Available at: http://www.ncbi.nlm.nih.gov/entrez/query.fcgi?cmd=Retrieve&db=PubMed&dopt=Citation&list_uids=7789426.

Weiss T, Miltner WHR, Huonker R, Friedel R, Schmidt I (2000) Rapid functional plasticity of the somatosensory cortex after finger amputation. Most:199–203.

Welker C (1971) Microelectrode delineation of fine grain somatotopic organization of (SmI) cerebral neocortex in albino rat. Brain Research 26:259–275 Available at: http://linkinghub.elsevier.com/retrieve/pii/S0006899371800045.

Welker C (1976) Receptive fields of barrels in the somatosensory neocortex of the rat. Journal of Comparative Neurology 166:173–189 Available at: http://www.ncbi.nlm.nih.gov/entrez/query.fcgi?cmd=Retrieve&db=PubMed&dopt=Citation&list_uids=770516.

Welker C, Woolsey TA (1974) Structure of layer IV in the somatosensory neocortex of the rat: description and comparison with the mouse. Journal of Comparative Neurology 158:437–453 Available at: http://www.ncbi.nlm.nih.gov/pubmed/4141363.

Welker E, Armstrong-James M, Loos H Van Der, Kraftsik R (1993) The mode of activation of a barrel column: response properties of single units in the somatosensory cortex of the mouse upon whisker deflection. European Journal of Neuroscience 5:691–712 Available at: http://www.ncbi.nlm.nih.gov/pubmed/8261141.

Weller RE, Sur M, Kaas JH (1987) Callosal and ipsilateral cortical connections of the body surface representations in SI and SII of tree shrews. Somatosensory research 5:107–33 Available at: http://www.ncbi.nlm.nih.gov/pubmed/3423531 [Accessed September 15, 2011].

White EL (1989) Cortical Circuits: Synaptic Organization of the Cerebral Cortex. Boston: Birkhauser.

White EL, DeAmicis RA (1977) Afferent and efferent projections of the region in mouse SmL cortex which contains the posteromedial barrel subfield. The Journal of Comparative Nurology 175:455–82 Available at: http://www.ncbi.nlm.nih.gov/pubmed/915034 [Accessed September 15, 2011].

Wieringen A van, Carlyon RP, Laneau J, Wouters J (2005) Effects of waveform shape on human sensitivity to electrical stimulation of the inner ear. Hearing research 200:73–86 Available at: http://www.ncbi.nlm.nih.gov/pubmed/15668040 [Accessed March 1, 2013].

Wiest MC, Bentley N, Nicolelis M a L (2005) Heterogeneous integration of bilateral whisker signals by neurons in primary somatosensory cortex of awake rats. Journal of neurophysiology 93:2966–73 Available at: http://www.ncbi.nlm.nih.gov/pubmed/15563555 [Accessed January 30, 2012].

Williams JC, Hippensteel J a, Dilgen J, Shain W, Kipke DR (2007) Complex impedance spectroscopy for monitoring tissue responses to inserted neural implants. Journal of neural engineering 4:410–23 Available at: http://www.ncbi.nlm.nih.gov/pubmed/18057508 [Accessed March 1, 2013].

Wise SP, Jones EG (1976) The organization and postnatal development of the commissural projection of the rat somatic sensory cortex. The Journal of Comparative Nurology 168:313–43 Available at: http://www.ncbi.nlm.nih.gov/pubmed/950383 [Accessed September 15, 2011].

Wise SP, Jones EG (1977)(a) Somatotopic and columnar organization in the corticotectal projection of the rat somatic sensory cortex. Brain research 133:223–35 Available at: http://www.mendeley.com/research-papers/search/?query="the+functional+status+and+columnar+organization+of+single+cells [Accessed August 21, 2011].

Wise SP, Jones EG (1977)(b) Cells of origin and terminal distribution of descending projections of the rat somatic sensory cortex. The Journal of comparative neurology 175:129–57 Available at: http://www.ncbi.nlm.nih.gov/pubmed/408380 [Accessed November 10, 2012].

Wong-Riley MTT, Welt C (1980) Histochemical changes in cytochrome oxidase of cortical barrels after vibrissal removal in neonatal and adult mice. Proceedings of the National Academy of Sciences 77:2333–2337 Available at: http://www.pnas.org/content/77/4/2333.full.pdf.

Woolsey TA (1967) Somatosensory, auditory and visual cortical areas of the mouse. The Johns Hopkins medical journal 121:91–112 Available at: http://www.ncbi.nlm.nih.gov/pubmed/6032827 [Accessed September 13, 2011].

Woolsey TA, Loos H Van Der (1970) The structural organization of layer IV in the somatosensory region (SI) of mouse cerebral cortex. The description of a cortical field composed of discrete cytoarchitectonic units. Brain Research 17:205–242 Available at: http://www.ncbi.nlm.nih.gov/pubmed/4904874.

Xu S, Talwar SK, Hawley ES, Li L, Chapin JK (2004) A multi-channel telemetry system for brain microstimulation in freely roaming animals. Journal of Neuroscience Methods 133:57–63 Available at: http://linkinghub.elsevier.com/retrieve/pii/S0165027003003108 [Accessed August 29, 2011].

Yorke CH, Caviness VS (1975) Interhemispheric neocortical connections of the corpus callosum in the normal mouse: a study based on anterograde and retrograde methods. Journal of Comparative Neurology 164:233–245 Available at: http://www.ncbi.nlm.nih.gov/entrez/query.fcgi?cmd=Retrieve&db=PubMed&dopt=Citation&list_uids=1184784.

Záborszky L, Wolff JR (1982) Distribution patterns and individual variations of callosal connections in the albino rat. Anatomy and embryology 165:213–32 Available at: http://www.ncbi.nlm.nih.gov/pubmed/6186162 [Accessed September 15, 2011].

APPENDIX A

This Appendix presents the interactive neuronal stimulation and recording device bill of materials (BOM). The system is divided into four sub-circuits: Wireless communication, Stimulator ABE, Recorder AFE, and PSoC. The BOM includes all passive device values and is given in Tables A.1 – A.4.

Table A.1: Wireless communication BOM

Device	Value	Package
C1	1 µF	0603
C2	470 pF	0603
C3	2.2 µF	Tantalum Size A
C4	100 nF	0603
R1	1 kΩ	0603
R2	0 kΩ	0603
R3	10 kΩ	0603
R4	10 kΩ	0603
LED1	Red	0603
LED2	Red	0603
LED3	Red	0603
U1	MIC5219-3.3BM5	5 pin SOT23-5
U2	RN-42	30 pin SMD

Table A.2: Stimulator Analog Back End BOM

Device	Value	Package
C1	0.33 µF	0603
C2	0.1 µF	0603
C3	0.1 µF	0603
C4	0.33 µF	0603
C5	0.1 µF	0603
C6	0.1 µF	0603
C7	100 nF	0603
C8	100 nF	0603
C9	100 nF	0603
C10	100 nF	0603
R1	10 kΩ	0603
R2	10 kΩ	0603
R3	100 kΩ	0603
R4	100 kΩ	0603
R5	10 kΩ	0603
R6	10 kΩ	0603
R7	1 kΩ	0603
R8	1 Ω	0603
R9	1 Ω	0603
R10	21.7 kΩ	0603
R11	5 kΩ	0603
R12	1 kΩ	0603
R13	100 kΩ	0603
R14	1 kΩ	0603
R15	1 kΩ	0603
LED1	Red	0603
LED2	Red	0603
AMP1	TL082, device A	8 pin
AMP2	OPA454	9 pin
U1	MC7812	Pack 3
U2	MC7912	Pack 3

Table A.3: Recorder Analog Front End Version 1.0 BOM

Device	Value	Package
C1	0.33 µF	0603
C2	0.1 µF	0603
C3	0.1 µF	0603
C4	0.33 µF	0603
C5	0.1 µF	0603
C6	0.1 µF	0603
C7	3.3nF	0603
C8	2.2 µF	0603
C9	0.068 µF	0603
C10	0.068 µF	0603
C11	0.047 µF	0603
C12	470 pF	0603
C13	100 nF	0603
C14	100 nF	0603
C15	100 nF	0603
C16	100 nF	0603
C17	100 nF	0603
C18	100 nF	0603
C19	100 nF	0603
R1	10 kΩ	0603
R2	10 kΩ	0603
R3	220 kΩ	0603
R4	200 Ω	0603
R5	110 kΩ	0603
R6	620 Ω	0603
R7	118 kΩ	0603
R8	2.4 kΩ	0603
R9	10 kΩ	0603
R10	93.1 kΩ	0603
R11	10 kΩ	0603
R12	10 kΩ	0603
R13	33 kΩ	0603
R14	33 kΩ	0603
LED1	Red	0603
LED2	Red	0603
AMP1	TL084, device A	8 pin
AMP2	TL084, device B	8 pin
AMP3	TL084, device C	8 pin
AMP4	TL084, device D	8 pin
U1	MC7812	Pack 3
U2	MC7912	Pack 3

Table A.3: Recorder Analog Front End Version 2.0 BOM

Device	Value	Package
C1	0.33 µF	0603
C2	0.1 µF	0603
C3	0.1 µF	0603
C4	0.33 µF	0603
C5	0.1 µF	0603
C6	0.1 µF	0603
C7	3.3nF	0603
C8	2.2 µF	0603
C9	0.068 µF	0603
C10	0.068 µF	0603
C11	0.047 µF	0603
C12	330 pF	0603
C13	100 nF	0603
C14	100 nF	0603
C15	100 nF	0603
C16	100 nF	0603
C17	100 nF	0603
C18	100 nF	0603
C19	100 nF	0603
R1	10 kΩ	0603
R2	10 kΩ	0603
R3	220 kΩ	0603
R4	270 Ω	0603
R5	150 kΩ	0603
R6	430 Ω	0603
R7	13 kΩ	0603
R8	3 kΩ	0603
R9	10 kΩ	0603
R10	56 kΩ	0603
R11	10 kΩ	0603
R12	10 kΩ	0603
R13	33 kΩ	0603
R14	33 kΩ	0603
LED1	Red	0603
LED2	Red	0603
AMP1	TL084, device A	8 pin
AMP2	TL084, device B	8 pin
AMP3	TL084, device C	8 pin
AMP4	TL084, device D	8 pin
U1	MC7812	Pack 3
U2	MC7912	Pack 3

Table A.4: PSoC BOM

Device	Value	Package
C1	100 nF	0603
R1	1 kΩ	0603
R2	1 kΩ	0603
R3	1 kΩ	0603
LED1	Blue	0603
LED2	Blue	0603
LED3	Blue	0603
PSoC1	CY8C28542	28 pin
Mini-Prog	PSoC Programmer	5 pin